

1N-02-CR
PT-1
2788/27

PREDICTION OF FORCES AND MOMENTS FOR
FLIGHT VEHICLE CONTROL EFFECTORS— FINAL REPORT

PART I: VALIDATION OF METHODS FOR PREDICTING
HYPERSONIC VEHICLE CONTROLS FORCES AND MOMENTS

NASA Grant NAG 1-849

The National Aeronautics and Space Administration
Langley Research Center
ATTN: Dr. John Shaughnessy
MS 494
Hampton, VA 23665

M. Maughmer, L. Ozoroski, T. Ozoroski, D. Straussfogel
Department of Aerospace Engineering
The Pennsylvania State University
233 Hammond Building
University Park, PA 16802

May 1990

(NASA-CR-186571) PREDICTION OF FORCES AND
MOMENTS FOR FLIGHT VEHICLE CONTROL
EFFECTORS. PART I: VALIDATION OF METHODS FOR
PREDICTING HYPERSONIC VEHICLE CONTROLS
FORCES AND MOMENTS Final Report

N90-21734

63/02
Unclas
0278827

Abstract

Many types of hypersonic aircraft configurations are currently being studied for their feasibility of future development. Since the control of the hypersonic configurations throughout the speed range has a major impact on acceptable designs, it must be considered in the conceptual design stage. Part I of this report examines the ability of the aerodynamic analysis methods contained in an industry standard conceptual design system, APAS II, to estimate the forces and moments generated through control surface deflections from low subsonic to high hypersonic speeds. Predicted control forces and moments generated by various control effectors are compared with previously published wind tunnel and flight test data for three configurations: the North American X-15, the Space Shuttle Orbiter, and a hypersonic research airplane concept. Qualitative summaries of the results are given for each longitudinal force and moment and each control derivative in the various speed ranges. Results show that all predictions of longitudinal stability and control derivatives are acceptable for use at the conceptual design stage. Results for most lateral/directional control derivatives are acceptable for conceptual design purposes; however, predictions at supersonic Mach numbers for the change in yawing moment due to aileron deflection and the change in rolling moment due to rudder deflection are found to be unacceptable. Including shielding effects in the analysis is shown to have little effect on lift and pitching moment predictions while improving drag predictions. Overall, lateral/directional control derivatives show better agreement when shielding effects are not included.

In Part II of this report, an investigation of the aerodynamic control effectiveness of highly swept delta planforms operating in ground effect is presented. A vortex-lattice computer program incorporating a free wake is developed as a tool to calculate aerodynamic stability and control derivatives. Data generated using this program are compared to experimental data and to data from other vortex-lattice programs. Results show that an elevon deflection produces greater increments in C_L and C_M in ground effect than the same deflection produces out of ground effect and that the free wake is indeed necessary for good predictions near the ground.

Table of Contents

	Page
Overview	1
Part I: Validation of Methods for Predicting Hypersonic Vehicle Controls Forces and Moments	
Introduction	3
North American X-15 Research Aircraft	4
<i>Low Speed: $M_\infty = .056$</i>	4
<i>Transonic: $M_\infty = 0.80, 1.03, 1.18$</i>	4
<i>Supersonic: $M_\infty = 2.96$</i>	7
<i>Hypersonic: $M_\infty = 4.65, 6.89$</i>	8
<i>Summary Results with Mach Number</i>	9
Hypersonic Research Airplane	9
<i>Low Speed: $M_\infty = 0.20$</i>	9
<i>Transonic: $M_\infty = 0.80, 0.98, 1.20$</i>	10
<i>Hypersonic: $M_\infty = 6.00$</i>	11
<i>Summary Results with Mach Number</i>	12
Rockwell Space Shuttle Orbiter	12
<i>Low Speed: $M_\infty = 0.20$</i>	12
<i>Transonic: $M_\infty = 0.80$</i>	14
<i>Hypersonic: $M_\infty = 5.00, 20.0$</i>	14
<i>Summary Results with Mach Number</i>	16
Conclusions and Recommendations	17
References	19
Nomenclature	21
Tables	22
Figures	24
Appendix: Bibliography of Experimental Force and Moment Data For Hypersonic Vehicle Configurations	

Table of Contents (cont'd)

	Page
Part II: An Analysis of Delta Wing Aerodynamic Control Effectiveness in Ground Effect	
Introduction	1
Motivation for the Investigation	1
Scope of the Research	2
Review of Previous Work	3
<i>Theoretical Predictions</i>	3
<i>Experimental Results</i>	4
Theoretical Developments	6
The Vortex-Lattice Method	6
The Biot-Savart Law	11
Determination of the Influence Coefficients	13
Calculation of the Lift Coefficient	16
The Free Wake	18
The Ground Effect	23
The Suction Analogy	27
<i>Total Lift</i>	27
<i>Total Pitching Moment</i>	30
Flap Deflections	31
Results and Discussion	33
Verification of Results	33
VLM-FIG Predictions	49
Summary and Conclusions	64
References	66
Appendix A: Computer Program Description	69
Programming Method	69
Output	79
Appendix B: Computer Program Listing	80
Nomenclature	109

Overview

The purpose of this final progress report is to present the findings of two research activities which focus on hypersonic vehicle configurations. The first of these activities, discussed in Part I of this report, is aimed at validating methods, suitable for conceptual design work, which can be used for predicting flight control forces and moments over the Mach number range from low subsonic through hypersonic. Specifically, the subsonic/supersonic panel methods of Woodward, called the Unified Distributed Panel method (UDP)¹, are examined for subsonic and supersonic flight Mach numbers, while an enhanced version of the Hypersonic Arbitrary Body Program (HABP) of Gentry² is considered for hypersonic speeds. All of these methods have been incorporated into a single analysis program called the Aerodynamic Preliminary Analysis System II (APAS)^{3,4}, which is used in this study. Although HABP has been widely used for conceptual design activities since the early 1970's and a number of studies have been undertaken to examine its ability to predict the overall vehicle aerodynamics, no comprehensive, systematic study has been found which has explored its ability to predict forces and moments generated by aerodynamic flight controls. Thus, the goal of the present effort is to determine the accuracy and range of validity of the simple local surface inclination methods for predicting control forces and moments for a variety of configurations.

The approach used in this validation effort is to compare predicted and experimental results for several vehicle configurations which cover a broad range of proposed hypersonic vehicle configurations and for which wind-tunnel data are available.

The second research activity, considered in Part II of this report, is directed at studying the flight control behaviour of highly swept delta wing planforms in close proximity to the ground. Because of the possibility that the stability characteristics and/or the control effectiveness of such configurations is altered significantly by ground effect, this is an important area of concern in considering the take-off and landing of proposed hypersonic

flight vehicles. Furthermore, any analysis of such configurations in ground effect must examine the coupling that exists between deflecting a control surface to achieve a proper moment for trim and the change that such a deflection causes in the total lift generated. In order to explore these issues, a vortex-lattice program, which includes a free-wake and a reflective image plane to model ground proximity, has been developed. With this program it is possible to examine the change in moment of the entire vehicle, as well as the change in control effectiveness, due to ground effect. In this way, it can be determined whether or not sufficient control power for trim in ground effect is available and if not, the vortex-lattice code should be useful in evaluating innovative ways of generating the required moments to trim.

Part I: Validation of Methods for Predicting Hypersonic Vehicle Control Forces and Moments

Introduction

Before a great deal of activity is undertaken in assessing different types of flight control systems for hypersonic vehicles, it is important to understand the strengths and limitations of the prediction tools most likely to be used in this effort. Towards this end, a number of supersonic/hypersonic methods have been evaluated. Specifically, because their inherent simplicity makes them ideally suited to conceptual design work, among the tools under examination are the classical local surface inclination methods, including Newtonian theory, tangent-wedge/tangent-cone methods, and shock expansion techniques. These methods are all part of an industry-standard computer program called the "Hypersonic Arbitrary Body Program (HABP)," originally prepared by Gentry² and now part of a more encompassing program, the "Aerodynamic Preliminary Analysis System (APAS)," detailed in Refs. 3,4. Although HABP has been widely used for conceptual design activities since the early 1970's and a number of studies have been undertaken to examine its ability to predict the overall vehicle aerodynamics, Refs. 5-9 for example, it is apparent that no comprehensive, systematic study has explored its ability to predict forces and moments generated by aerodynamic flight controls. Thus, the goal of the present effort is to determine the accuracy and range of validity of the simple local surface inclination methods for predicting control forces and moments for a variety of configurations.

In addition to exploring the validity of the hypersonic capability of APAS, results using the subsonic and supersonic panel methods of that program, including a wetted-area drag prediction, were also compared with experimental data. Although more sophisticated methods are available for predicting control forces and moments in subsonic and supersonic flows, few offer the generality, simplicity and speed of the panel methods.

The approach taken in this validation effort is to examine several vehicle configurations which cover a broad range of proposed hypersonic vehicle configurations, and for which wind-tunnel data are available. For each configuration, the theoretical and experimental results are compared across the entire speed range of subsonic, transonic, supersonic, and hypersonic Mach numbers. The configurations analyzed are the X-15, shown in Fig. 1, the Hypersonic Research Airplane, a wing-body vehicle, as shown in Fig. 2, and the Space Shuttle Orbiter, presented in Fig. 3. Details concerning the geometry specification and the program implementation for this study are contained in Ref. 10. The experimental data to which the theoretical results are compared are included in the Appendix of this report, "Bibliography of Experimental Force and Moment Data for Hypersonic Vehicle Configurations," which is a rather extensive survey of available sources for such data.

North American X-15 Research Aircraft

The North American X-15 research airplane was developed in the late 1950's and flown in the early 1960's. It was designed to reach flight velocities of 6,600 ft/sec and altitudes of 250,000 feet. The wind tunnel data used to compare with theoretical predictions are taken from Refs. 11-14.

Low Speed: $M_{\infty} = .056$

Comparisons of the longitudinal subsonic panel method results of APAS are compared to low-speed experimental data ($M_{\infty} = .056$) in Figs. 4-8. In each figure, the theoretical zero-flap deflection results are given by the solid line, while the dashed line is for a 40 degree flap deflection. From the lift-curve data of Fig. 4, it is seen that over the linear range up to about 25 degrees angle of attack, the predicted results are within approximately 15% of the experimental ones. As expected, because separated flow is unaccounted for in the method, the rounding off of the lift curve is not captured. This likewise probably contributes to the lift-curve slope not being well predicted. Over the

linear range of the data, the theoretical method predicts the change in lift due to a flap deflection reasonable well, although for the most part the change in lift is slightly underestimated.

The general behavior of the drag as it depends on angle of attack is predicted fairly well by the wetted-area build-up method used in APAS, Fig. 5, although the absolute drag values, particularly at higher angles of attack because separation drag is not taken into account, are underpredicted. The errors in lift and drag as they depend on angle of attack compensate one another in the plot of C_D against C_L , Fig. 6. In this case, up until the drag increases due to separated flow become appreciable, the method does a good job when compared to the experimental results.

Pitching moment coefficient versus angle of attack, Fig. 7, and versus lift coefficient, Fig. 8, demonstrate the well-known difficulty of predicting pitching moments using methods which do not account for separation. In fact, only the predictions of the zero-lift values of the moment coefficient with zero flap deflection are even close to the experimental values. The change in moment with flap deflection is, in particular, not well predicted. Above about 20 degrees angle of attack where the results are largely affected by separation, the method, of course, produces a very poor estimation of the experimental results.

Results are presented for a downward elevator deflection of 5 degrees in Figs. 9-13. In this case, while the absolute values of the coefficients are somewhat in error, the changes due to the control deflection are all reasonably well predicted. In particular, the change in pitching moment due to the elevator deflection is predicted quite well, although other features of the pitching moment curves, Figs. 12 and 13, are not even approximated well.

In the comparisons of the predicted and experimental lateral/directional coefficients, Figs. 14-19, the different line types correspond to different treatments of the leading and side-edge suction forces. Included are purely potential flow with no edge treatment, potential flow plus the leading edge suction force, and potential flow plus leading and side-

edge modifications. The change in side force, yawing moment and rolling moment with differentially deflected elevons are presented as they depend on angle of attack in Figures 14–16, respectively. Although not accounting for flow separation probably contributes to the discrepancy at higher angles of attack between the theoretical and experimental results for $C_{n\delta_a}$, Fig. 15, all of the other results are certainly good enough for conceptual design work. In addition, for these cases, the inclusion of leading edge and/or side-edge suction analogies does not make a great deal of difference in the results.

The change in side force, yawing moment, and rolling moment with deflection of the vertical tail are presented with their dependence on angle of attack in Figures 17–19. Although not as good as the previous results, these too are probably close enough for many conceptual design studies. Note that in these figures, only the potential flow plus leading edge suction force results have been included. Unfortunately, some of the trends with changes in angle of attack are not captured and, in particular, it should be noted that the theoretical method misses the loss in control effectiveness at higher angles of attack, as seen in Fig. 18, probably because the method does not account for the separated flow off the fuselage which blankets the vertical tail.

Transonic: $M_\infty = 0.80, 1.03, 1.18$

For transonic Mach numbers of $M_\infty = 0.80, 1.03,$ and $1.18,$ the subsonic and supersonic panel method results are compared for experimental data only for the longitudinal aerodynamic derivatives at elevon deflections of 0 degrees, -3 degrees, and -6 degrees. The plots of these comparisons are presented in Figs. 20–31. In all cases, the angle of attack range is limited to less than 20 degrees such that the influence of separated flow on the results is limited.

As observed in Figs. 20, 24, and 28, both the trends and absolute levels of the lift curves are predicted quite well. In addition, the change in lift coefficient with elevon deflection is predicted well. Figs. 21, 25, and 29 demonstrate that the drag curves are well predicted, particularly at the lower angles of attack, for Mach numbers of 0.80 and 1.18.

Near $M_\infty = 1.00$, however, the drag coefficient is over-predicted and some unexplained discontinuities exist in the drag curve. In all cases, the drag increment due to a control deflection is not resolved well, although the trends are correct. Similar comments apply to the drag polar curves, Figs. 22, 26, and 30.

The pitching moment coefficient is plotted against the lift coefficient for the three Mach numbers in Figs. 23, 27, and 31. The zero-lift values of the pitching moment coefficient, as well as the change in moment coefficient with elevon deflection, are possibly predicted close enough for some purposes. The slope of the curve (static stability, $\partial C_m / \partial C_L$) is not predicted all that well; however, it improves as the Mach number moves away from $M_\infty = 1.00$.

Supersonic: $M_\infty = 2.96$

Comparisons of experimental and theoretical results for longitudinal coefficients at a Mach number of 2.96 are presented in Figs. 32-35. Lift and drag comparisons are not unlike those at lower speeds. The prediction of the slope of moment coefficient against lift coefficient curve, Fig. 35, is better than at lower speeds. Also, it is seen that the prediction of the change in moment coefficient with elevon deflection is not too bad for smaller deflections, where presumably the amount of separated flow on the surface is small, but deteriorates at larger deflection angles.

The prediction of lateral/directional coefficients with a differential elevon deflection are presented in Figs. 36-38. In these plots the potential flow result overlays that with the leading-edge modification included. While the predictions entirely miss some of the non-linear behavior observed in the experimental results, they are probably good enough for conceptual design work. Similar comments can be made for the vertical tail deflection results, Figs. 39-41. In particular, the directional control effectiveness, Fig. 40, is predicted quite well provided the vehicle angle of attack is not too great. Above an angle of attack of 25 degrees, the control effectiveness falls off rapidly, most likely due to the blanketing of the vertical tail in separated flow off the body.

Hypersonic: $M_\infty = 4.65, 6.89$

For Mach numbers of 4.65 and 6.83, experimental results are compared with theoretical results obtained using the Hypersonic Arbitrary Body Program (HABP) which is contained in APAS. When using HABP, the user has the choice of whether or not to ignore the aerodynamic contributions of components "shielded" (or shadowed) in the wake of upstream parts of the vehicle. For the X-15 runs, it was found that the use of shielding had very little impact on the results. Consequently, except where noted, the predictions presented are calculated without the shielding option.

The comparison of theoretical and experimental results of the longitudinal data for a Mach number of 4.65 are presented in Figs. 42-45. The lift-curve, Fig. 42, clearly demonstrates the non-linear behavior typical of hypersonic flow. While the general shape of this curve, as well as those of Figs. 43-45, is captured adequately, the effect of a symmetrical elevon deflection is not. Because the effect of a control deflection on the C_D vs. α curve, Fig. 43, is small compared to the effect on C_L , the underprediction of the effects of a control deflection observed in Figs. 44 and 45 is likely due to the problems of predicting the effect on lift.

Theoretical and experimental comparisons of lateral/directional coefficients are given in Figs. 46-51. Near zero angle of attack, the side force and yaw due to an unsymmetrical elevon deflection, Figs. 46 and 47, respectively, are predicted reasonably well; however, at higher angles of attack, only the sign of the force and moment is predicted correctly. Although the rolling moment due to the unsymmetrical elevon deflection is not predicted too badly, the control effectiveness is underpredicted, particularly at higher angles of attack. The prediction of side force, yawing moment, and rolling moment due to a vertical tail deflection is relatively good and certainly adequate for conceptual design studies.

Comparisons are presented for a Mach number of 6.83 in Figs. 52-64. The comments made for the $M_\infty = 4.65$ case apply to these results as well. Note the negligible

impact of shielding, Figs. 56-58, on lift, drag, and moment coefficients.

Summary Results with Mach Number

Some of the preceding lateral/directional comparisons are replotted versus Mach number in Figs. 65-70. The change in side force, yawing moment, and rolling moment due to an unsymmetrical elevon deflection are presented for two angles of attack in Figs. 65-67. Away from $M_\infty = 1.00$, the zero angle-of-attack predictions are quite good. From Fig. 67 it is seen that at higher Mach numbers the roll control power is considerably less than it is at low speeds. Although not predicted by HABP, it does increase somewhat as the Mach number increases. As should be expected, the change in angle of attack has little impact on the change in side force and yawing moment with unsymmetrical elevon deflection, Figs. 65 and 66, and the trends are predicted fairly well. Unfortunately, in the case of change in rolling moment with unsymmetrical elevon deflection, the effect of an angle of attack change is not predicted.

The changes in the lateral/directional control derivatives for a vertical tail deflection are presented in Figs. 68-70. For the Mach numbers shown and zero angle of attack, the predicted results agree quite well with those obtained experimentally.

Hypersonic Research Airplane

Comparison of theoretical predictions with experimental data for the Hypersonic Research Airplane (HRA), Ref. 15, are now considered. This blended wing/body aircraft has many configuration characteristics typical of proposed hypersonic vehicles. The wind-tunnel results which will be used for this comparison are taken from Refs. 15-17.

Low Speed: $M_\infty = 0.20$

Experimental results are compared with APAS subsonic panel method predictions of the longitudinal aerodynamic characteristics of the HRA in Figs. 71-75. Overall, the agreement between the experimental values with those calculated is similar to that obtained for the X-15 aircraft. The lift coefficient versus angle of attack, Fig. 71, is like

the X-15. The lift coefficient is underpredicted at higher angles of attack. Possibly, the extent of vortex lift is not fully taken into account. The change in lift coefficient with a symmetrical elevon deflection, $C_{L\delta_e}$, is predicted well enough for conceptual design activities. Also as was the case for the X-15 and observed in Fig. 72, the drag coefficient is increasingly underpredicted as the angle of attack increases. The agreement between experiment and theory in the C_D-C_L curve, Fig 73, reflects the characteristics of the C_L and C_D versus angle of attack results.

The pitching moment coefficient predictions, Figs. 74 and 75, are much better for the HRA than for the X-15. Also, as is the case for the X-15 and more important from a flight controls point of view, the prediction of the elevon control power, $C_{m\delta_e}$, is reasonable. It is observed, however, that the magnitude of the control power for the X-15, possibly because of the all-moving tail and the longer moment arm, is considerably greater than that of the HRA.

In considering the prediction of the lateral/directional coefficients, Figs. 76-81, results are presented for calculations using potential flow, potential flow with leading edge suction analogy, and potential flow with leading and side edge suction analogies. In the case of the change in side force, yawing moment, and rolling moment with differentially deflected elevons, $C_{Y\delta_a}$, $C_{n\delta_a}$, and $C_{l\delta_a}$ the predictions using potential flow plus the leading edge modification agree quite well with the experimental results. The changes in the coefficients with a vertical tail deflection, $C_{Y\delta_v}$, $C_{n\delta_v}$, and $C_{l\delta_v}$ are not well predicted and are typically in error by 50% or more. In all cases, use of potential flow plus the leading edge suction treatment gives the best results. The inclusion of the side edge modification makes little difference or causes the agreement between the experimental and predicted results to be worse.

Transonic: $M_\infty = 0.80, 0.98, 1.20$

For the case of $M_\infty = 0.80$, the comparison between the experimental and predicted results, presented in Figs. 82-89, is very similar to that for $M_\infty = 0.20$ and additional

comments are not necessary. As the Mach number increases, the prediction of $C_{L_{\delta_e}}$ deteriorates, Fig. 90, as does that of elevator control power, $C_{m_{\delta_e}}$ Figs. 93 and 94. The drag coefficient, Fig. 91, is further underpredicted when compared to the lower Mach number cases. The predicted values of the change in the side force, yawing moment, and rolling moment coefficients with differential elevon deflection, $C_{Y_{\delta_a}}$, $C_{n_{\delta_a}}$, and $C_{l_{\delta_a}}$, Figs. 95-97, are certainly adequate for conceptual design activities. The deterioration of $C_{L_{\delta_e}}$ and $C_{m_{\delta_e}}$ predictions noted for $M_\infty = 0.80$ continues as the Mach number increases to $M_\infty = 1.20$. Comparison of experimental and theoretical results for this Mach number are presented in Figs. 98-105.

Hypersonic: $M_\infty = 6.00$

Comparisons of experimental results with predictions using HABP without shielding for the longitudinal aerodynamics are presented in Figs. 106-110. While the C_L vs. α data shown in Fig. 106 appears better than that for the X-15, it should be noted that the values of C_L , as well as $C_{L_{\delta_e}}$ are considerably less. In any case, with the exception of missing that $C_{L_{\delta_e}}$ decreases as the angle of attack decreases, the magnitudes of the forces and most of the trends are predicted reasonably well. In the case of the drag coefficient, Figs. 107 and 108, the trends are captured fairly well although, opposite of what happens in the case of the X-15, the drag coefficient is consistently overpredicted. The moment coefficient predictions for this case, Figs. 109 and 110, are also not too bad and probably good enough for conceptual design activities. Certainly the trends, as well as the values of the elevator control power, $C_{m_{\delta_e}}$, are reasonably well predicted.

The longitudinal cases just presented without shielding are repeated with shielding in Figs. 111-115. In all cases here, the use of shielding improves the predictions considerably. In particular, incorporating shielding produces much better agreement between the experimental data and the calculated coefficients at lower angles of attack. As a consequence, the values of the control derivatives, $C_{L_{\delta_e}}$ and $C_{m_{\delta_e}}$ are much improved.

Comparisons of wind-tunnel findings with HABP predictions with and without

shielding for the changes in the lateral coefficients with differentially deflected elevons are given in Figs. 116–119. For these cases, the predictions without shielding agree somewhat better with experimental data than those with shielding. In either case, while the predictions are good, it should be noted that the control power, $C_{l_{\delta a}}$, is very low. Similar comments apply to the change in coefficients due to a vertical tail deflection, $C_{Y_{\delta v}}$, $C_{n_{\delta v}}$, and $C_{l_{\delta v}}$, as presented in Figs. 119–121.

Summary Results with Mach Number

Summaries of the lateral control derivatives as they depend on Mach number and at two angles of attack are given in Figs. 122–124. Overall, $C_{Y_{\delta a}}$, $C_{n_{\delta a}}$, and $C_{l_{\delta a}}$ are predicted well at low speeds, reasonably well in the transonic range, and very well at $M_{\infty} = 6.00$. With the exception of the prediction at $M_{\infty} = 6.00$, this is not the case for $C_{Y_{\delta v}}$, $C_{n_{\delta v}}$, and $C_{l_{\delta v}}$, presented for zero angle of attack as a function of Mach number in Figs. 125–127. In fact, the trends as well as the values of these derivatives are not well predicted. This was not the case for the X-15, which achieved directional control by means of very large all-moving, wedge cross-sectioned surfaces both above and below the vehicle centerline.

Rockwell Space Shuttle Orbiter

The third hypersonic vehicle configuration for which theoretical and experimental results are compared is the Rockwell Space Shuttle Orbiter. All of the experimental data used for this comparison is taken from Ref. 18.

Low Speed: $M_{\infty} = 0.20$

Longitudinal aerodynamic coefficients as predicted using the subsonic panel method of APAS are compared with experimental findings in Figs. 128–132. Included in these comparisons are results for full-span elevon deflections of -20, -10, 0, and 10 degrees. As observed in Fig. 128, the predicted lift coefficients as a function of angle of attack are, for the most part, within about 10%. While both the predicted and experimental results

are close to linear for the range of angles of attack presented, the lift-curve slopes are not well predicted. This causes fairly large discrepancies between the predicted and experimental results at low angles of attack and large negative elevon deflections. In spite of these problems, the flap effectiveness of the elevon, $C_{L_{\delta_e}}$, is predicted reasonably well except at low angles of attack and large negative deflection angles for which not accounting for separated flow evidently causes the control effectiveness to be overpredicted.

Comparisons of predicted and experimental drag coefficients are presented versus angle of attack in Fig. 129, and versus lift coefficient in Fig. 130. In both cases the predicted results are probably good enough for conceptual design activities.

Predicted and experimental pitching moment coefficients are presented as a function of angle of attack in Fig. 131, and as a function of lift coefficient in Fig. 132. In both cases the predicted values of the coefficients are not too good. In fact, the slopes of the predicted and experimental curves are sometimes of the opposite sign. Although slightly overpredicted, however, the predicted elevon control effectiveness, $C_{m_{\delta_e}}$, is reasonably close to that found experimentally. Predicted values of the lateral control derivatives for the Shuttle are compared with experimental values in Fig. 133-135. These panel method predictions for differentially deflected elevons are made using potential flow only, potential flow plus leading-edge effects, and potential flow plus leading- and side-edge effects. As was the case for the other vehicles examined, the potential flow, modified with the leading-edge suction analogy only, yields the best agreement with experiment. This agreement is probably acceptable for conceptual design work.

Predicted and experimental comparisons for directional control derivatives, $C_{Y_{\delta_v}}$, $C_{n_{\delta_v}}$, and $C_{l_{\delta_v}}$, are shown in Figs. 136-138. In these cases, only the potential flow plus leading-edge effects are presented. As before, the predictions are not too bad. At worst, the control effectiveness, $C_{n_{\delta_v}}$, is predicted to be 30% greater than the value found experimentally.

Transonic: $M_\infty = 0.80$

Predicted lift curves for different elevon deflections are compared with experimental results at $M_\infty = 0.80$ in Fig. 139. Although similar to the $M_\infty = 0.25$ comparison, the problem areas are more pronounced. For example, the lift-curve slopes are generally not well predicted, the bending over of the curves due to flow separation is not captured, and the control effectiveness, $C_{l_{\delta_e}}$, while not too bad for $\delta_e = \pm 10^\circ$, is poorly predicted for $\delta_e = -20^\circ$. In the case of C_D versus α and C_D versus C_L , Figs. 140 and 141, the comparisons are similar to those for $M_\infty = 0.25$. While significant errors are present as separated flow strongly influences the results at higher angles of attacks, the drag predictions capture the trends correctly and are acceptable for conceptual design activities. In the case of C_M plotted against α , Fig. 142, and against C_L , Fig. 143, the $\delta_e = 0$ prediction is reasonably close to the experimental data. Other than that, about all that can be said is that the predicted trends are more or less correct.

As in the $M_\infty = 0.25$ case, the best lateral control derivative predictions are obtained using the potential flow results modified with leading-edge effects. The predicted values of $C_{Y_{\delta_a}}$, $C_{n_{\delta_a}}$, and $C_{l_{\delta_a}}$ as they depend on angle of attack, Figs. 144–146, are reasonably close to the experimental values. The directional derivatives, $C_{Y_{\delta_v}}$ and $C_{n_{\delta_v}}$, however, presented in Figs. 147 and 148, are in error by over 100% in some cases. The predicted values of $C_{l_{\delta_v}}$, as observed in Fig. 149, are somewhat better.

Hypersonic: $M_\infty = 5.00, 20.0$

Values of C_L , C_D , and C_m predicted using HABP without employing the shadowing of downstream components are compared with experimental results for $M_\infty = 5.00$ in Figs. 150–154. The predicted lift coefficient as it depends on angle of attack, Fig. 150, is in excellent agreement with the experimental data at angles of attack below 20° , and is not too bad even up to 40° . The flap effectiveness for a symmetrical elevon deflection, $C_{l_{\delta_e}}$, is predicted very well. Likewise, comparison of the predicted C_D - α and C_D - C_L curves with experiment, Figs. 151 and 152, are adequate for conceptual design studies.

For the comparisons with experiment of the predicted $C_m - \alpha$, Fig. 153, and $C_m - C_L$, Fig. 154, certainly the characteristic trends are captured; however, the control effectiveness is significantly overpredicted for large negative elevon deflections.

Predicted and experimental changes in C_L , C_D , and C_m due to deflecting the Shuttle body flap are presented in Figs. 155–157. In each case, the overall trends are more or less predicted by the methods in HABP. Most likely, the discrepancies in predicting these results are due to the fact that the effects of flow separation are not taken into account.

The influence on the longitudinal aerodynamic coefficients of shadowing panels which are shielded from the oncoming flow by upstream elements is demonstrated by the results presented in Figs. 158–162. It is observed that, while shielding does not make a critical difference in the cases of lift and drag coefficients, Figs. 158–160, the shielded results are uniformly better. For the pitching moment coefficient, Figs. 161–162, the shielded results are better in the low angle of attack and lift coefficient range, while the unshielded results are better at higher angles of attack and lift coefficients. In view of the fact that for these cases the use of shadowing produces superior results, at least for lift and drag, Figs. 163–167 repeat the previous predictions for lift, drag, and moment coefficients but with downstream components shielded.

Comparisons between HABP predictions for the lateral control derivatives and experiment are presented in Figs. 168–170. None of the calculated results employ shielding; however, the predictions are seen to capture both trends and magnitudes quite well. Unfortunately, this success is not repeated for the directional control derivatives, Figs. 171–173. It should be noted, however, that the magnitudes of these derivatives are, in general, quite small.

The comparisons generated for $M_\infty = 5.00$ are repeated in Figs. 174–197 for $M_\infty = 20.0$. Basic unshielded results are given in Figs. 174–178 while corresponding shielded results are presented in Figs. 187–191. For the most part, the comments di-

rected to the $M_\infty = 5.00$ comparisons also apply to the $M_\infty = 20.0$ results. If anything, the HABP predictions generally improve as the Mach number increases. As before, the predicted values of the pitching moment coefficients, Figs. 177-178 and 190-191, are not good; however, the values of $C_{m_{\delta_e}}$ are reasonable. Also, it should be noted that the directional control derivative predictions (without shielding) are considerably better at $M_\infty = 20.0$ than at $M_\infty = 5.00$. Again, it should be noted that the control effectivenesses, $C_{l_{\delta_a}}$ and $C_{n_{\delta_v}}$, are quite low.

Summary Results with Mach Number

Plots of the predicted and experimental values of the lateral/directional control derivations at fixed angles of attack as they depend on Mach number are presented in Figs. 198-203. Each of these plots indicate that the prediction improves as Mach number increases although, with the exception of the transonic region, they are reasonably good elsewhere. In every case, it should be noted that the control derivatives, including those of control effectiveness, decrease as the Mach number increases.

Conclusions and Recommendations

The suitability of the methods contained in APAS for flight control force and moment prediction are summarized in Table 1 for longitudinal quantities and Table 2 for lateral/directional derivatives. Based on the comparisons between experimental and predicted results made in this study, the assessment of predicting a particular quantity in a given speed range is ranked as: (1) capable of predicting magnitudes within 40%, as well as the proper trends, over a significant portion of the operating range; (2) capable of predicting trends reasonably well but not magnitudes; (3) generally unacceptable for conceptual design work.

In considering the results presented in Table 1, it is concluded that, provided the results are interpreted carefully and major decisions are not based on predictions which are known to be suspect, all of the longitudinal results can be of some use in conceptual design studies. As expected, the most questionable calculations are those in which neglected separated flow can significantly influence the results. In the case of predicting lateral/directional control derivatives, some results are found to be unacceptable. Fortunately, however, for the most part the primary control derivatives, $C_{l_{\delta_a}}$ and $C_{n_{\delta_v}}$, are found to provide reasonable results.

Given that for conceptual design work, the trade-off between accuracy and speed of computation leans very heavily toward speed, all of the prediction methods contained in APAS are reasonable. It should be noted, however, that in the case of the subsonic and supersonic methods, a great deal of flexibility exists in controlling the trade-off between accuracy and speed. The panel methods considered are basically as fast and robust as possible at the expense of accuracy. If more accuracy is desired, a number of improvements are possible between panel methods and a full-blown Navier-Stokes computation. For example, in the direction of increasing complexity and accuracy, a more complete boundary layer model could improve the drag predictions and, combined with empiri-

cal correlations, could greatly improve the derivatives strongly influenced by separation effects. If better accounting for the effects of compressibility is required, the flowfield could be modelled using the Euler equation rather than the linearized potential equation.

While in the case of subsonic and supersonic Mach numbers there is a great deal of flexibility for achieving a desired level of accuracy by implementing a sufficiently rigorous theoretical model, this is not the case in the hypersonic flight regime. Essentially, there is nothing in the way of a more sophisticated theoretical model between the flow inclination methods contained in HABP and a full Navier-Stokes computation. Unfortunately at present, the time required for setting up computational grids, as well as execution requirements, are much too great for the full computational methods to be routinely used for conceptual design activities. Thus, methods such as those contained in HABP will likely remain the primary tools for preliminary flight control force and moment prediction for some time. For such work these methods can be expected to provide reasonable estimates provided they are applied to situations not dominated by strong viscous/inviscid interactions, real gas and/or rarefied gas effects, or flowfields containing extensive regions of separated flow.

Finally, while little can be done to remove the noted limitations of the hypersonic flow inclination methods, the following should be considered to improve their usefulness and accuracy:

- (1) guided by the existing data base, make empirical adjustments in the methods to account for the anomalies seen between predicted and experimental results
- (2) add a more sophisticated boundary-layer theory, including a transition model, to better account for viscous effects
- (3) develop an unsteady Newtonian Theory (based on piston theory) to allow the computation of dynamic stability and control derivatives.

References

1. Woodward, F., "Analysis and Design of Wing-Body Combinations at Subsonic and Supersonic Speeds," *Journal of Aircraft*, Nov.-Dec. 1968.
2. Gentry, A.E., "Hypersonic Arbitrary-Body Aerodynamic Computer Program (Mark III Version). Vol. 1—User's Manual," Report DAC 61552, McDonnell-Douglas Corporation, April 1968.
3. Bonner, E., Clever, W., and Dunn, K., "Aerodynamic Preliminary Analysis System II—Part I, Theory," NASA CR-165627, 1981.
4. Sova, G. and Divan, P., "Aerodynamic Preliminary Analysis System II— Part II, User's Manual, North American Aircraft Operations, Rockwell International.
5. Middleton, W.D., Lundry, J.L., and Coleman, R.G., "A System for Aerodynamic Design and Analysis of Supersonic Aircraft, Part 1—Development," NASA CR 3352, 1980.
6. Fisher, C.M.E., "Experience Using the Mark IV Supersonic Hypersonic Arbitrary Body Program," *Aerodynamics of Hypersonic Lifting Vehicles*, AGARD CP-428, Paper 31, April 1987.
7. Covell, P.F., Wood, R.M., Bauer, S.X., and Malaker, I.J., "Configuration Trade and Code Validation Study on a Conical Hypersonic Vehicle," AIAA Paper 88-4505, September 1988.
8. Moore, M.E. and Williams, J.E., "Aerodynamic Prediction Rationale for Analyses of Hypersonic Configurations," AIAA Paper 89-0525, January 1989.
9. Cruz, C.I., and Wilhite, A.W., "Prediction of High-Speed Aerodynamic Characteristics Using The Aerodynamic Preliminary Analysis System (APAS), AIAA Paper 89-2173, August 1989.
10. Ozoroski, L.P., "Evaluation of Methods for Predicting the Forces and Moments Generated by Control Surface Deflections on Hypersonic Vehicles," M.S. Thesis, Pennsylvania State University, 1990.
11. Boisseau, Peter C., "Investigation of the Low-speed Stability and Control Characteristics of a 1/7-Scale Model of the North American X-15 Airplane," NACA RM L57D09, 1957.
12. Osbourne, R.S., "Aerodynamic Characteristics of a 0.0667 Scale Model of the N.A. X-15 Research Airplane at Transonic Speeds," NASA TM X-24, 1959.
13. Penland, J.A. and Fetterman, D.E. Jr., "Static Longitudinal, Directional, and Lateral Stability and Control Data at a Mach Number of 6.83 of the Final Configuration of the X-15 Research Airplane," NASA TM X-236, April 1960.

14. McKinney, R.L. and Lancaster, J.A., "Investigation of the Aerodynamic Characteristics of a 0.02-Scale Model of the X-15 Airplane at Mach Numbers of 2.96, 3.96, and 4.65 at High Angles of Attack," NASA TM X-820, June 1963.
15. Dillon, J.L. and Pittman, J.L., "Aerodynamic Characteristics at Mach Numbers from 0.33 to 1.20 of a Wing-Body Design Concept for a Hypersonic Research Airplane," NASA TP 1044, 1977.
16. Dillon, J.L. and Creel, T.R. Jr., "Aerodynamic Characteristics at Mach Number 0.2 of a Wing Body Concept for a Hypersonic Research Airplane," NASA TP 1189, 1978.
17. Dillon, J.L. and Pittman, J.L., "Aerodynamic Characteristics at Mach 6 of a Wing-Body Concept for a Hypersonic Research Airplane," NASA TP 1249, August 1978.
18. "Aerodynamic Design Data Book," Vol. I, Shuttle Orbiter Vehicle, October 1978.

Nomenclature

$C_D =$	drag coefficient
$C_L =$	lift coefficient
$C_Y =$	side force coefficient
$C_l =$	rolling moment coefficient
$C_m =$	pitching moment coefficient
$C_n =$	yawing moment coefficient

Subscripts

$\delta_a =$	aileron or differential elevon deflection
$\delta_{bf} =$	body flap deflection
$\delta_e =$	elevator or synchronous elevon deflection
$\delta_f =$	flap deflection
$\delta_h =$	horizontal tail deflection
$\delta_v =$	rudder or vertical tail deflection

M_∞	C_L	C_{L_a}	$C_{L_{\delta_e}}$	C_D	$C_{D_{\delta_e}}$	C_m	C_{m_a}	$C_{m_{\delta_e}}$
Subsonic $M_\infty < 0.8$	○	○	○	●	●	●	●	○
Transonic $0.8 < M_\infty < 1.2$	○	○	○	●	●	●	●	●
Supersonic $1.2 < M_\infty < 4.5$	○	○	○	○	○	●	●	●
Low Hypersonic ¹ $4.5 < M_\infty < 8.0$	○	○	○ ³	○	○	● ²	● ^{2,3}	○ ^{2,3}
High Hypersonic ¹ $8.0 < M_\infty < 20.0$	○	○	○ ³	●	○	●	●	○

- Trends predicted well and magnitudes are within 40% over a significant portion of the operating range.
- Results should be regarded cautiously— Magnitudes near zero angle of attack or trends with angle of attack, but not both, are predicted reasonably well.
- Not useful

Notes: 1. Longitudinal results are generally better with shielding.
2. Moment results for low angles of attack are generally better with shielding, while high angle of attack results are generally better without shielding.
3. Some problems in predicting results for X-15

Table 1 Qualitative Assessment of the Ability of APAS to Predict Longitudinal Stability and Control Derivatives Categorized By Speed Range

M_∞	$C_{Y\delta_a}$	$C_{n\delta_a}$	$C_{l\delta_a}$	$C_{Y\delta_e}$	$C_{n\delta_e}$	$C_{l\delta_e}$
Subsonic $M_\infty < 0.8$	○ ³	○ ³	○	●	● ²	●
Transonic $0.8 < M_\infty < 1.2$	○	○ ³	○	●	●	●
Supersonic $1.2 < M_\infty < 4.5$	○	●	●	○	○	●
Low Hypersonic ¹ $4.5 < M_\infty < 8.0$	● ²	○ ²	○ ²	○ ³	○ ³	○ ³
High Hypersonic ¹ $8.0 < M_\infty < 20.0$	○	○	○ ³	○	○	○

- Trends predicted well and magnitudes are within 40% over a significant portion of the operating range.
- Results should be regarded cautiously—Magnitudes near zero angle of attack or trends with angle of attack, but not both, are predicted reasonably well.
- Not useful

Notes: 1. Lateral/directional results are generally better without shielding.
 2. Some problems in predicting results for X-15
 3. Some problems in predicting results for Space Shuttle Orbiter

Table 2 Qualitative Assessment of the Ability of APAS to Predict Lateral/Directional Control Derivatives Categorized By Speed Range

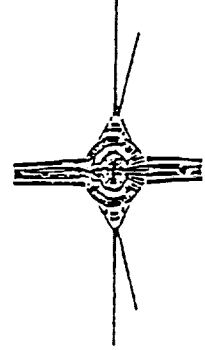
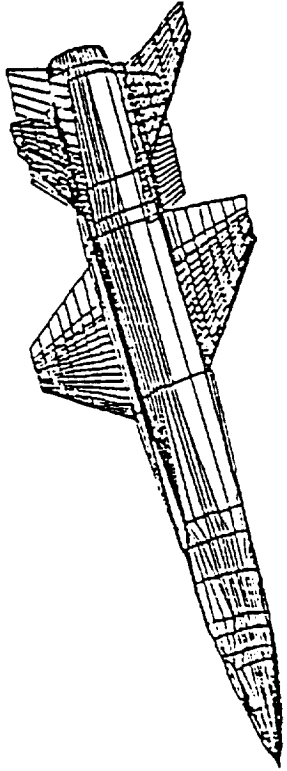
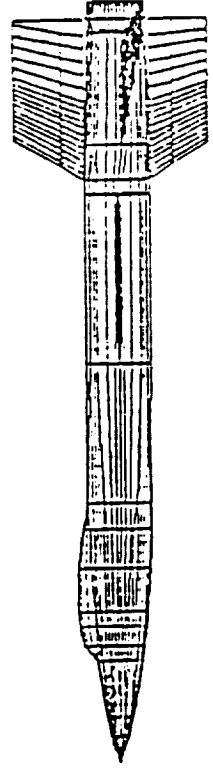
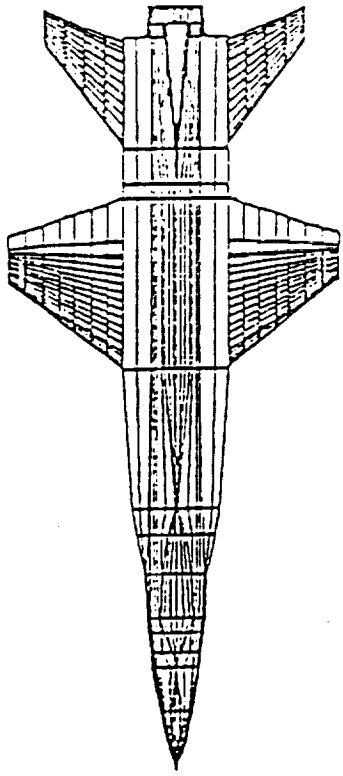


Fig. 1 X-15 Configuration

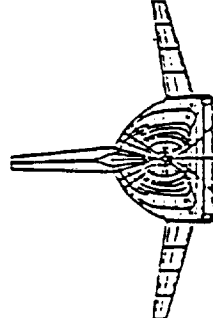
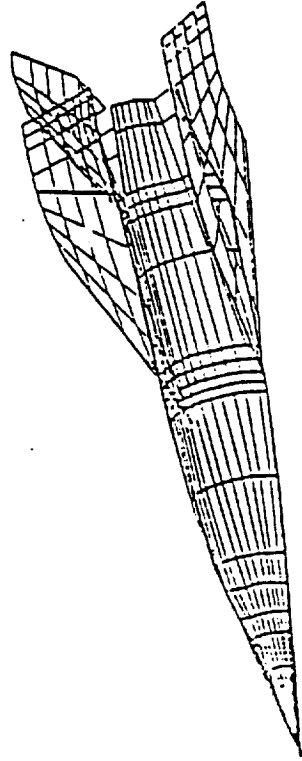
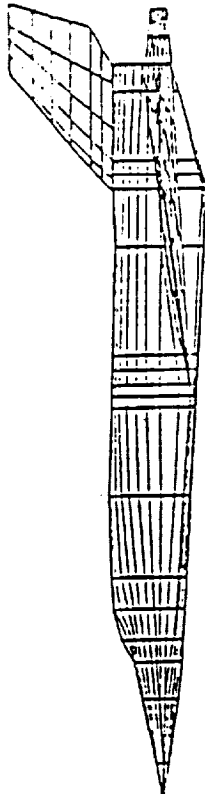
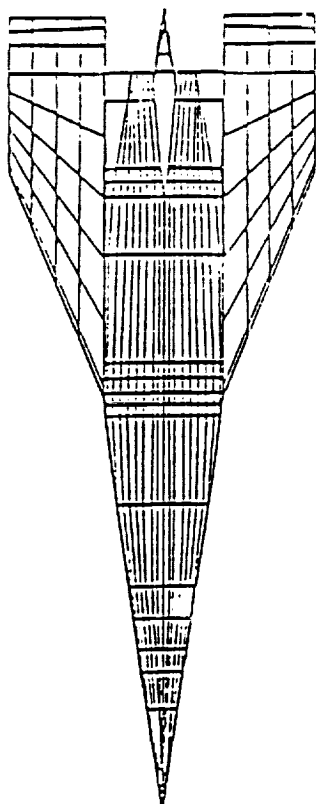


Fig. 2 Hypersonic Wing-Body Configuration

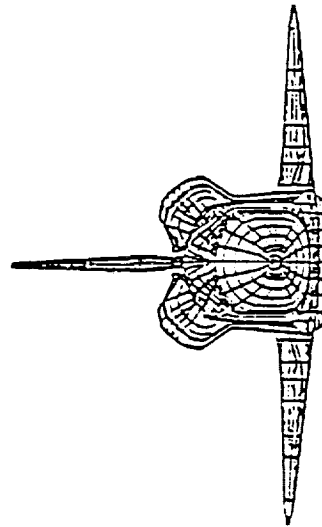
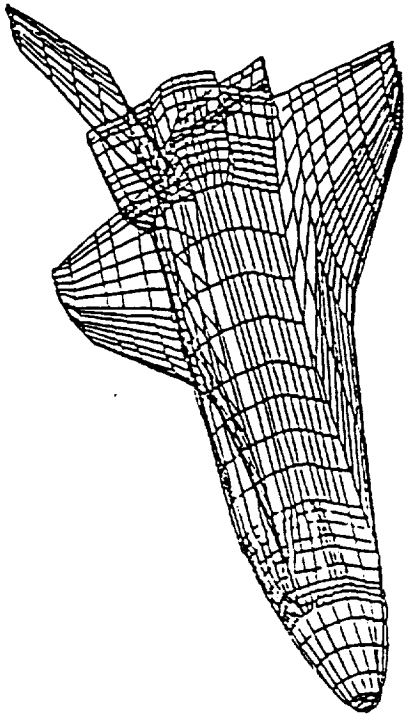
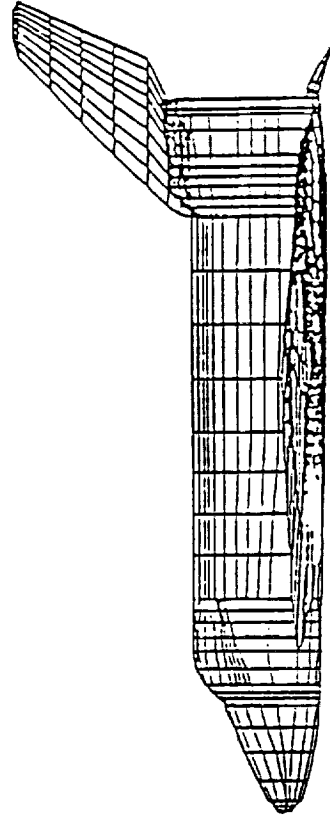
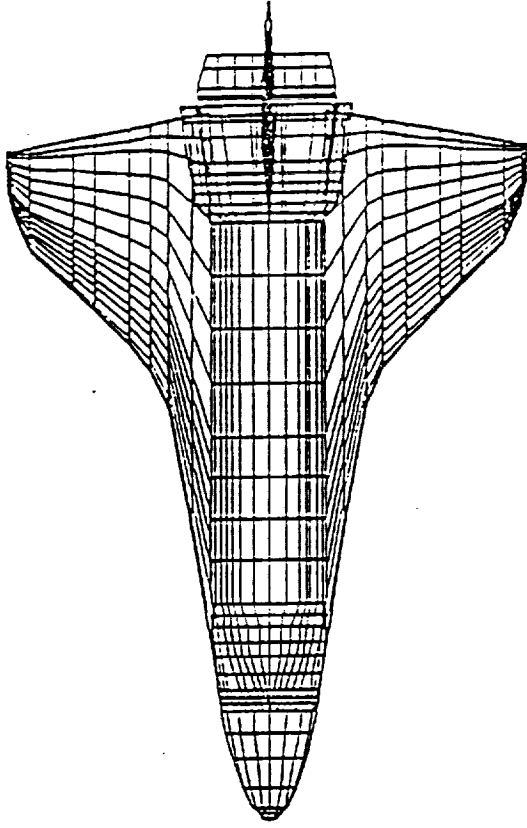


Fig. 3 Space Shuttle Configuration

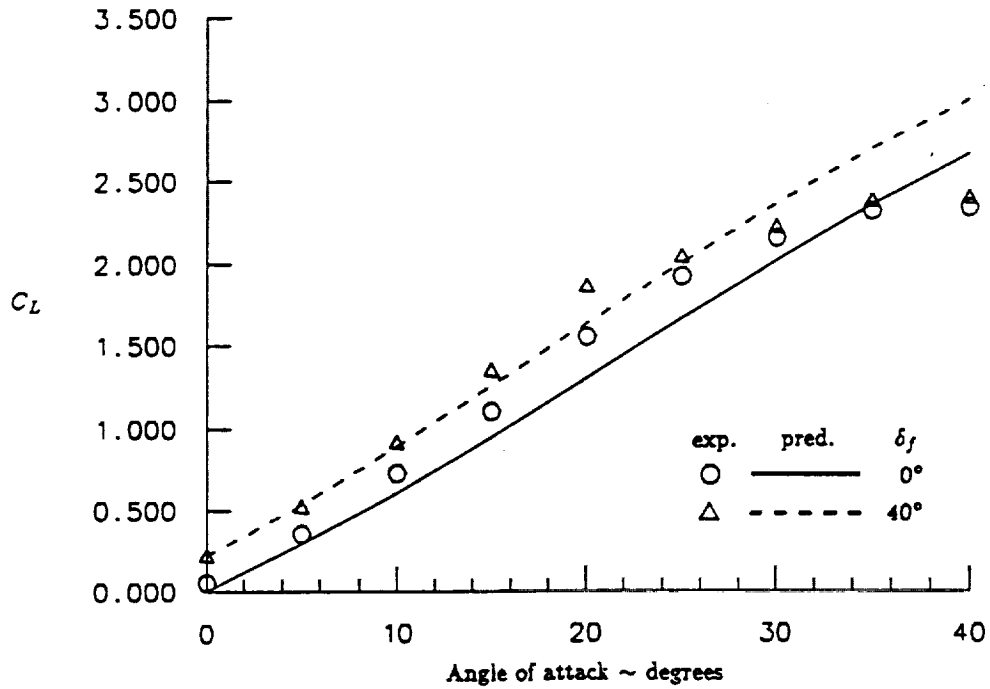


Fig. 4 Comparison Between Predicted and Experimentally Measured Lift on X-15 Vehicle at Low Speed Including the Effect of Flap Deflection. X-15 ; C_L vs. α ; $M = .056$; $\delta_f = 0^\circ$ and 40°

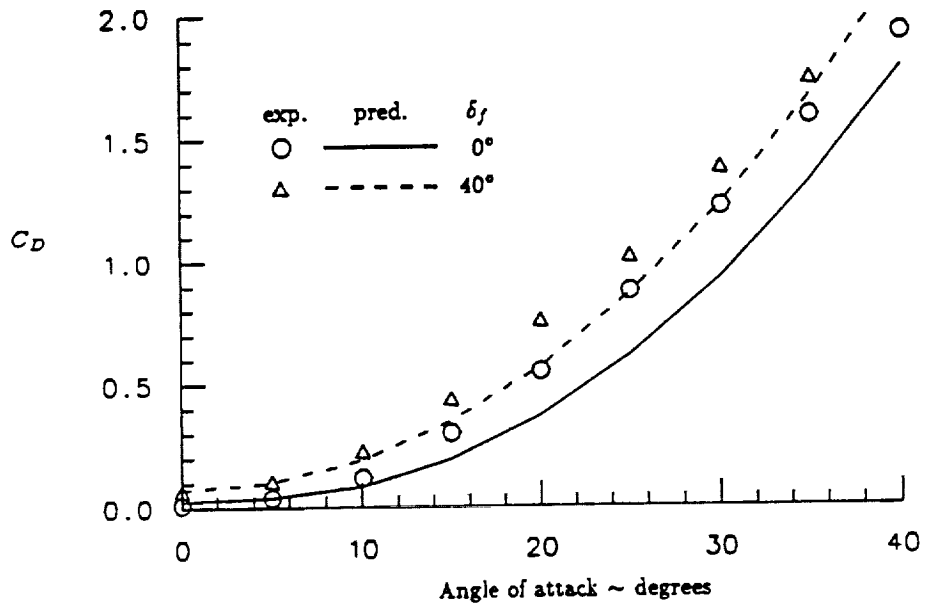


Fig. 5 Comparison Between Predicted and Experimentally Measured Drag on X-15 Vehicle at Low Speed Including the Effect of Flap Deflection. X-15 ; C_D vs. α ; $M = .056$; $\delta_f = 0^\circ$ and 40°

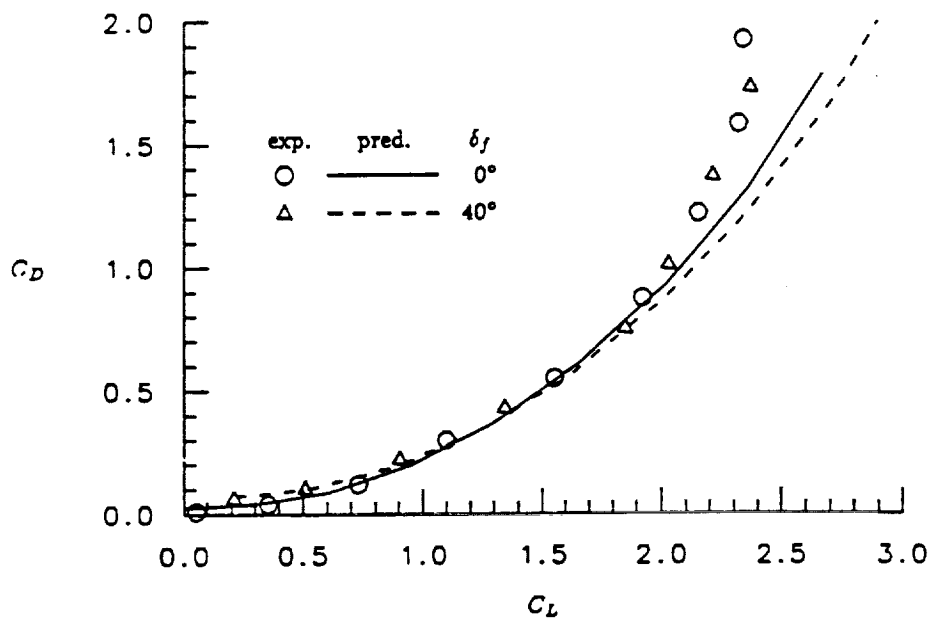


Fig. 6 Comparison Between Predicted and Experimentally Measured Drag as a Function of Lift on the X-15 Vehicle Including the Effect of Flap Deflection.
 X-15 ; C_D vs. C_L ; $M = .056$; $\delta_f = 0^\circ$ and 40°

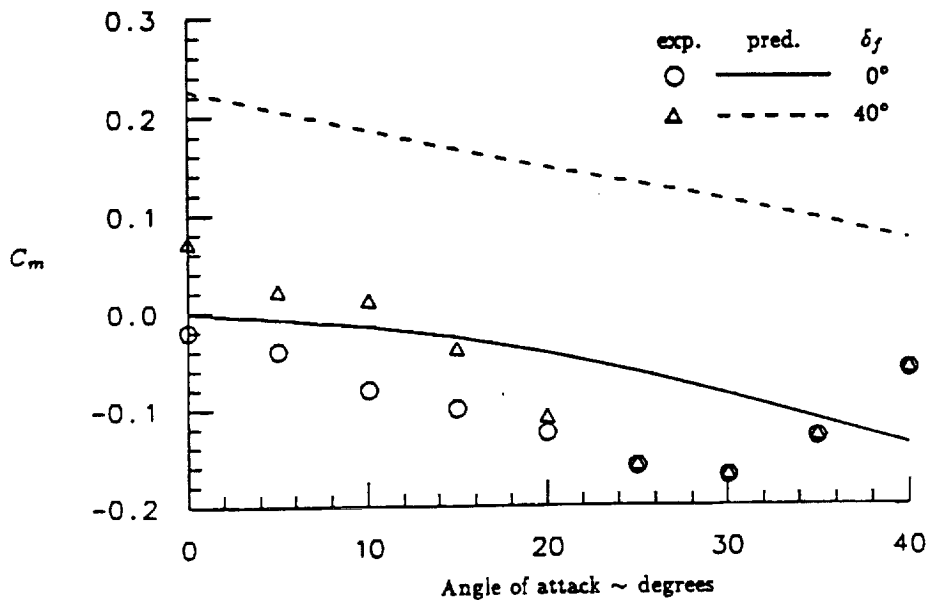


Fig. 7 Comparison Between Predicted and Experimentally Measured Moment on X-15 Vehicle at Low Speed Including the Effect of Flap Deflection.
 X-15 ; C_m vs. α ; $M = .056$; $\delta_f = 0^\circ$ and 40°

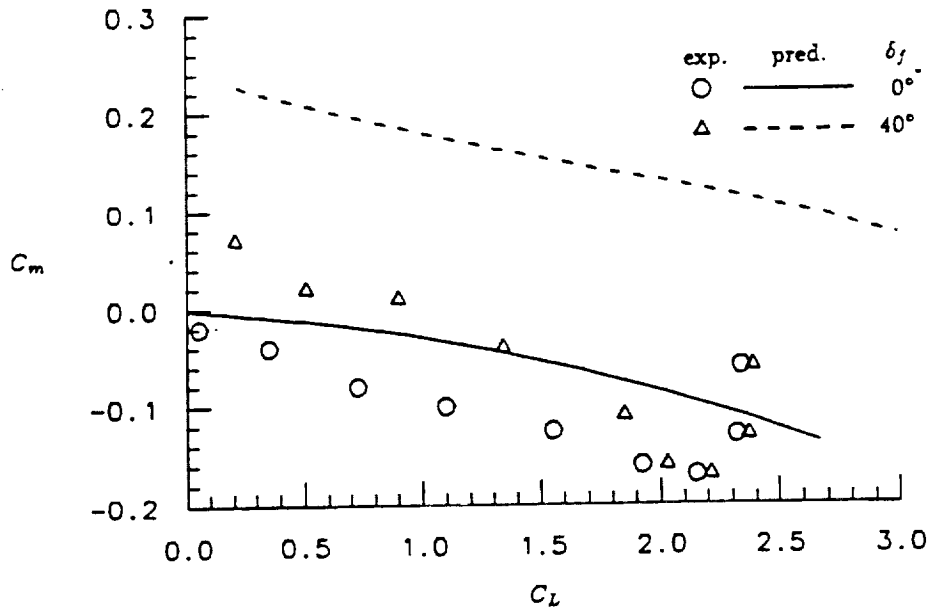


Fig. 8 Comparison Between Predicted and Experimentally Measured Moment as a Function of Lift on the X-15 Vehicle at Low Speed Including the Effect of Flap Deflection.
 X-15 ; C_m vs. C_L ; $M = .056$; $\delta_f = 0^\circ$ and 40°

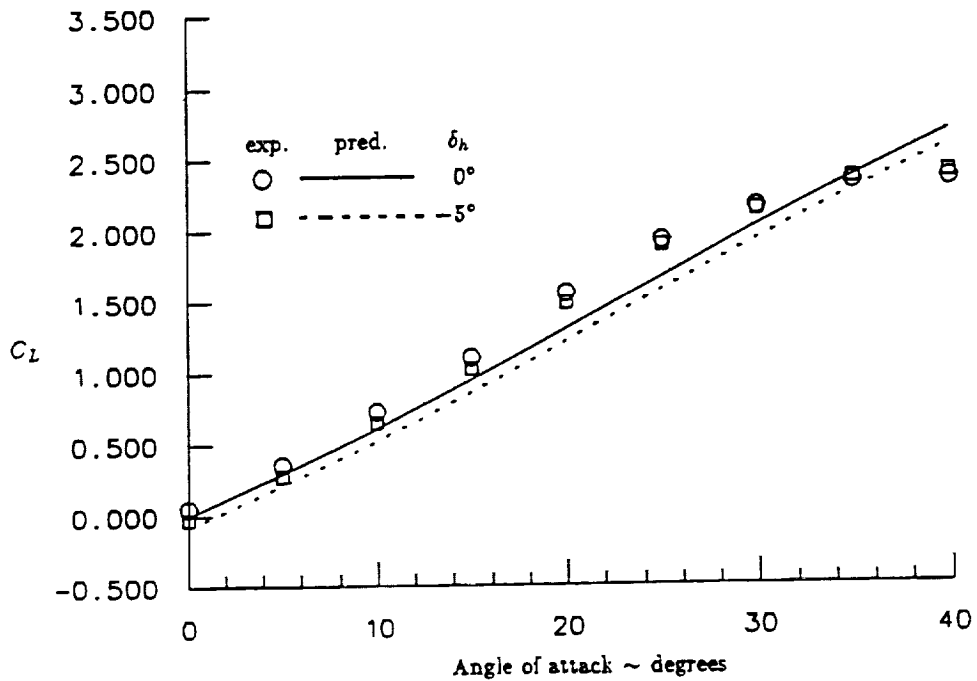


Fig. 9 Comparison Between Predicted and Experimentally Measured Lift on X-15 Vehicle at Low Speed Including the Effect of Horizontal Tail Deflection.
 X-15 ; C_L vs. α ; $M = .056$; $\delta_h = 0^\circ$ and -5°

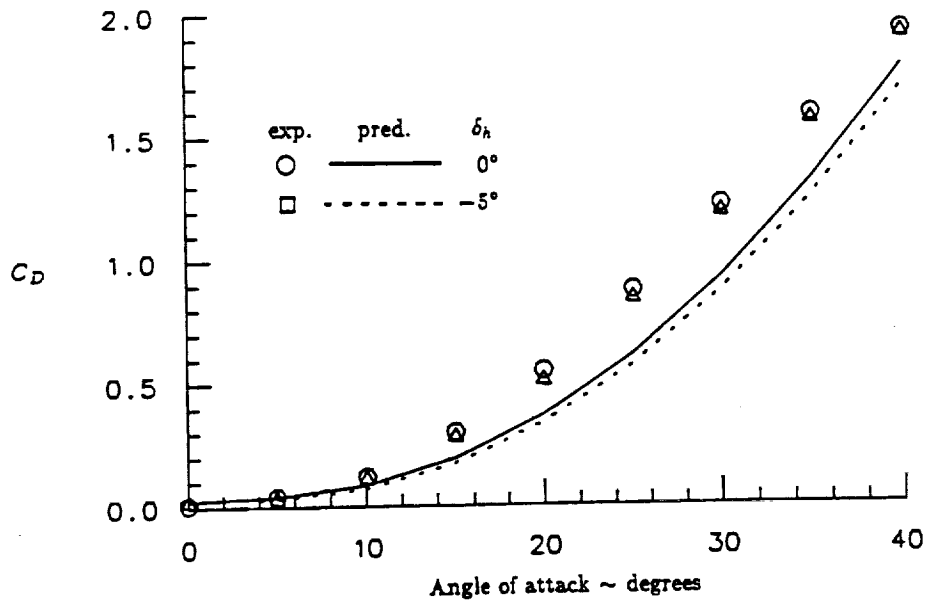


Fig. 10 Comparison Between Predicted and Experimentally Measured Drag on X-15 Vehicle at Low Speed Including the Effect of Horizontal Tail Deflection.
 X-15 ; C_D vs. α ; $M = .056$; $\delta_h = 0^\circ$ and -5°

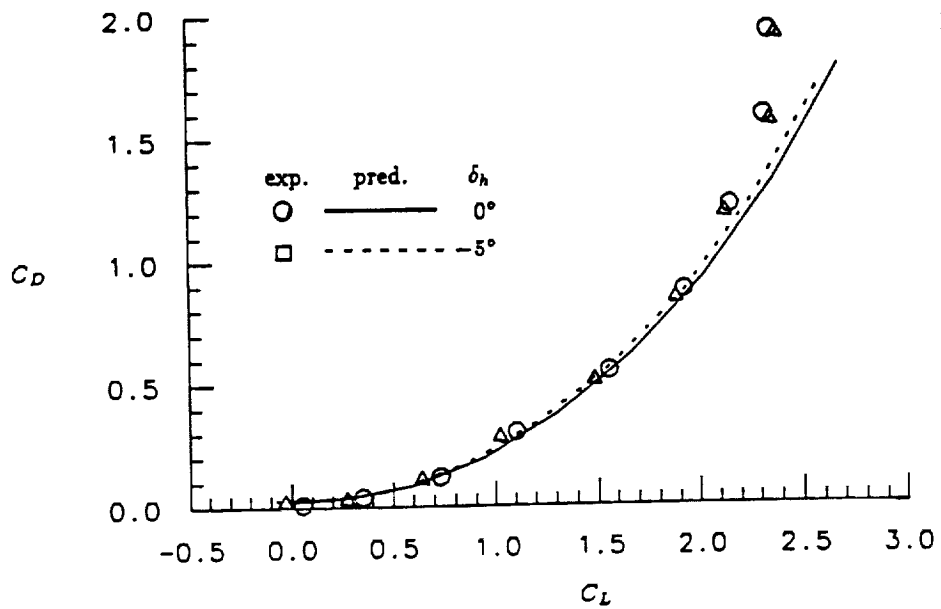


Fig. 11 Comparison Between Predicted and Experimentally Measured Drag as a Function of Lift on the X-15 Vehicle at Low Speed Including the Effect of Horizontal Tail Deflection.
 X-15 ; C_D vs. C_L ; $M = .056$; $\delta_h = 0^\circ$ and -5°

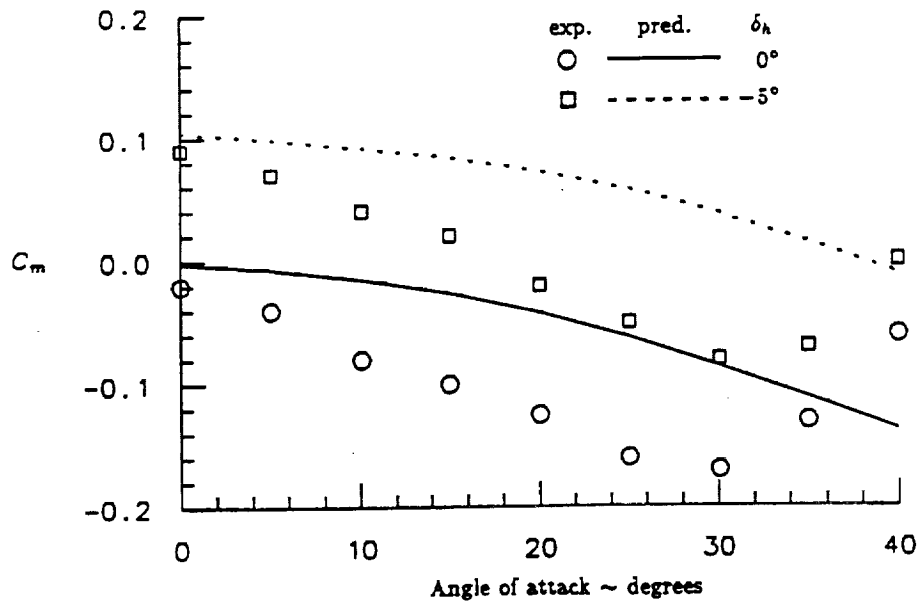


Fig. 12 Comparison Between Predicted and Experimentally Measured Moment on X-15 Vehicle at Low Speed Including the Effect of Horizontal Tail Deflection.
 X-15 ; C_m vs. α ; $M = .056$; $\delta_h = 0^\circ$ and -5°

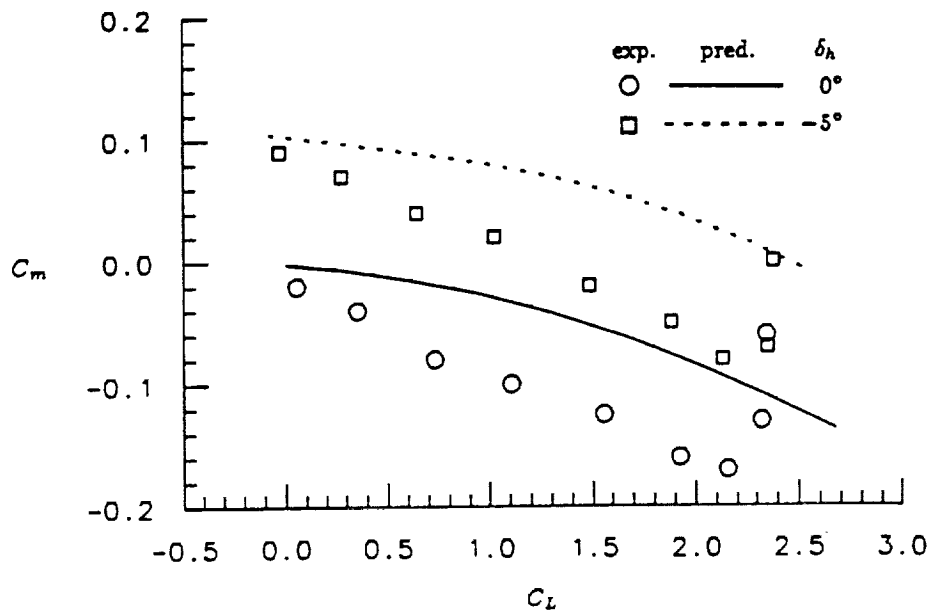


Fig. 13 Comparison Between Predicted and Experimentally Measured Drag as a Function of Lift on the X-15 Vehicle at Low Speed Including the Effect of Horizontal Tail Deflection.
 X-15 ; C_m vs. C_L ; $M = .056$; $\delta_h = 0^\circ$ and -5°

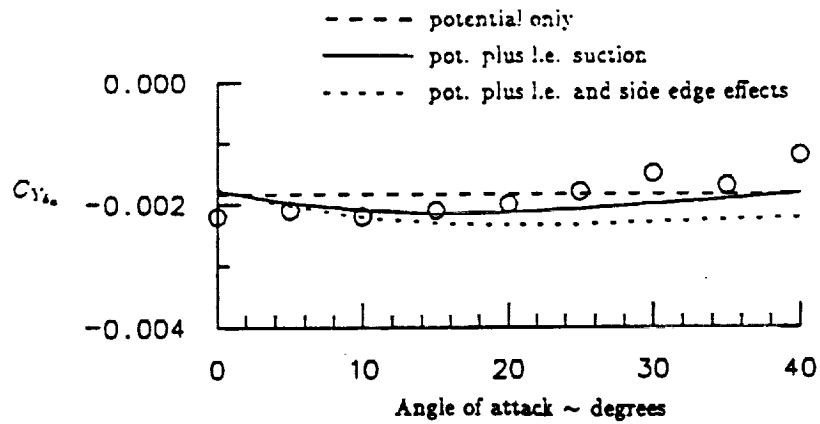


Fig. 14 Comparison Between Predicted and Experimentally Measured Side Force Due to Aileron Deflection on the X-15 Vehicle at Low Speed Including the Effect of Different Modelling Techniques.
 X-15 ; $C_{Y_{\delta_a}}$ vs. α ; $M = .056$

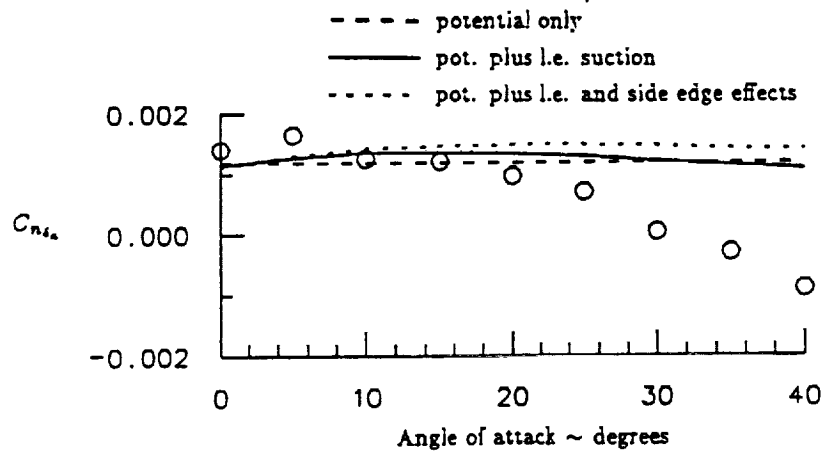


Fig. 15 Comparison Between Predicted and Experimentally Measured Yawing Moment Due to Aileron Deflection on the X-15 Vehicle at Low Speed Including the Effect of Different Modelling Techniques.
 X-15 ; $C_{n_{\delta_a}}$ vs. α ; $M = .056$

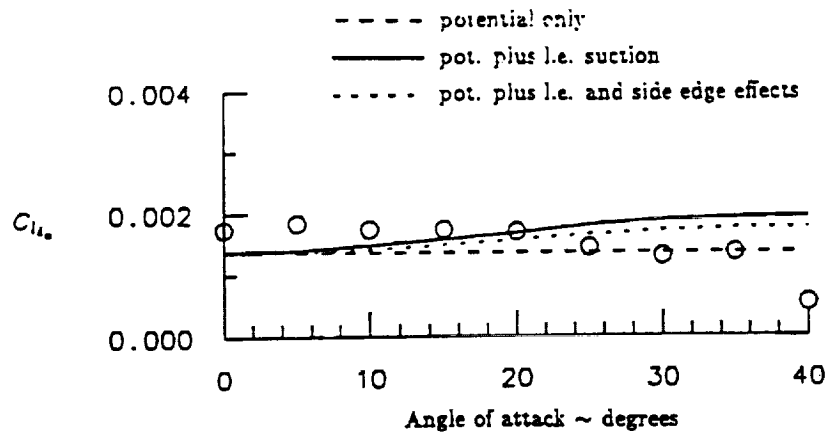


Fig. 16 Comparison Between Predicted and Experimentally Measured Rolling Moment Due to Aileron Deflection on the X-15 Vehicle at Low Speed Including the Effect of Different Modelling Techniques. X-15 ; $C_{l_{\delta_a}}$ vs. α ; $M = .056$

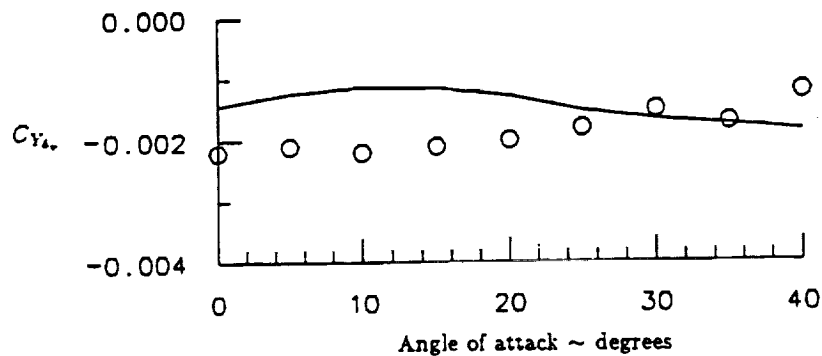


Fig. 17 Comparison Between Predicted and Experimentally Measured Side Force Due to Vertical Tail Deflection on the X-15 Vehicle at Low Speed. X-15 ; $C_{Y_{\delta_v}}$ vs. α ; $M = .056$

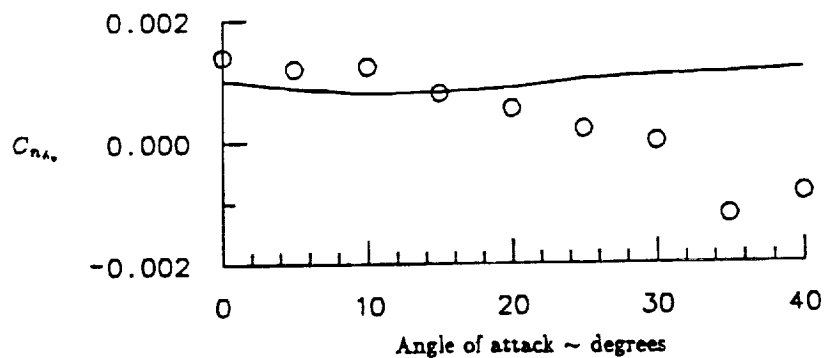


Fig. 18 Comparison Between Predicted and Experimentally Measured Yawing Moment Due to Vertical Tail Deflection on the X-15 Vehicle at Low Speed. X-15 ; $C_{n\delta_v}$ vs. α ; $M = .056$

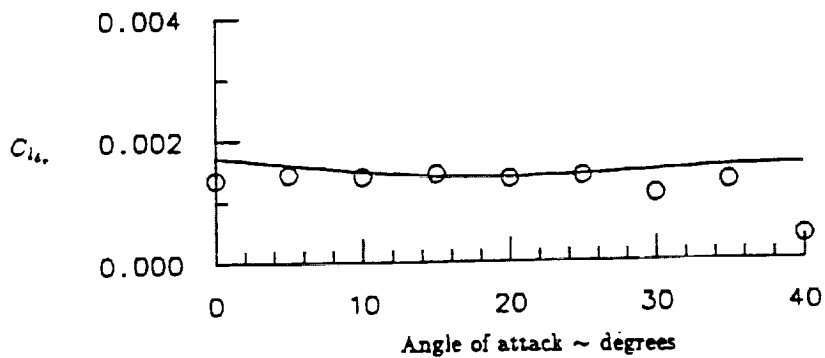


Fig. 19 Comparison Between Predicted and Experimentally Measured Rolling Moment Due to Vertical Tail Deflection on the X-15 Vehicle at Low Speed. X-15 ; $C_{l\delta_v}$ vs. α ; $M = .056$

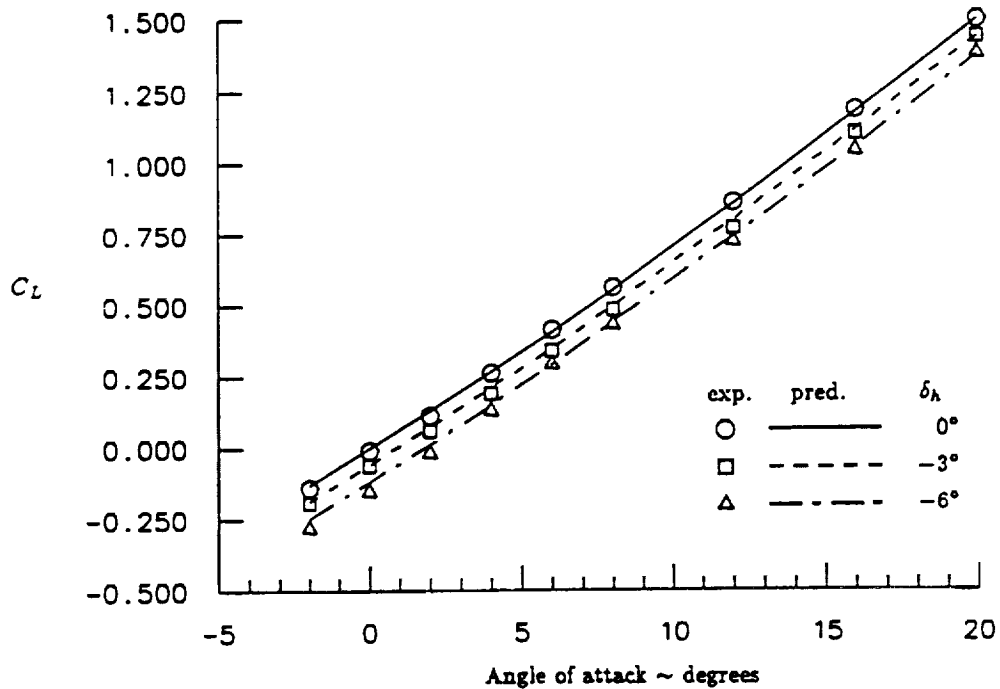


Fig. 20 Comparison Between Predicted and Experimentally Measured Lift on X-15 Vehicle at High Subsonic Speed Including the Effect of Horizontal Tail Deflection.
 X-15 ; C_L vs. α ; $M = 0.8$; $\delta_h = 0^\circ, -3^\circ, \text{ and } -6^\circ$

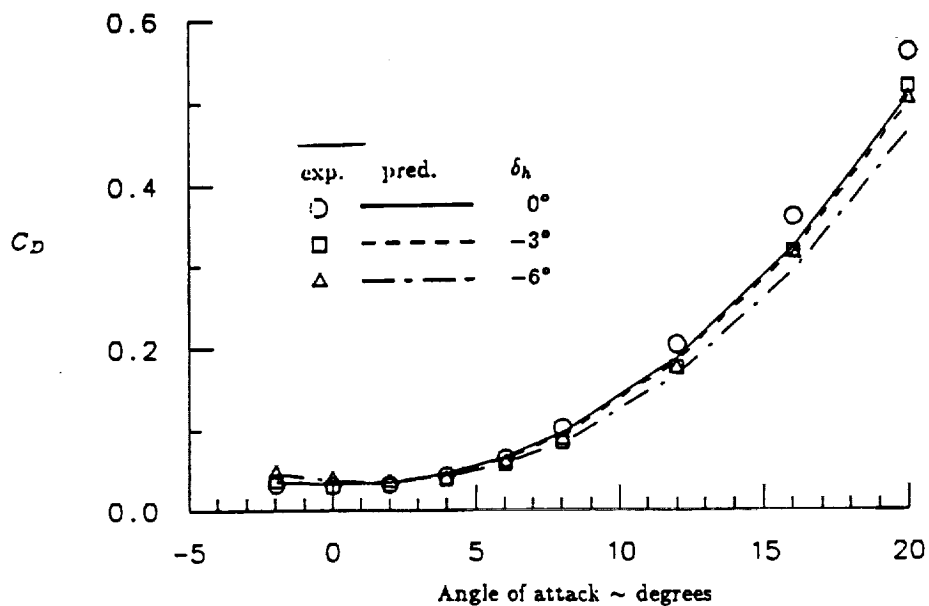


Fig. 21 Comparison Between Predicted and Experimentally Measured Drag on X-15 Vehicle at High Subsonic Speed Including the Effect of Horizontal Tail Deflection.
 X-15 ; C_D vs. α ; $M = 0.8$; $\delta_h = 0^\circ, -3^\circ, \text{ and } -6^\circ$

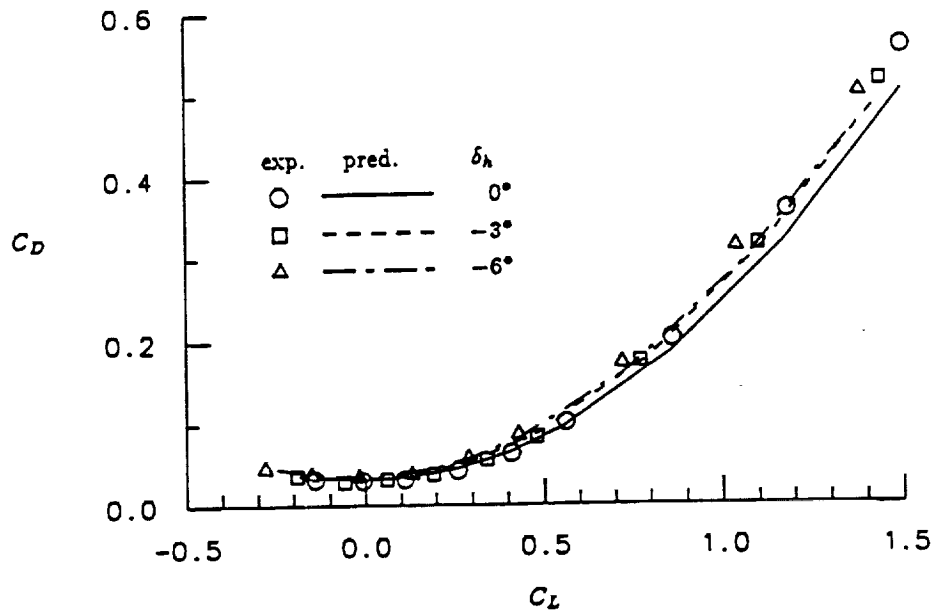


Fig. 22 Comparison Between Predicted and Experimentally Measured Drag as a Function of Lift on the X-15 Vehicle at High Subsonic Speed Including the Effect of Horizontal Tail Deflection. X-15 ; C_D vs. C_L ; $M = 0.8$; $\delta_h = 0^\circ, -3^\circ, \text{ and } -6^\circ$

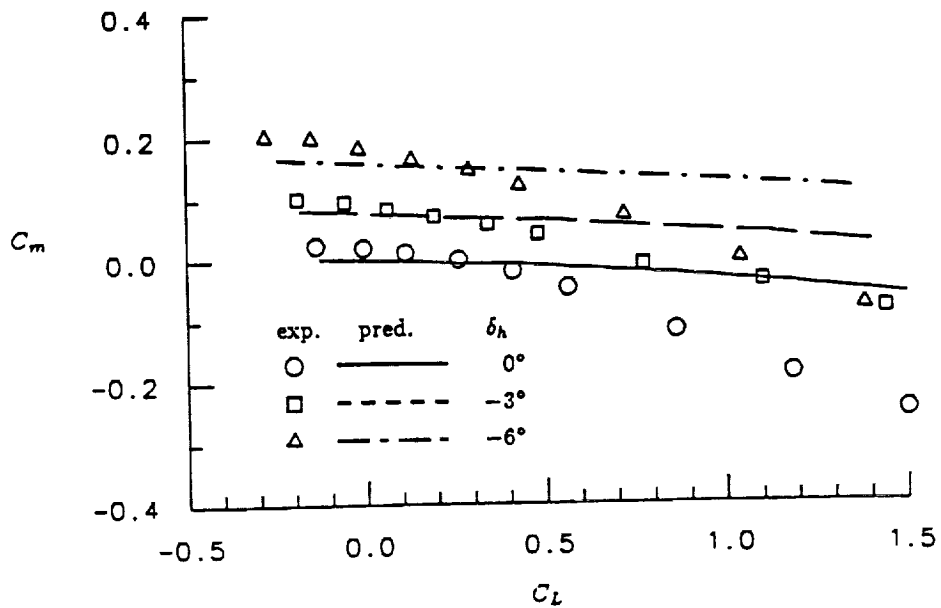


Fig. 23 Comparison Between Predicted and Experimentally Measured Moment as a Function of Lift on the X-15 Vehicle at High Subsonic Speed Including the Effect of Horizontal Tail Deflection. X-15 ; C_m vs. C_L ; $M = 0.8$; $\delta_h = 0^\circ, -3^\circ, \text{ and } -6^\circ$

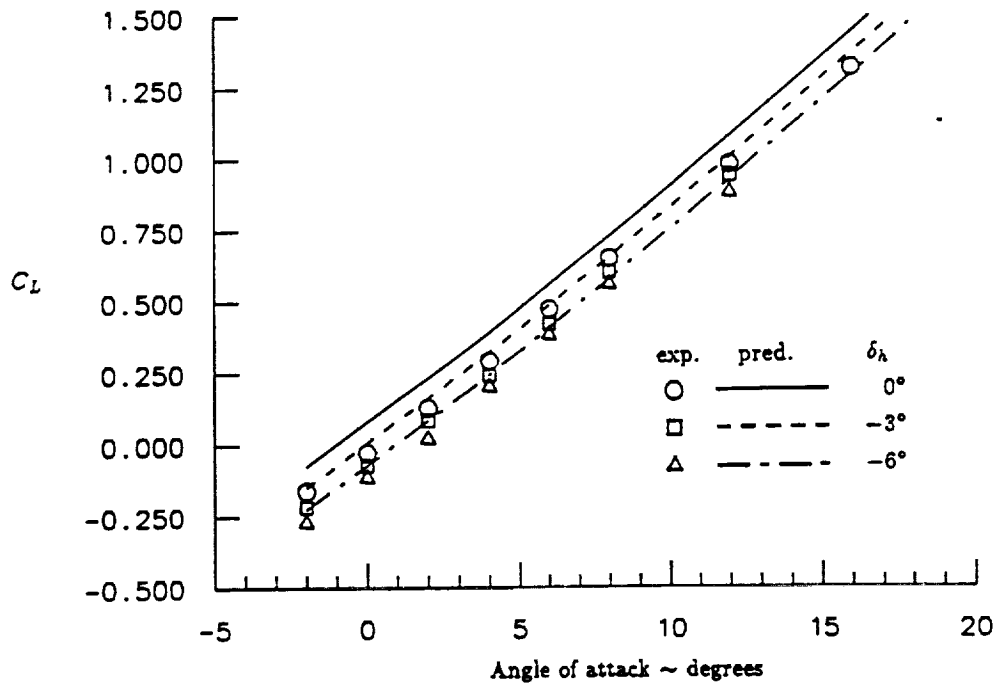


Fig. 24 Comparison Between Predicted and Experimentally Measured Lift on X-15 Vehicle at Transonic Speed Including the Effect of Horizontal Tail Deflection.
 X-15 ; C_L vs. α ; $M = 1.03$; $\delta_h = 0^\circ, -3^\circ, \text{ and } -6^\circ$

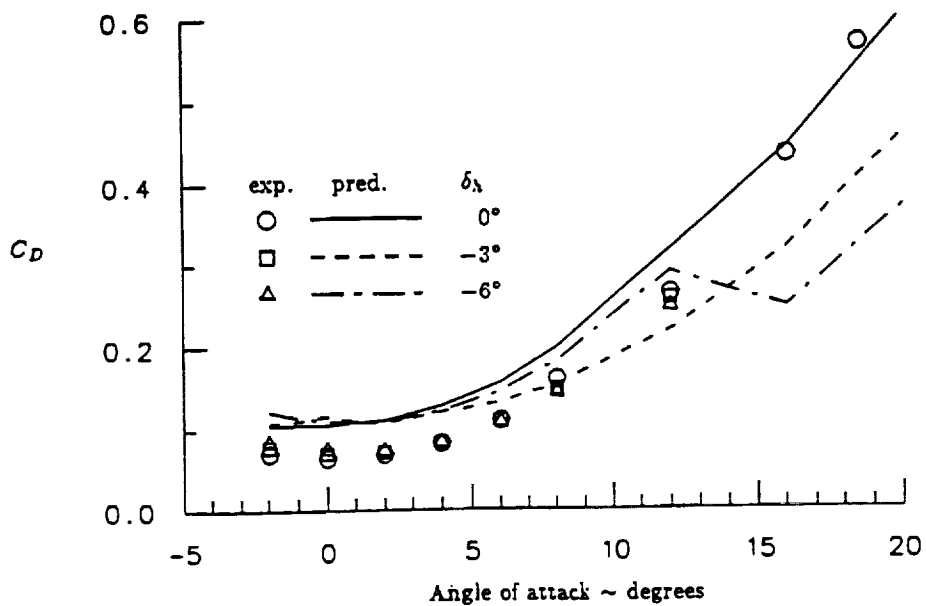


Fig. 25 Comparison Between Predicted and Experimentally Measured Drag on X-15 Vehicle at Transonic Speed Including the Effect of Horizontal Tail Deflection.
 X-15 ; C_D vs. α ; $M = 1.03$; $\delta_h = 0^\circ, -3^\circ, \text{ and } -6^\circ$

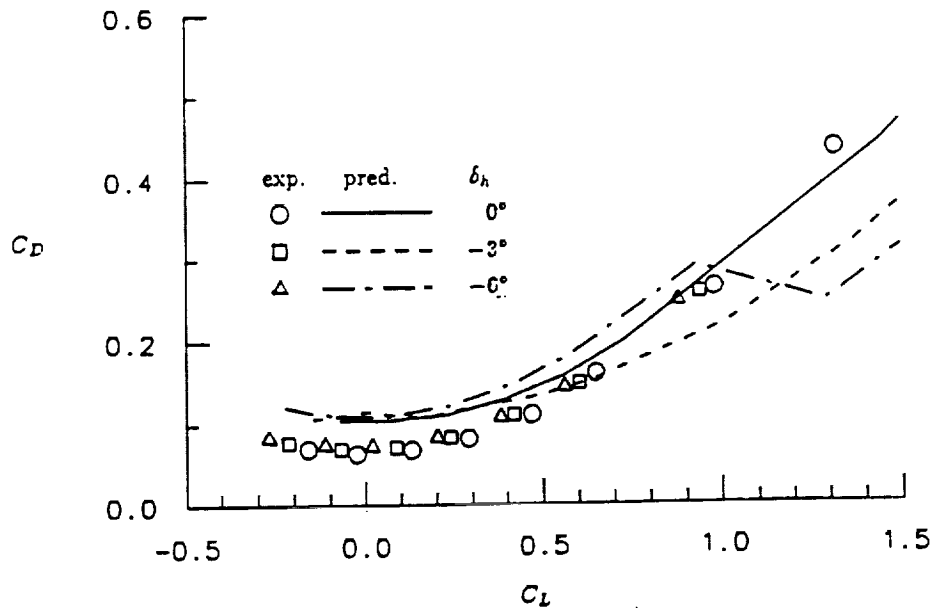


Fig. 26 Comparison Between Predicted and Experimentally Measured Drag as a Function of Lift on the X-15 Vehicle at Transonic Speed Including the Effect of Horizontal Tail Deflection.
 X-15 ; C_D vs. C_L ; $M = 1.03$; $\delta_h = 0^\circ, -3^\circ, \text{ and } -6^\circ$

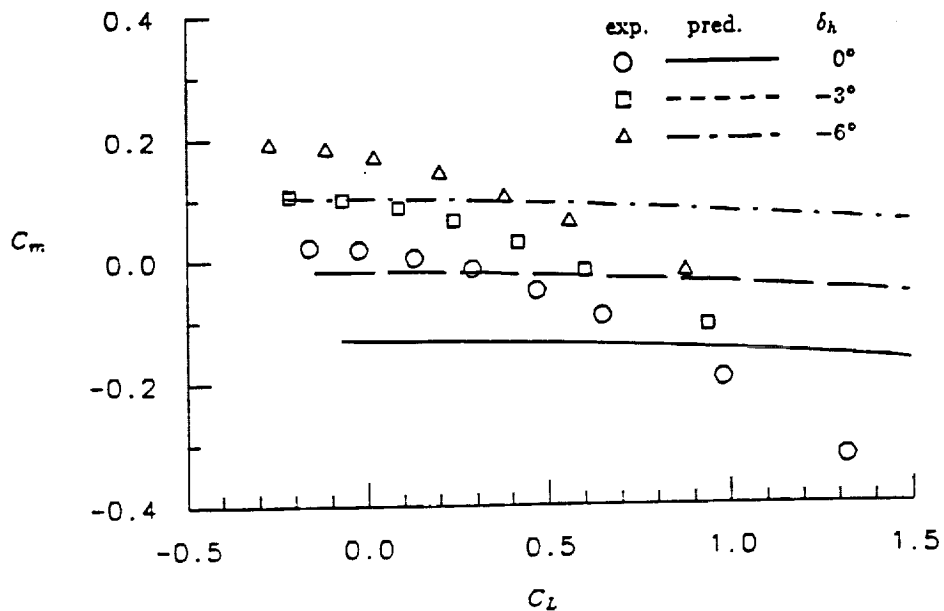


Fig. 27 Comparison Between Predicted and Experimentally Measured Moment as a Function of Lift on the X-15 Vehicle at Transonic Speed Including the Effect of Horizontal Tail Deflection.
 X-15 ; C_m vs. C_L ; $M = 1.03$; $\delta_h = 0^\circ, -3^\circ, \text{ and } -6^\circ$

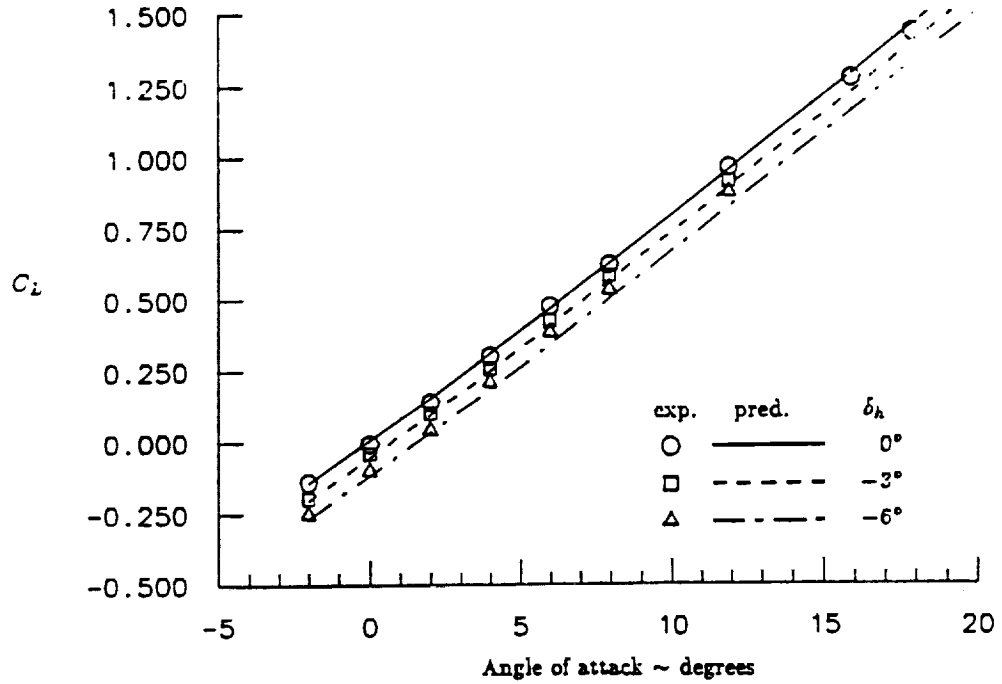


Fig. 28 Comparison Between Predicted and Experimentally Measured Lift on X-15 Vehicle at High Transonic Speed Including the Effect of Horizontal Tail Deflection.
 X-15 ; C_L vs. α ; $M = 1.18$; $\delta_h = 0^\circ, -3^\circ, \text{ and } -6^\circ$

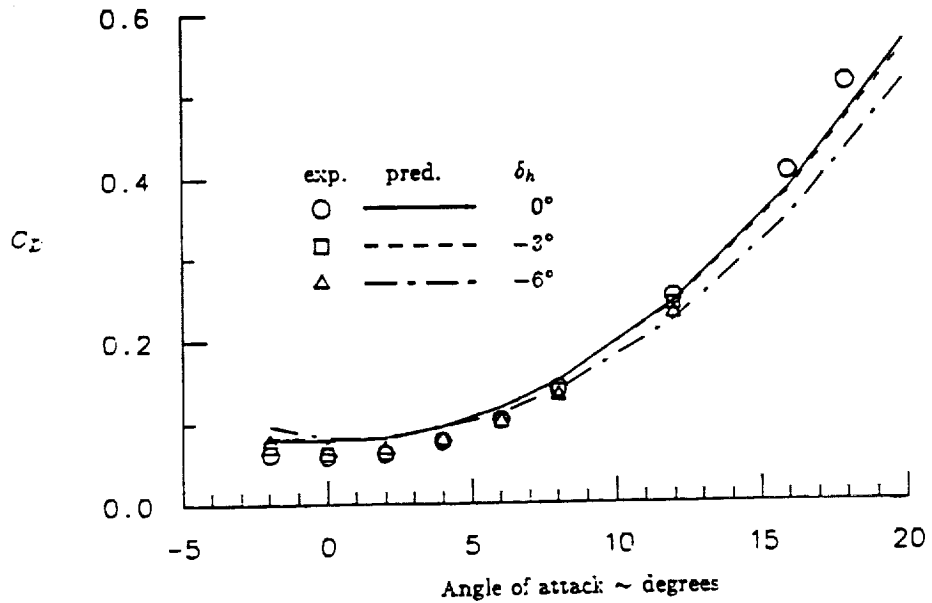


Fig. 29 Comparison Between Predicted and Experimentally Measured Drag on X-15 Vehicle at High Transonic Speed Including the Effect of Horizontal Tail Deflection.
 X-15 ; C_D vs. α ; $M = 1.18$; $\delta_h = 0^\circ, -3^\circ, \text{ and } -6^\circ$

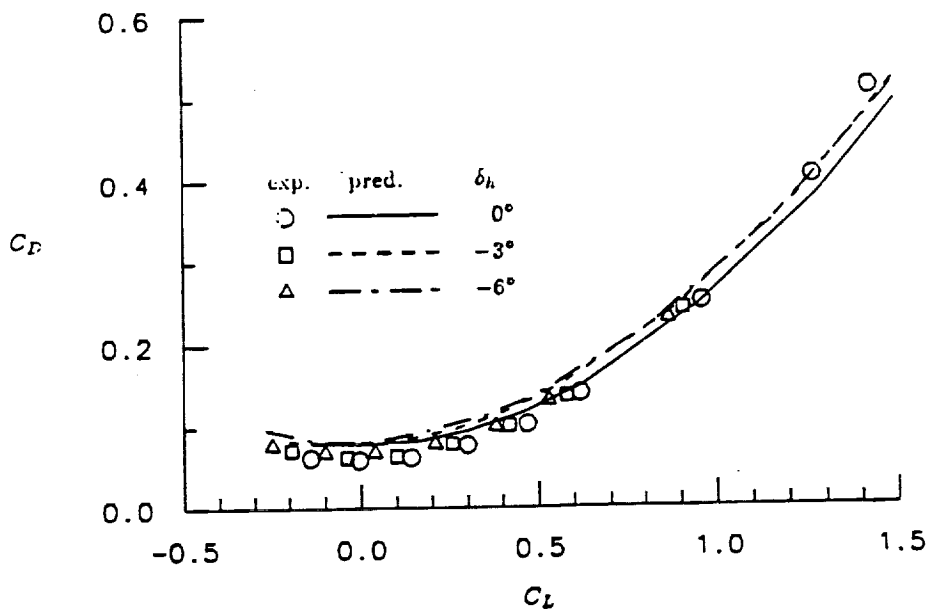


Fig. 30 Comparison Between Predicted and Experimentally Measured Drag as a Function of Lift on the X-15 Vehicle at High Transonic Speed Including the Effect of Horizontal Tail Deflection.
 X-15 ; C_D vs. C_L ; $M = 1.18$; $\delta_h = 0^\circ, -3^\circ, \text{ and } -6^\circ$

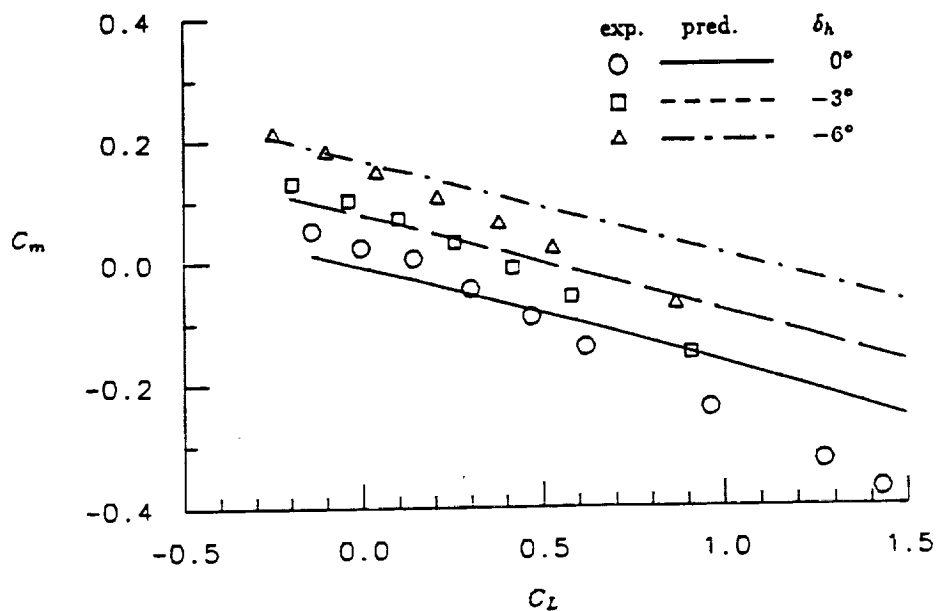


Fig. 31 Comparison Between Predicted and Experimentally Measured Moment as a Function of Lift on the X-15 Vehicle at High Transonic Speed Including the Effect of Horizontal Tail Deflection.
 X-15 ; C_m vs. C_L ; $M = 1.18$; $\delta_h = 0^\circ, -3^\circ, \text{ and } -6^\circ$

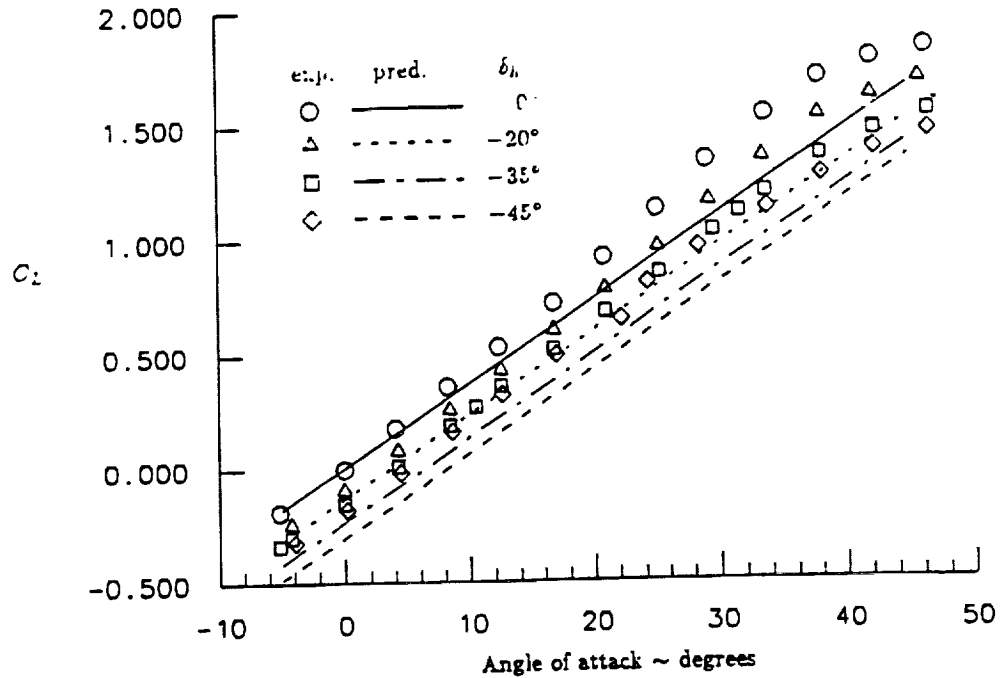


Fig. 32 Comparison Between Predicted and Experimentally Measured Lift on X-15 Vehicle at Supersonic Speed Including the Effect of Horizontal Tail Deflection.
 X-15 ; C_L vs. α ; $M = 2.96$; $\delta_h = 0^\circ, -20^\circ, -35^\circ, \text{ and } -45^\circ$

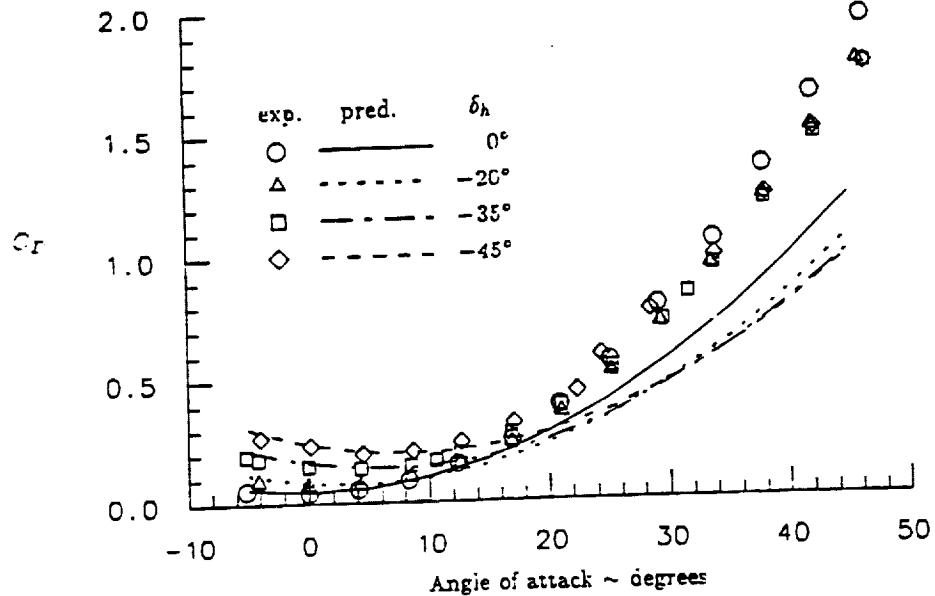


Fig. 33 Comparison Between Predicted and Experimentally Measured Drag on X-15 Vehicle at Supersonic Speed Including the Effect of Horizontal Tail Deflection.
 X-15 ; C_D vs. α ; $M = 2.96$; $\delta_h = 0^\circ, -20^\circ, -35^\circ, \text{ and } -45^\circ$

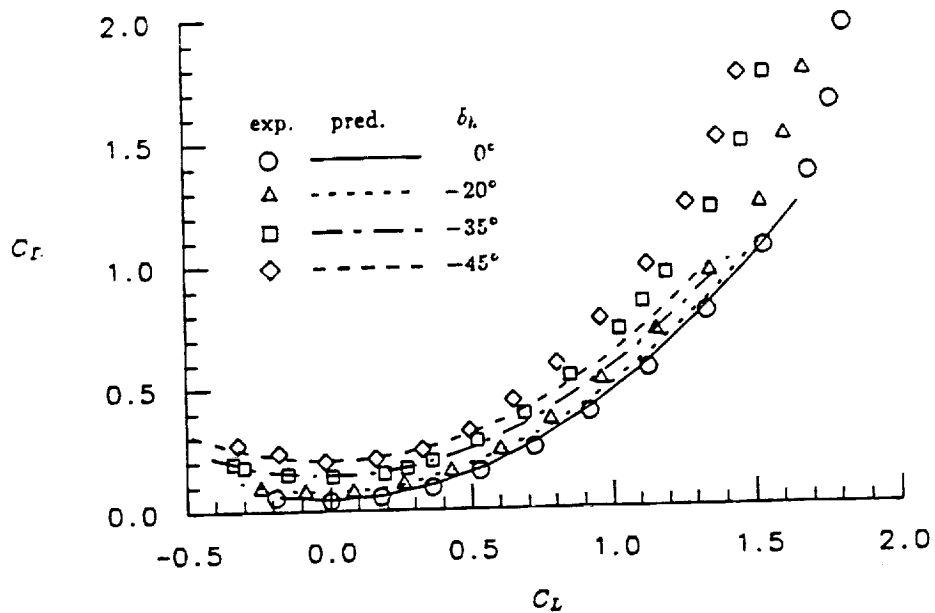


Fig. 34 Comparison Between Predicted and Experimentally Measured Drag as a Function of Lift on the X-15 Vehicle at Supersonic Speed Including the Effect of Horizontal Tail Deflection.
 X-15 ; C_D vs. C_L ; $M = 2.96$; $\delta_h = 0^\circ, -20^\circ, -35^\circ, \text{ and } -45^\circ$

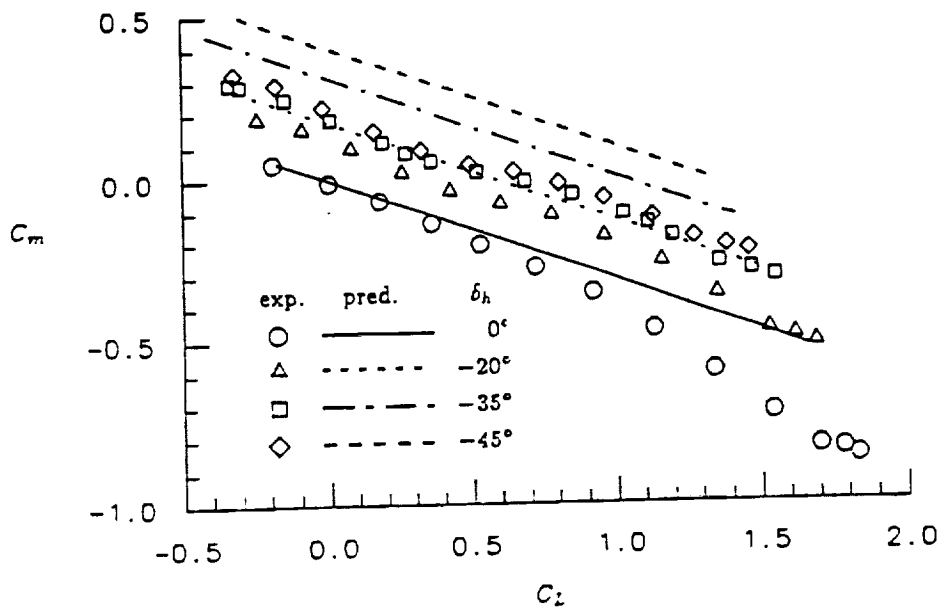


Fig. 35 Comparison Between Predicted and Experimentally Measured Moment as a Function of Lift on the X-15 Vehicle at Supersonic Speed Including the Effect of Horizontal Tail Deflection.
 X-15 ; C_m vs. C_L ; $M = 2.96$; $\delta_h = 0^\circ, -20^\circ, -35^\circ, \text{ and } -45^\circ$

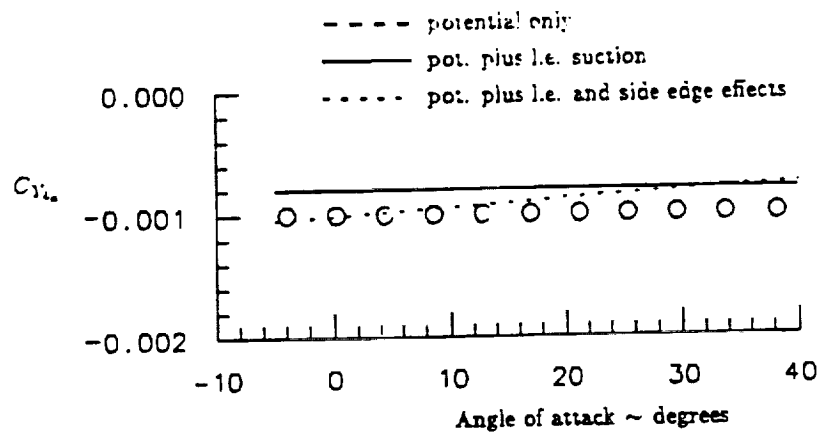


Fig. 36 Comparison Between Predicted and Experimentally Measured Side Force Due to Aileron Deflection on the X-15 Vehicle at Supersonic Speed Including the Effect of Different Modelling Techniques.
 X-15 ; $C_{Y_{\delta a}}$ vs. α ; $M = 2.96$

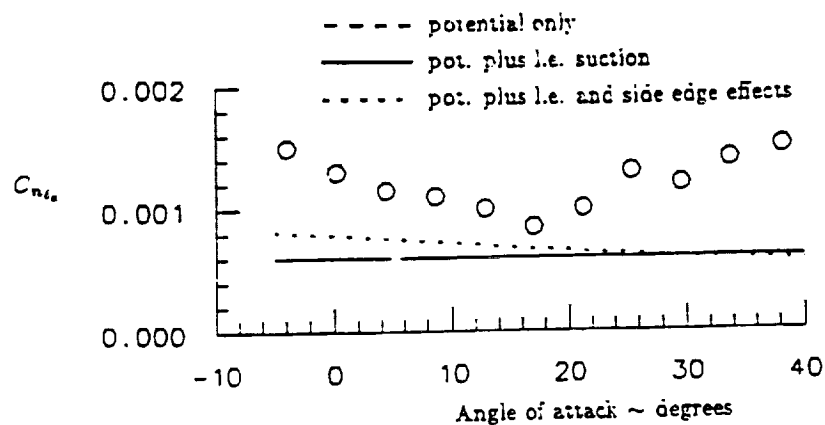


Fig. 37 Comparison Between Predicted and Experimentally Measured Yawing Moment Due to Aileron Deflection on the X-15 Vehicle at Supersonic Speed Including the Effect of Different Modelling Techniques.
 X-15 ; $C_{n_{\delta a}}$ vs. α ; $M = 2.96$

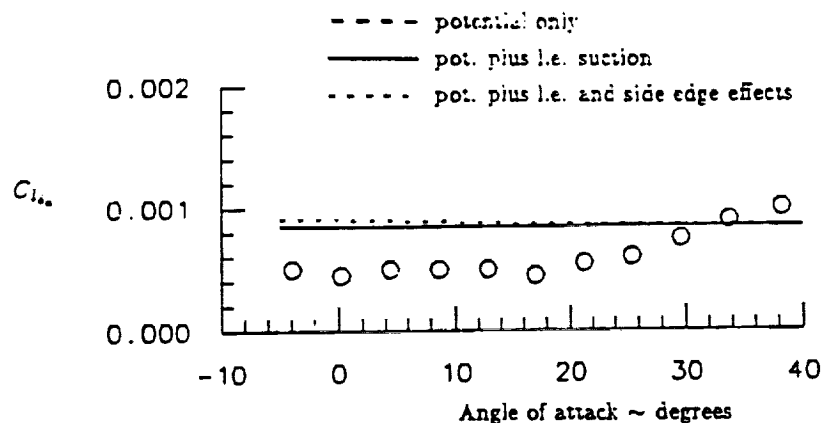


Fig. 38 Comparison Between Predicted and Experimentally Measured Rolling Moment Due to Aileron Deflection on the X-15 Vehicle at Supersonic Speed Including the Effect of Different Modelling Techniques.
 X-15 ; $C_{l_{\delta_a}}$ vs. α ; $M = 2.96$

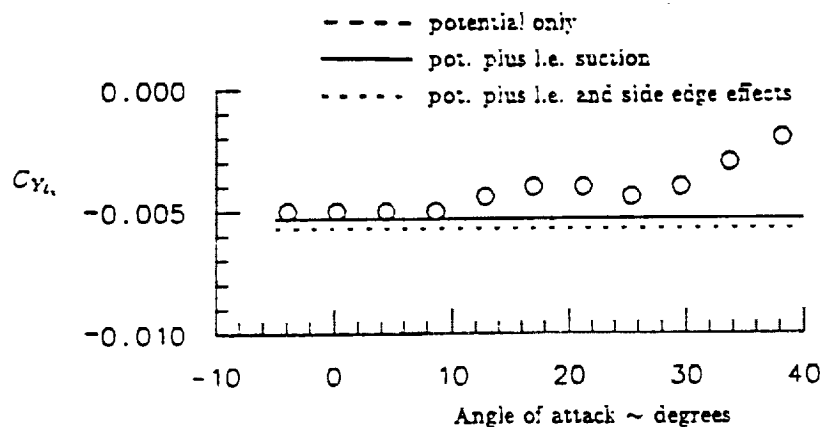


Fig. 39 Comparison Between Predicted and Experimentally Measured Side Force Due to Vertical Tail Deflection on the X-15 Vehicle at Supersonic Speed Including the Effect of Different Modelling Techniques.
 X-15 ; $C_{Y_{\delta_v}}$ vs. α ; $M = 2.96$

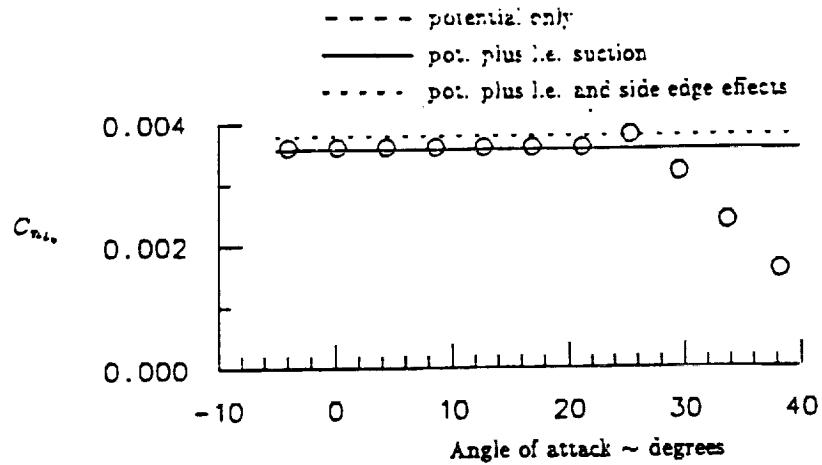


Fig. 40 Comparison Between Predicted and Experimentally Measured Yawing Moment Due to Vertical Tail Deflection on the X-15 Vehicle at Supersonic Speed Including the Effect of Different Modelling Techniques.
 X-15 ; $C_{n_{\dot{\alpha}}}$ vs. α ; $M = 2.96$

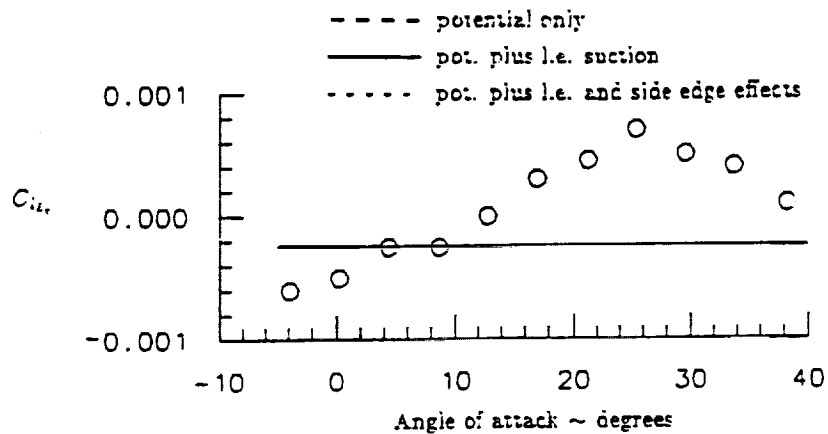


Fig. 41 Comparison Between Predicted and Experimentally Measured Rolling Moment Due to Vertical Tail Deflection on the X-15 Vehicle at Supersonic Speed Including the Effect of Different Modelling Techniques.
 X-15 ; $C_{l_{\dot{\alpha}}}$ vs. α ; $M = 2.96$

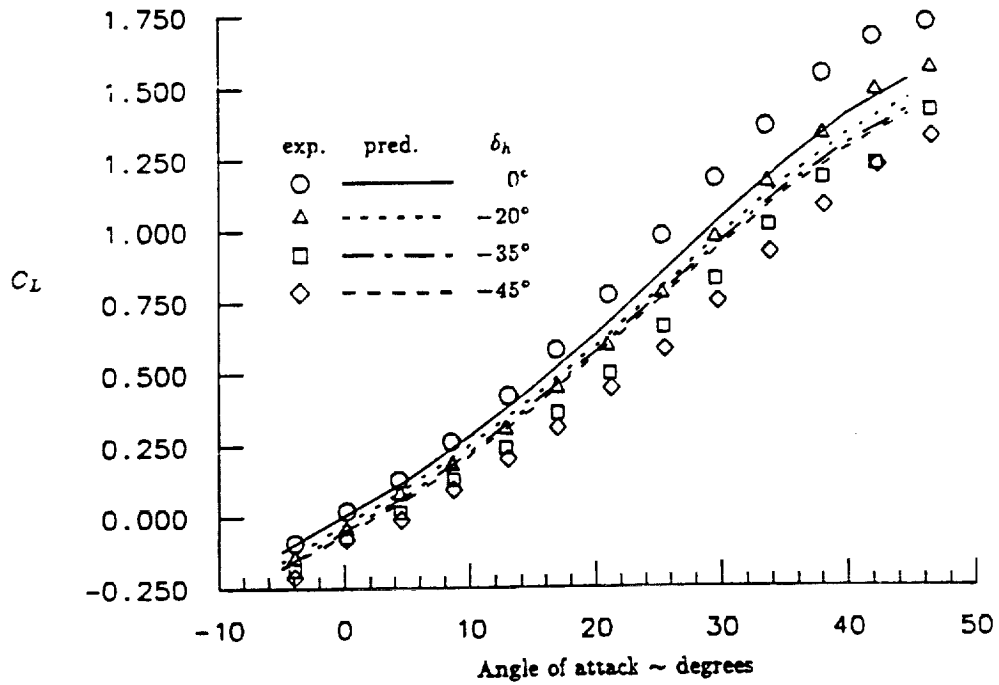


Fig. 42 Comparison Between Predicted and Experimentally Measured Lift on X-15 Vehicle at High Supersonic Speed Including the Effect of Horizontal Tail Deflection.
X-15 ; C_L vs. α ; $M = 4.65$

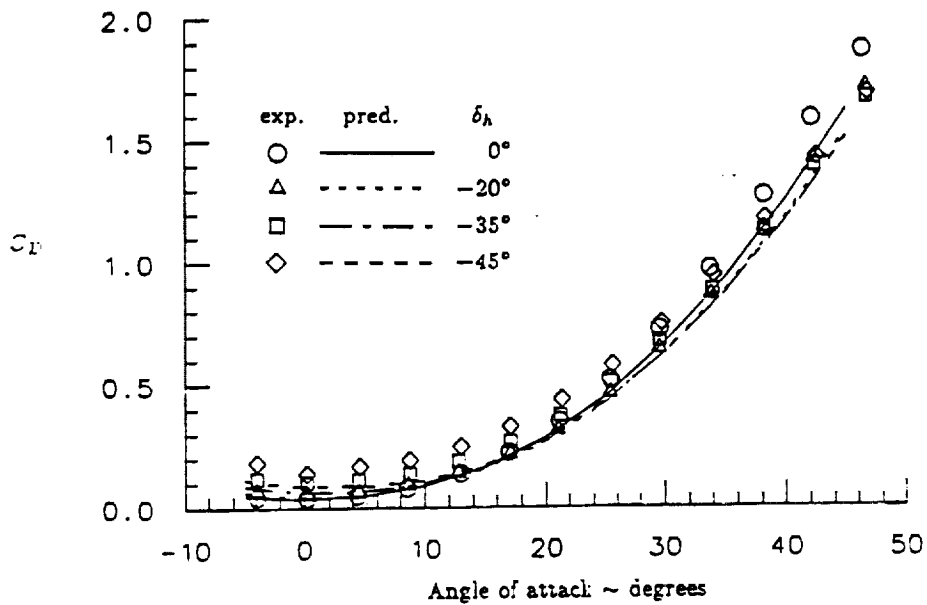


Fig. 43 Comparison Between Predicted and Experimentally Measured Drag on X-15 Vehicle at High Supersonic Speed Including the Effect of Horizontal Tail Deflection.
X-15 ; C_D vs. α ; $M = 4.65$

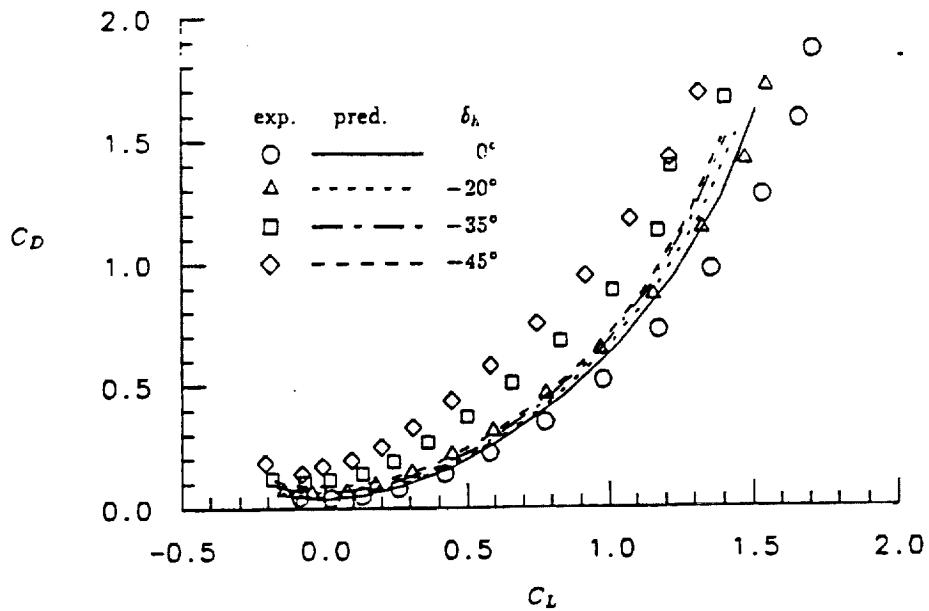


Fig. 44 Comparison Between Predicted and Experimentally Measured Drag as a Function of Lift on the X-15 Vehicle at High Supersonic Speed Including the Effect of Horizontal Tail Deflection.
 X-15 ; C_D vs. C_L ; $M = 4.65$

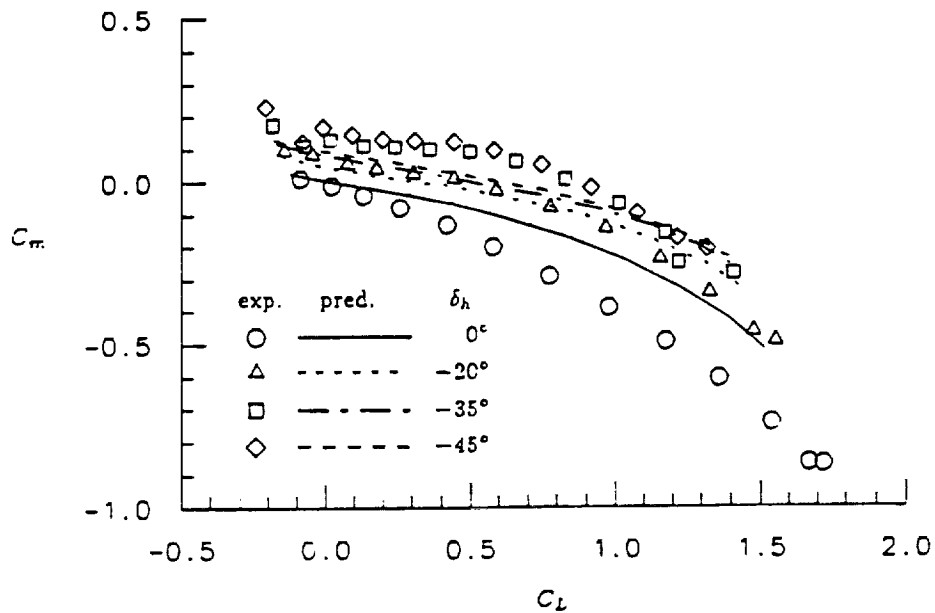


Fig. 45 Comparison Between Predicted and Experimentally Measured Moment as a Function of Lift on the X-15 Vehicle at High Supersonic Speed Including the Effect of Horizontal Tail Deflection.
 X-15 ; C_m vs. C_L ; $M = 4.65$

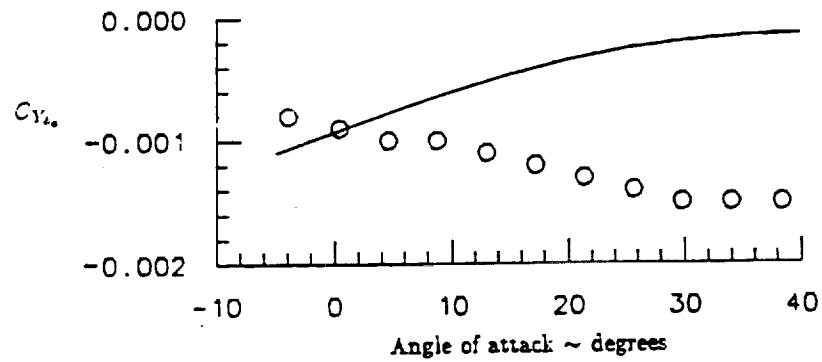


Fig. 46 Comparison Between Predicted and Experimentally Measured Side Force Due to Aileron Deflection on the X-15 Vehicle at High Supersonic Speed. X-15 ; $C_{Y_{\delta_a}}$ vs. α ; $M = 4.65$

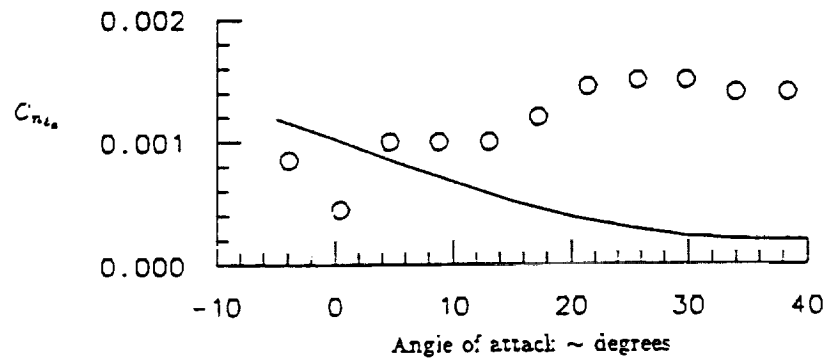


Fig. 47 Comparison Between Predicted and Experimentally Measured Yawing Moment Due to Aileron Deflection on the X-15 Vehicle at High Supersonic Speed. X-15 ; $C_{n_{\delta_a}}$ vs. α ; $M = 4.65$

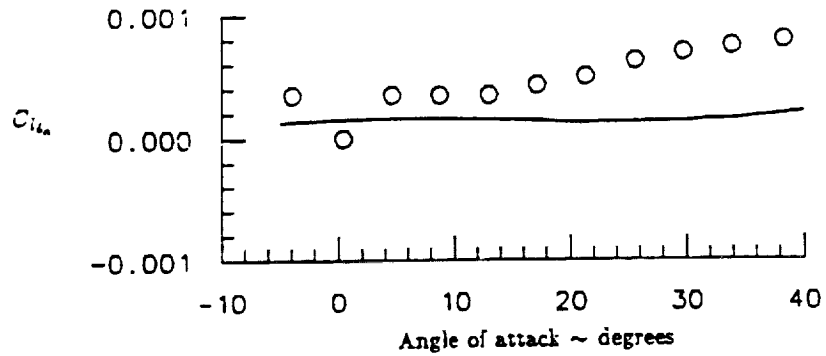


Fig. 48 Comparison Between Predicted and Experimentally Measured Rolling Moment Due to Aileron Deflection on the X-15 Vehicle at High Supersonic Speed.
 X-15 ; $C_{l_{\delta_a}}$ vs. α ; $M = 4.65$

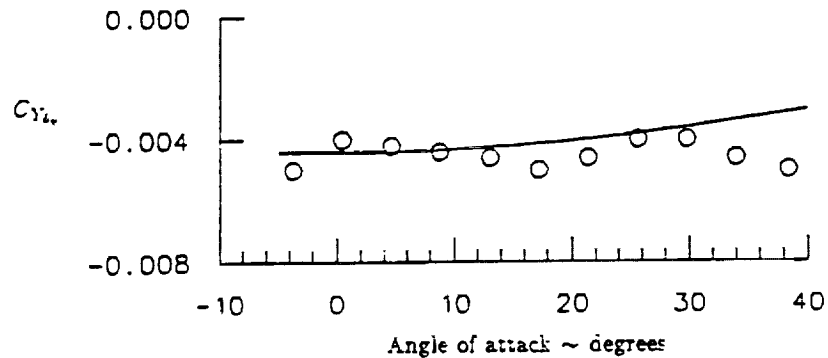


Fig. 49 Comparison Between Predicted and Experimentally Measured Side Force Due to Vertical Tail Deflection on the X-15 Vehicle at High Supersonic Speed.
 X-15 ; $C_{Y_{\delta_v}}$ vs. α ; $M = 4.65$

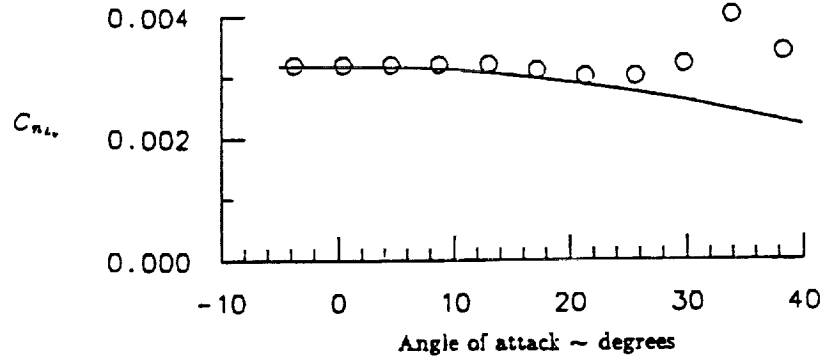


Fig. 50 Comparison Between Predicted and Experimentally Measured Yawing Moment Due to Vertical Tail Deflection on the X-15 Vehicle at High Supersonic Speed.
 X-15 ; C_{n1v} vs. α ; $M = 4.65$

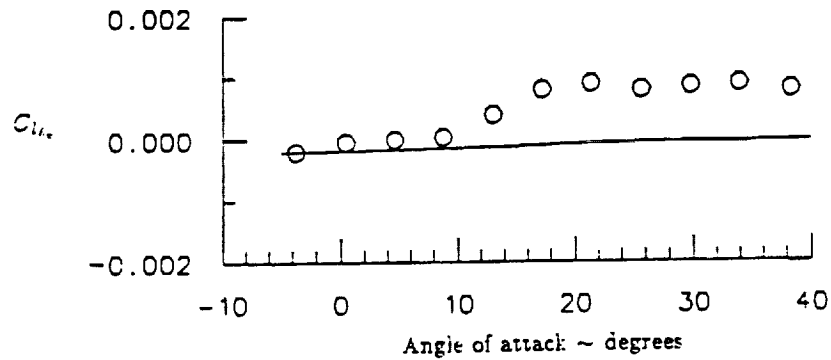


Fig. 51 Comparison Between Predicted and Experimentally Measured Rolling Moment Due to Vertical Tail Deflection on the X-15 Vehicle at High Supersonic Speed.
 X-15 ; C_{l1v} vs. α ; $M = 4.65$

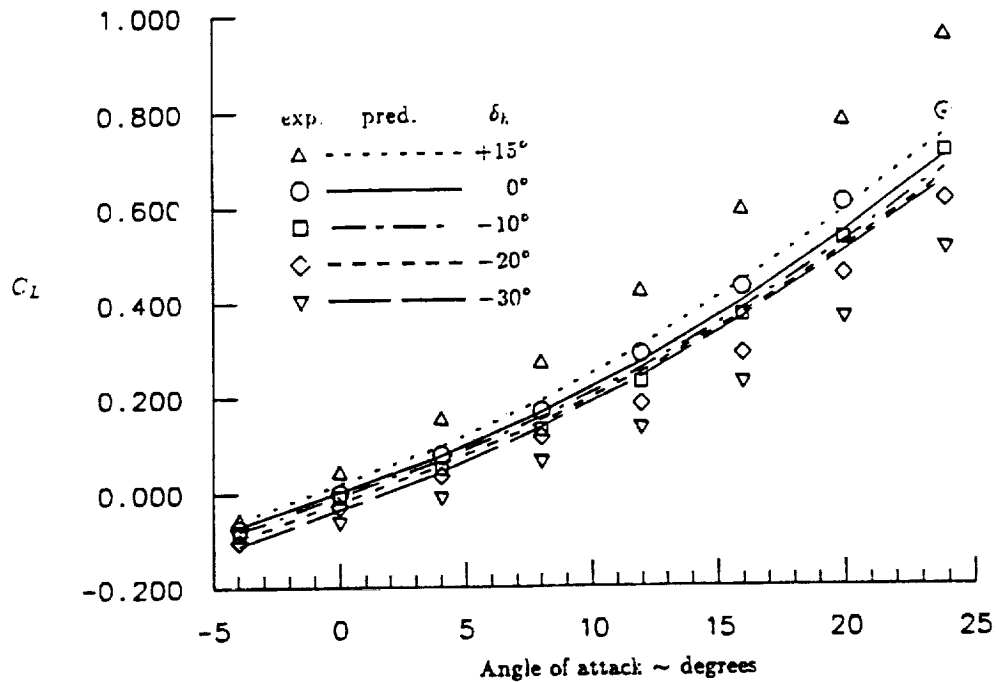


Fig. 52 Comparison Between Predicted and Experimentally Measured Lift on X-15 Vehicle at Hypersonic Speed Including the Effect of Horizontal Tail Deflection.
 X-15 ; C_L vs. α ; $M = 6.83$

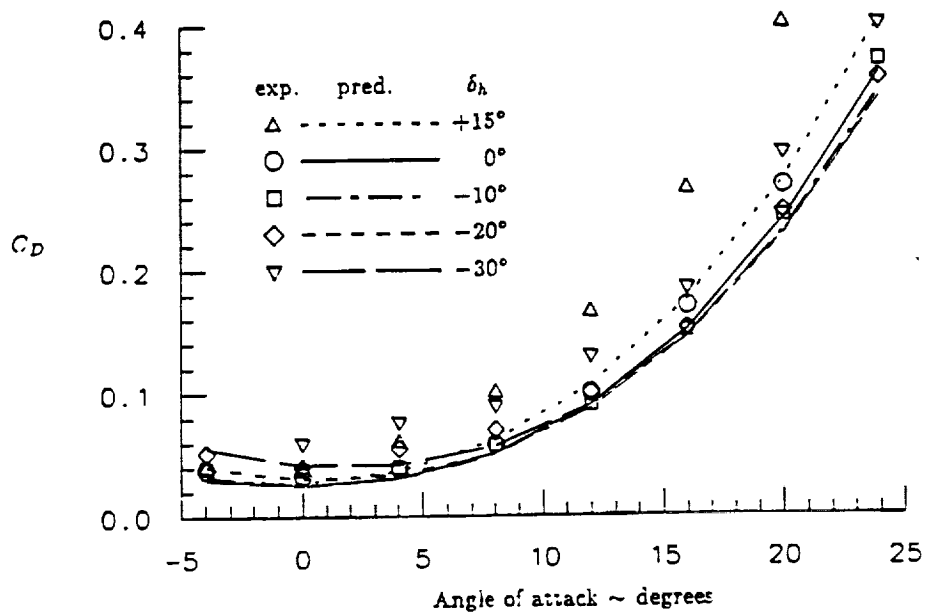


Fig. 53 Comparison Between Predicted and Experimentally Measured Drag on X-15 Vehicle at Hypersonic Speed Including the Effect of Horizontal Tail Deflection.
 X-15 ; C_D vs. α ; $M = 6.83$

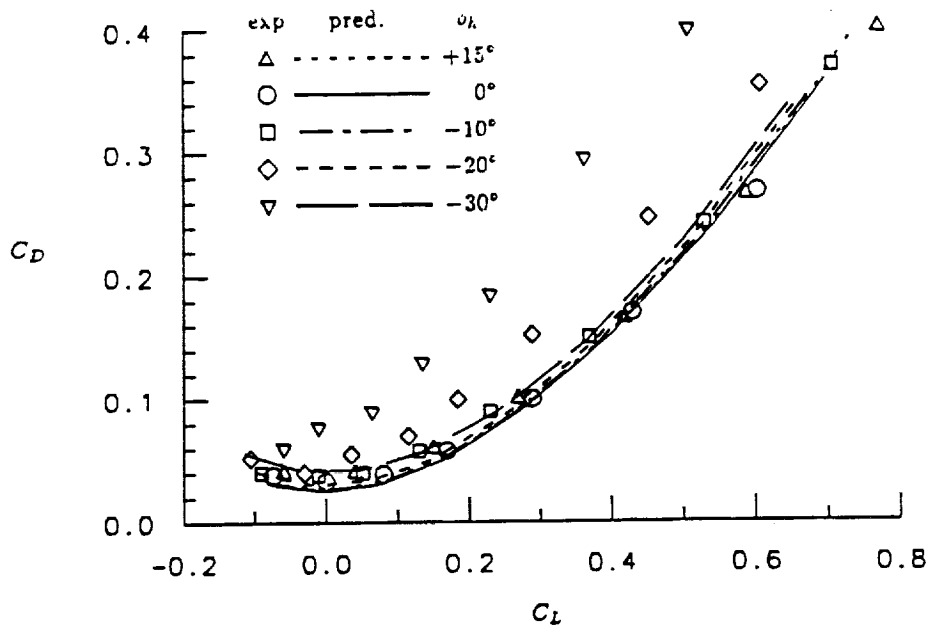


Fig. 54 Comparison Between Predicted and Experimentally Measured Drag as a Function of Lift on the X-15 Vehicle at Hypersonic Speed Including the Effect of Horizontal Tail Deflection.
 X-15 ; C_D vs. C_L ; $M = 6.83$

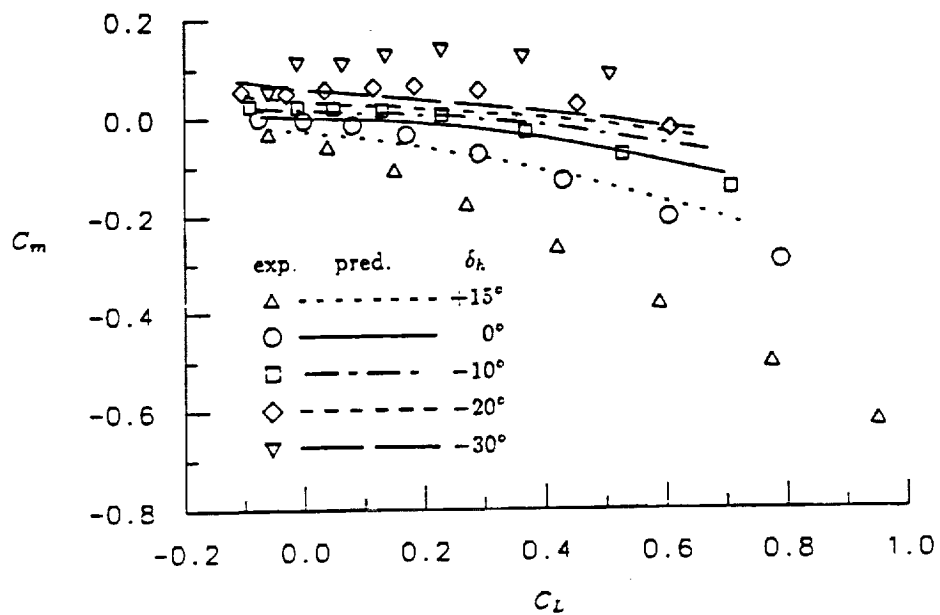


Fig. 55 Comparison Between Predicted and Experimentally Measured Moment as a Function of Lift on the X-15 Vehicle at Hypersonic Speed Including the Effect of Horizontal Tail Deflection.
 X-15 ; C_m vs. C_L ; $M = 6.83$

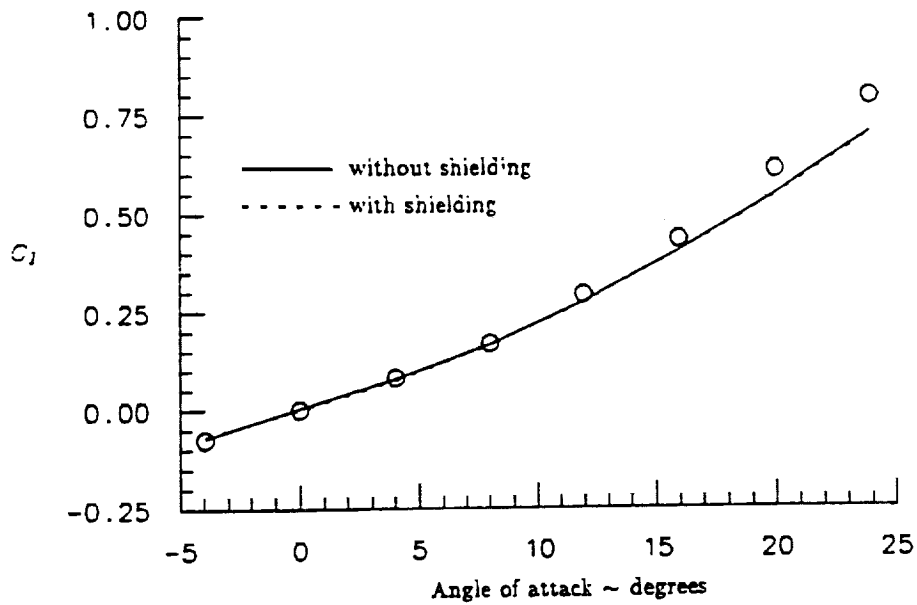


Fig. 56 The Effect of Shielding on the Predicted Lift on the X-15 Vehicle at Hypersonic Speed.
 X-15 ; C_L vs. α ; $M = 6.83$; with and without shielding

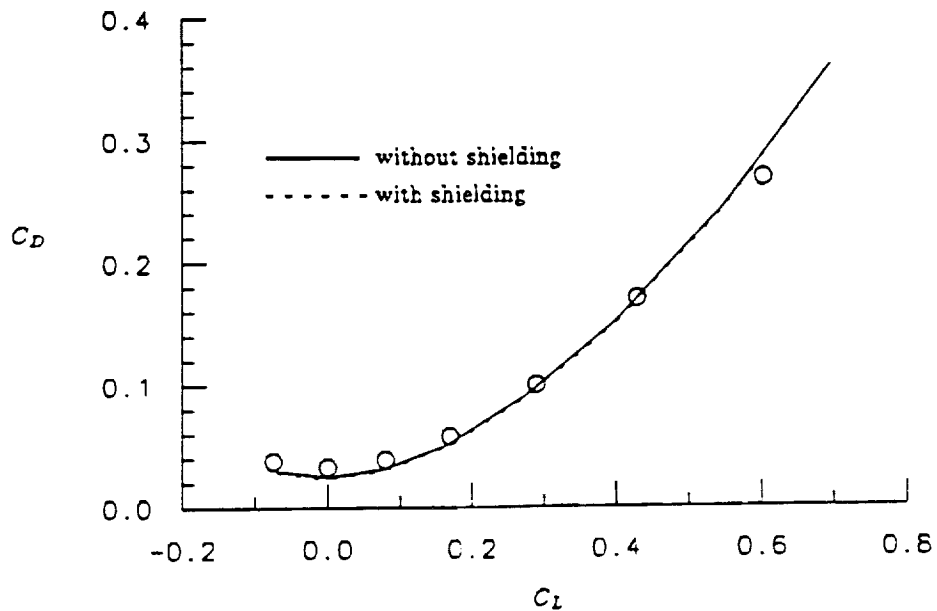


Fig. 57 The Effect of Shielding on the Predicted Drag on the X-15 Vehicle at Hypersonic Speed.
 X-15 ; C_D vs. C_L ; $M = 6.83$; with and without shielding

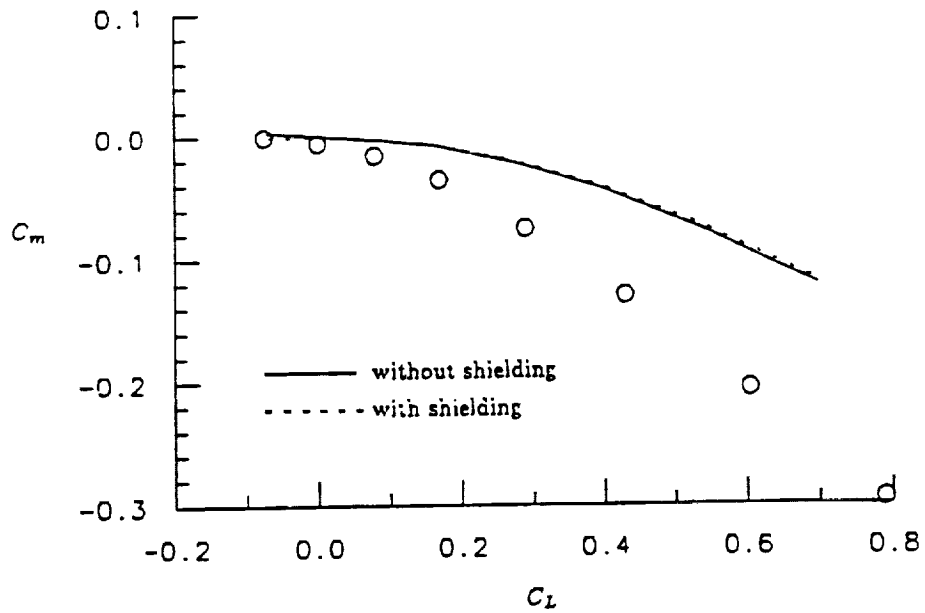


Fig. 58 The Effect of Shielding on the Predicted Moment of the X-15 Vehicle at Hypersonic Speed.
 X-15 ; C_m vs. C_L ; $M = 6.83$; with and without shielding

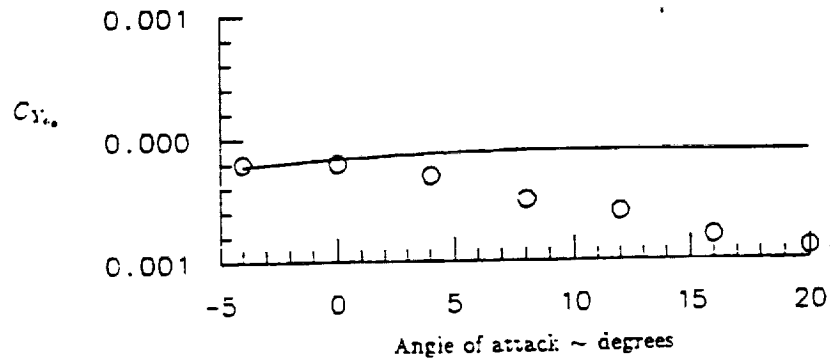


Fig. 59 Comparison Between Predicted and Experimentally Measured Side Force Due to Aileron Deflection on the X-15 Vehicle at Hypersonic Speed.
 X-15 ; C_{Y_a} vs. α ; $M = 6.83$

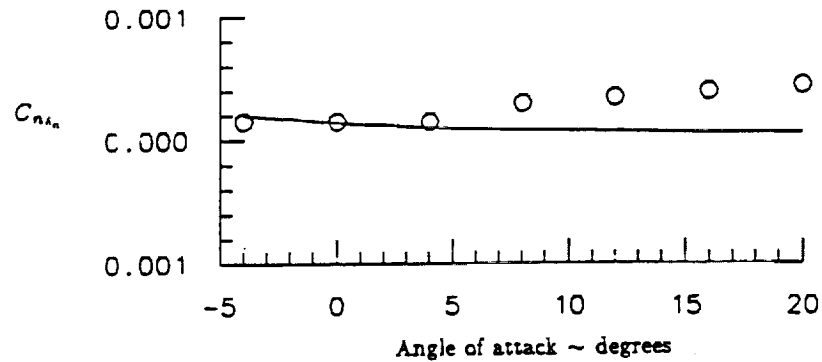


Fig. 60 Comparison Between Predicted and Experimentally Measured Yawing Moment Due to Aileron Deflection on the X-15 Vehicle at Hypersonic Speed.
 X-15 ; $C_{n\delta_a}$ vs. α ; $M = 6.83$

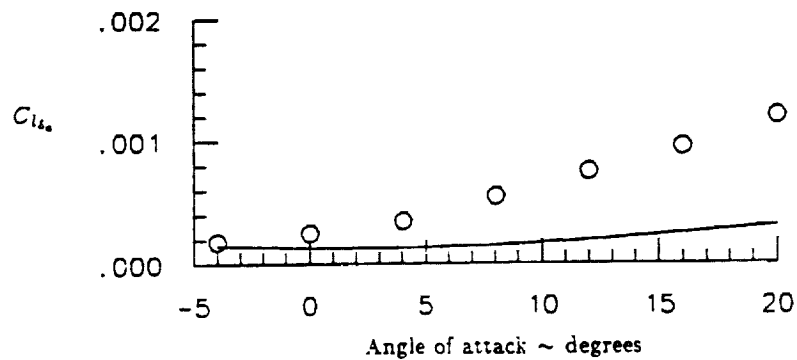


Fig. 61 Comparison Between Predicted and Experimentally Measured Rolling Moment Due to Aileron Deflection on the X-15 Vehicle at Hypersonic Speed.
 X-15 ; $C_{l\delta_a}$ vs. α ; $M = 6.83$

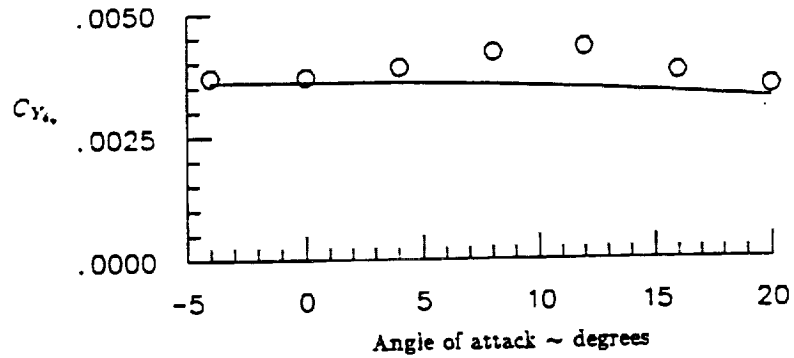


Fig. 62 Comparison Between Predicted and Experimentally Measured Side Force Due to Vertical Tail Deflection on the X-15 Vehicle at Hypersonic Speed. X-15 ; $C_{Y_{\delta_0}}$ vs. α ; $M = 6.83$

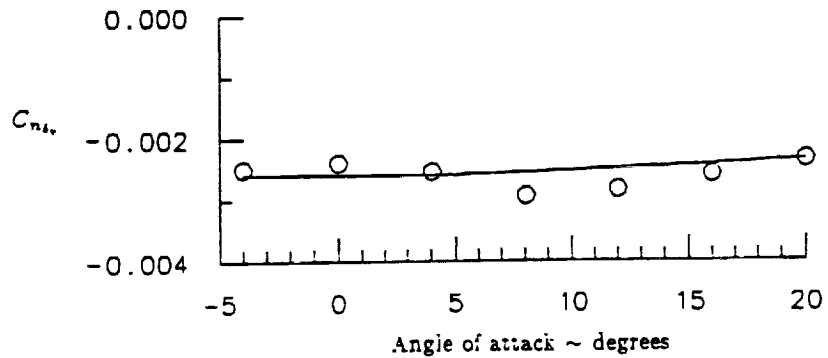


Fig. 63 Comparison Between Predicted and Experimentally Measured Yawing Moment Due to Vertical Tail Deflection on the X-15 Vehicle at Hypersonic Speed. X-15 ; $C_{n_{\delta_0}}$ vs. α ; $M = 6.83$

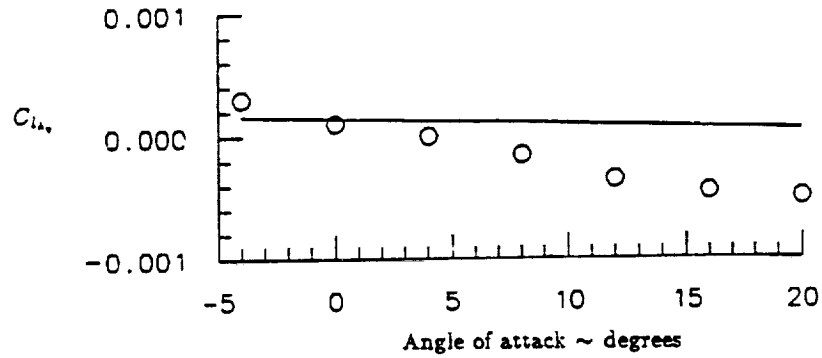


Fig. 64 Comparison Between Predicted and Experimentally Measured Rolling Moment Due to Vertical Tail Deflection on the X-15 Vehicle at Hypersonic Speed.
 X-15 ; $C_{l_{\delta_a}}$ vs. α ; $M = 6.83$

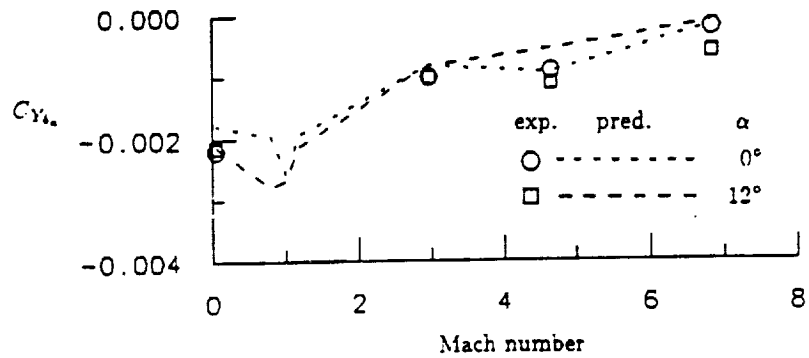


Fig. 65 Comparison Between Predicted and Experimentally Measured Side Force Due to Aileron Deflection on the X-15 Vehicle as a Function of Mach Number.
 X-15 ; $C_{Y_{\delta_a}}$ vs. M ; $\alpha = 0^\circ$ and 12°

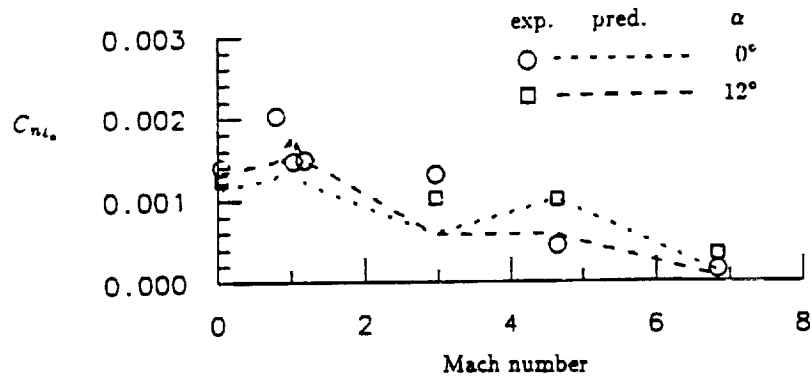


Fig. 66 Comparison Between Predicted and Experimentally Measured Yawing Moment Due to Aileron Deflection on the X-15 Vehicle as a Function of Mach Number.
X-15 ; $C_{n_{\delta_a}}$ vs. M ; $\alpha = 0^\circ$ and 12°

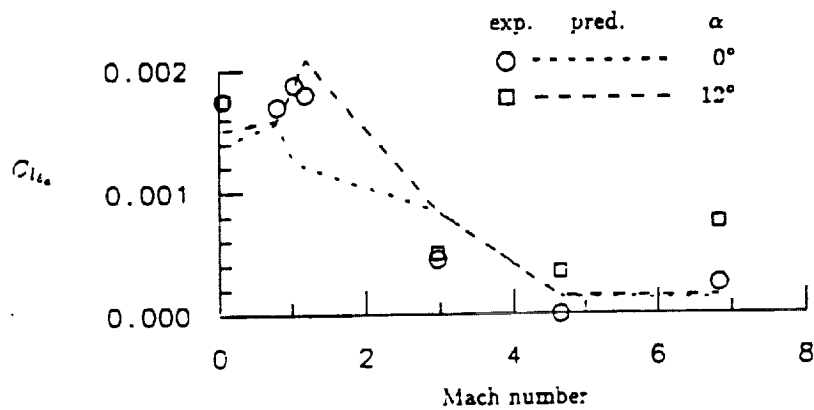


Fig. 67 Comparison Between Predicted and Experimentally Measured Rolling Moment Due to Aileron Deflection on the X-15 Vehicle as a Function of Mach Number.
X-15 ; $C_{l_{\delta_a}}$ vs. M ; $\alpha = 0^\circ$ and 12°

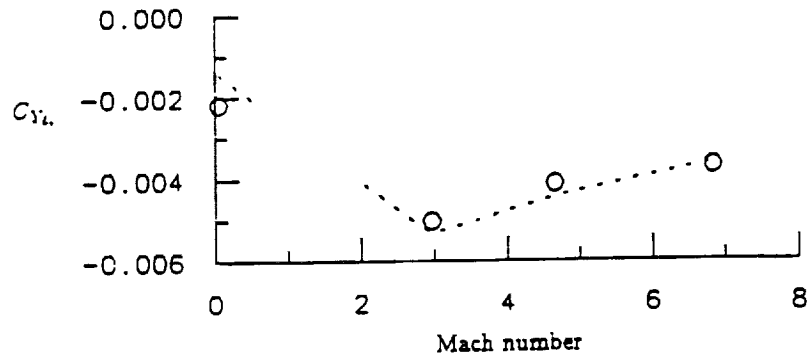


Fig. 68 Comparison Between Predicted and Experimentally Measured Side Force Due to Vertical Tail Deflection on the X-15 Vehicle as a Function of Mach Number.
 X-15 ; $C_{Y_{\delta}}$ vs. M ; $\alpha = 0^\circ$

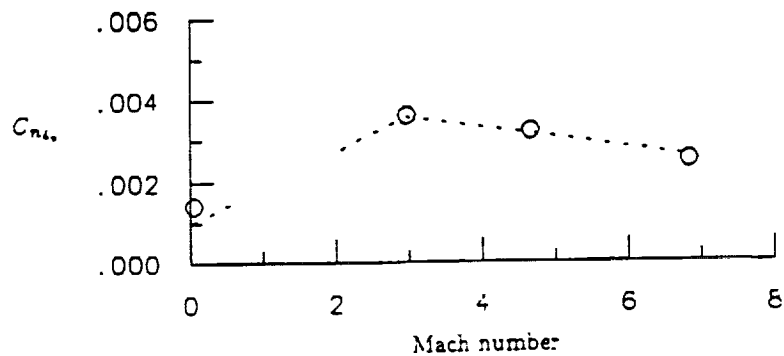


Fig. 69 Comparison Between Predicted and Experimentally Measured Yawing Moment Due to Vertical Tail Deflection on the X-15 Vehicle as a Function of Mach Number.
 X-15 ; $C_{n_{\delta}}$ vs. M ; $\alpha = 0^\circ$

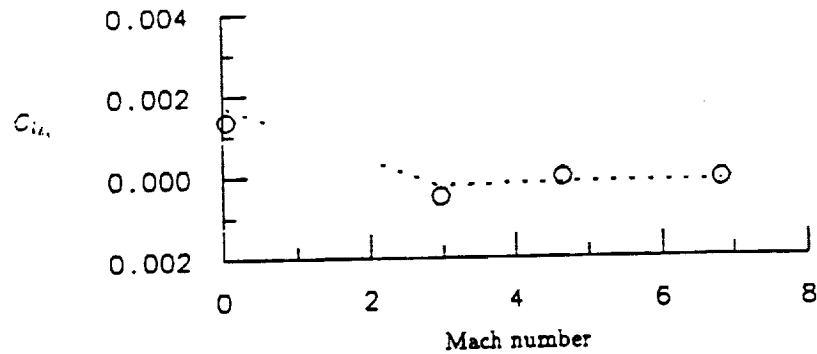


Fig. 70 Comparison Between Predicted and Experimentally Measured Rolling Moment Due to Vertical Tail Deflection on the X-15 Vehicle as a Function of Mach Number.
 X-15 ; $C_{l_{\delta_e}}$ vs. M ; $\alpha = 0^\circ$

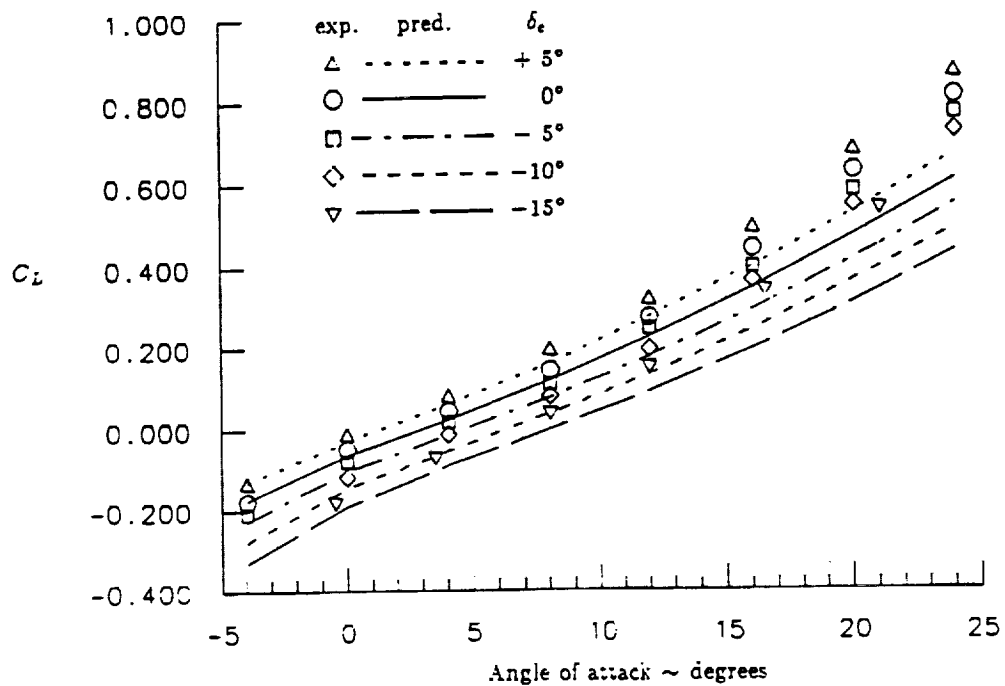


Fig. 71 Comparison Between Predicted and Experimentally Measured Lift on Hypersonic Research Airplane at Low Speed Including the Effect of Elevator Deflection.
 HRA ; C_L vs. α ; $M = 0.2$; $\delta_e = +5^\circ, 0^\circ, -5^\circ, -10^\circ, \text{ and } -15^\circ$

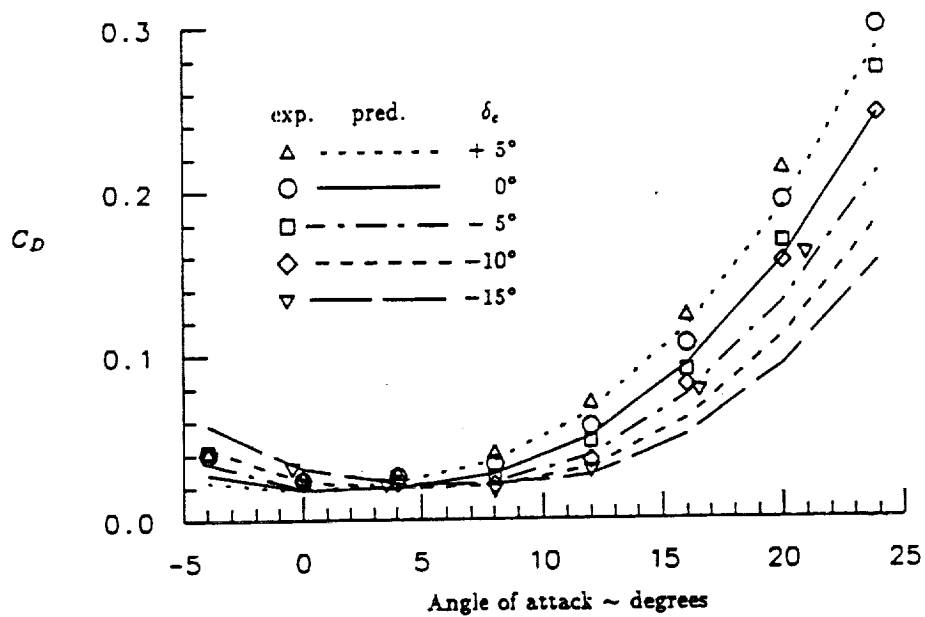


Fig. 72 Comparison Between Predicted and Experimentally Measured Drag on Hypersonic Research Airplane at Low Speed Including the Effect of Elevator Deflection.
 HRA ; C_D vs. α ; $M = 0.2$; $\delta_e = +5^\circ, 0^\circ, -5^\circ, -10^\circ, \text{ and } -15^\circ$

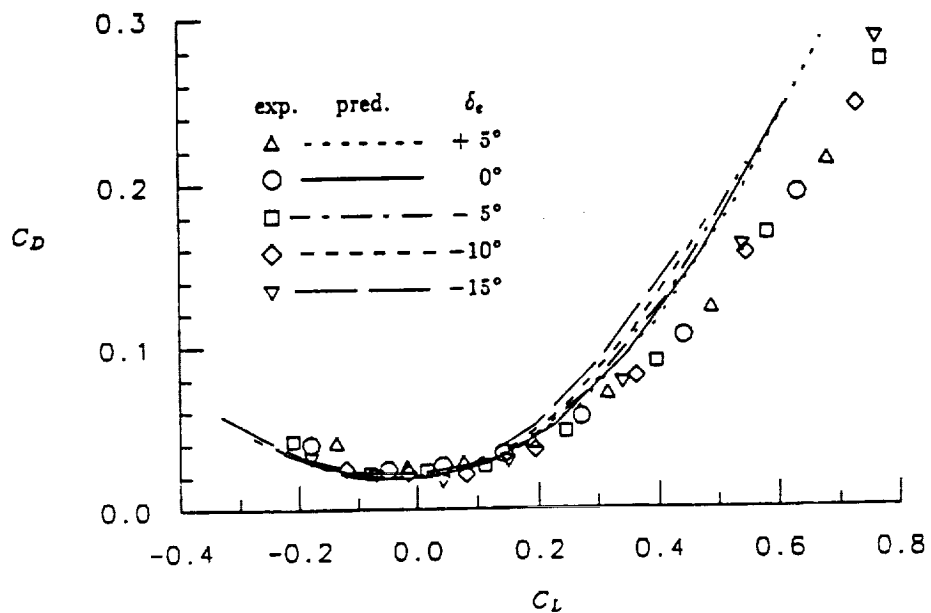


Fig. 73 Comparison Between Predicted and Experimentally Measured Drag as a Function of Lift on the Hypersonic Research Airplane at Low Speed Including the Effect of Elevator Deflection.
 HRA ; C_D vs. C_L ; $M = 0.2$; $\delta_e = +5^\circ, 0^\circ, -5^\circ, -10^\circ, \text{ and } -15^\circ$

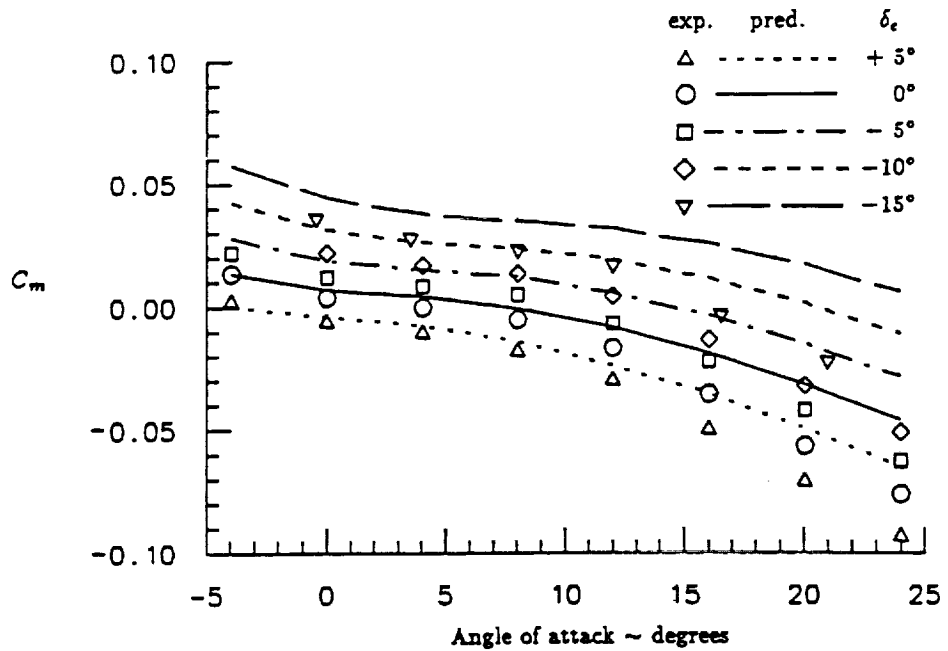


Fig. 74 Comparison Between Predicted and Experimentally Measured Moment on Hypersonic Research Airplane at Low Speed Including the Effect of Elevator Deflection.
HRA ; C_m vs. α ; $M = 0.2$; $\delta_e = +5^\circ, 0^\circ, -5^\circ, -10^\circ, \text{ and } -15^\circ$

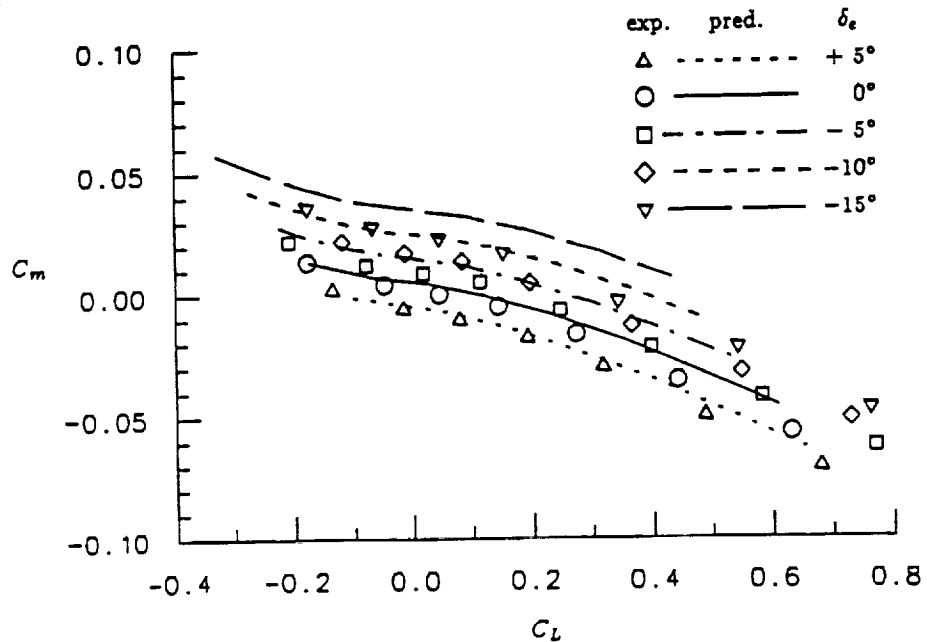


Fig. 75 Comparison Between Predicted and Experimentally Measured Moment as a Function of Lift on the Hypersonic Research Airplane at Low Speed Including the Effect of Elevator Deflection.
HRA ; C_m vs. C_L ; $M = 0.2$; $\delta_e = +5^\circ, 0^\circ, -5^\circ, -10^\circ, \text{ and } -15^\circ$

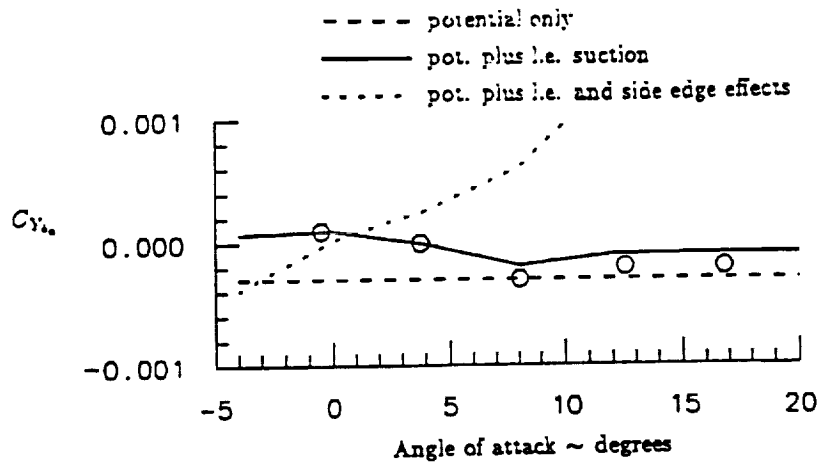


Fig. 76 Comparison Between Predicted and Experimentally Measured Side Force Due to Aileron Deflection on the Hypersonic Research Airplane at Low Speed Including the Effect of Different Modelling Techniques. HRA ; $C_{Y_{\delta a}}$ vs. α ; $M = 0.2$

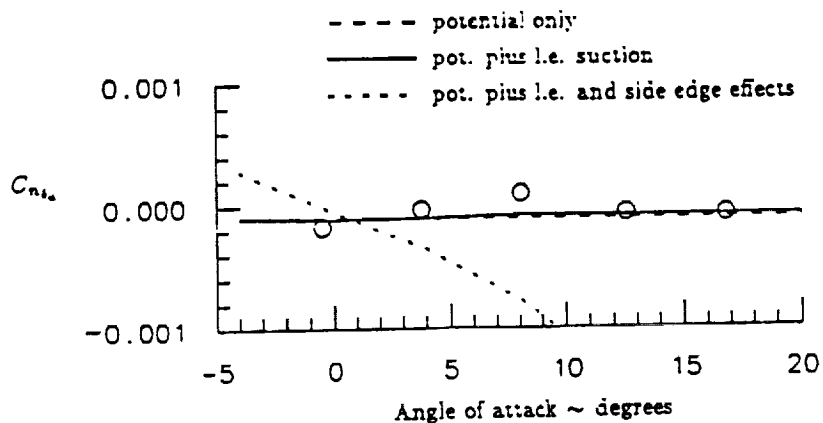


Fig. 77 Comparison Between Predicted and Experimentally Measured Yawing Moment Due to Aileron Deflection on the Hypersonic Research Airplane at Low Speed Including the Effect of Different Modelling Techniques. HRA ; $C_{n_{\delta a}}$ vs. α ; $M = 0.2$

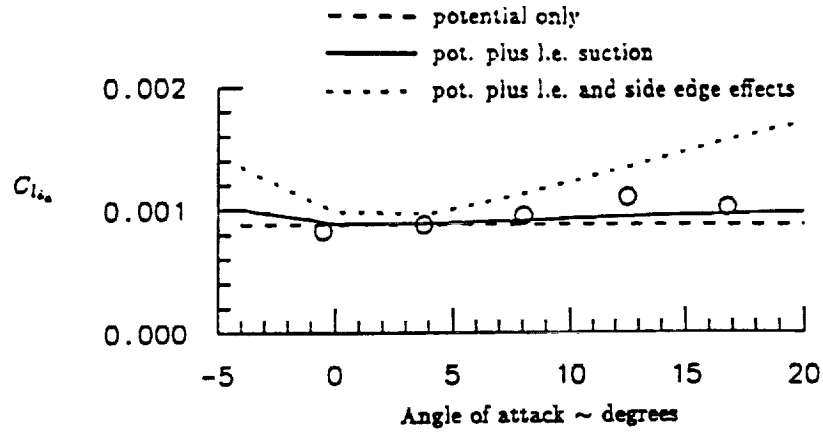


Fig. 78 Comparison Between Predicted and Experimentally Measured Rolling Moment Due to Aileron Deflection on the Hypersonic Research Airplane at Low Speed Including the Effect of Different Modelling Techniques. HRA ; $C_{l_{\delta_a}}$ vs. α ; $M = 0.2$

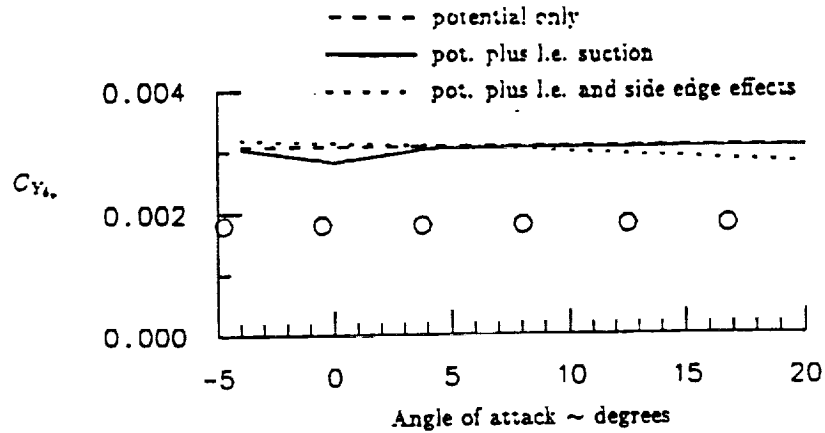


Fig. 79 Comparison Between Predicted and Experimentally Measured Side Force Due to Rudder Deflection on the Hypersonic Research Airplane at Low Speed Including the Effect of Different Modelling Techniques. HRA ; $C_{Y_{\delta_r}}$ vs. α ; $M = 0.2$

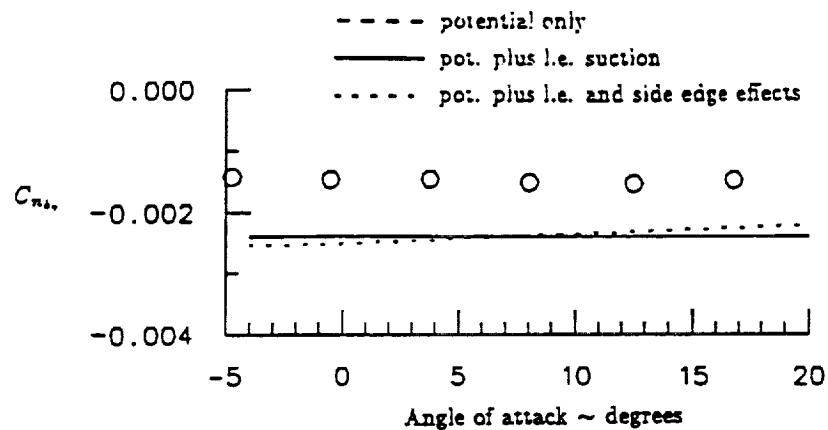


Fig. 80 Comparison Between Predicted and Experimentally Measured Yawing Moment Due to Rudder Deflection on the Hypersonic Research Airplane at Low Speed Including the Effect of Different Modelling Techniques. HRA ; $C_{n_{\delta_r}}$ vs. α ; $M = 0.2$

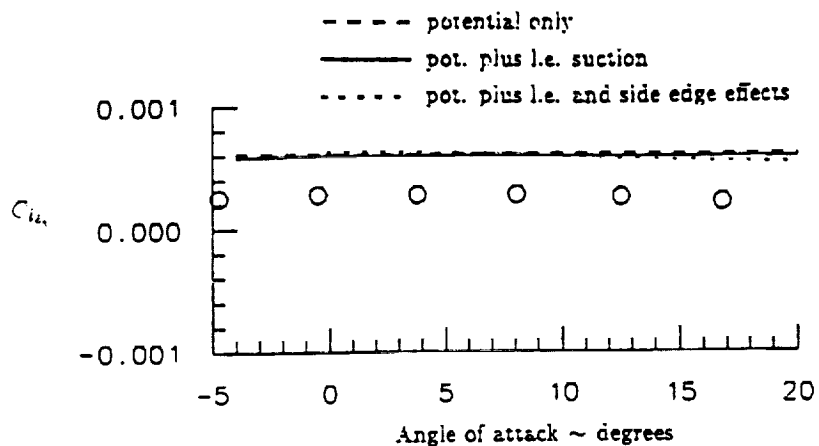


Fig. 81 Comparison Between Predicted and Experimentally Measured Rolling Moment Due to Rudder Deflection on the Hypersonic Research Airplane at Low Speed Including the Effect of Different Modelling Techniques. HRA ; $C_{l_{\delta_r}}$ vs. α ; $M = 0.2$

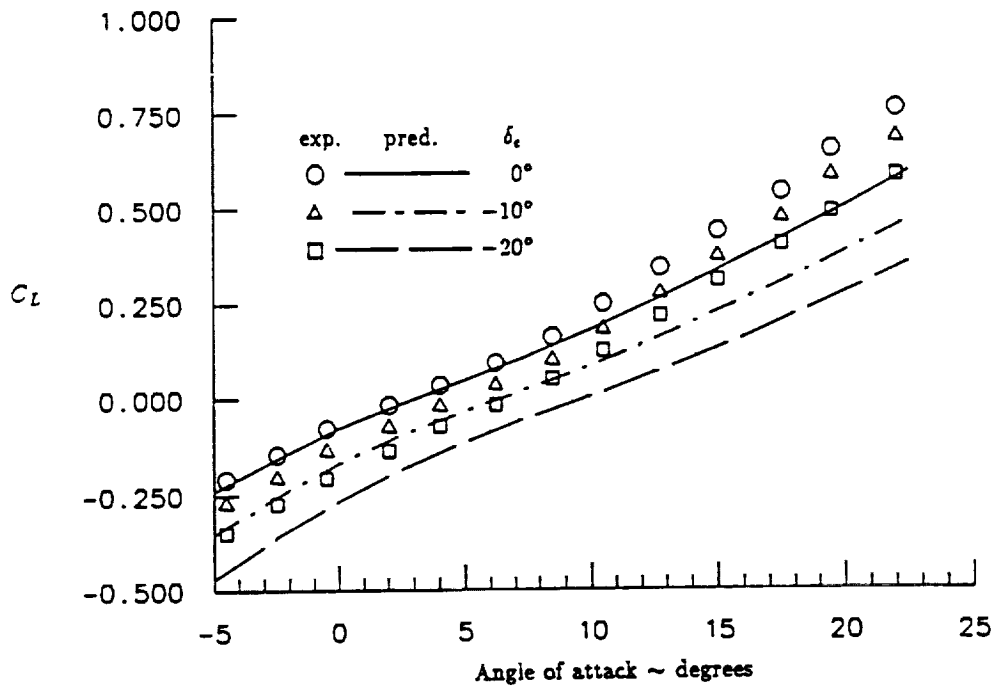


Fig. 82 Comparison Between Predicted and Experimentally Measured Lift on Hypersonic Research Airplane at High Subsonic Speed Including the Effect of Elevator Deflection.
HRA ; C_L vs. α ; $M = 0.8$; $\delta_e = 0^\circ, -10^\circ, \text{ and } -20^\circ$

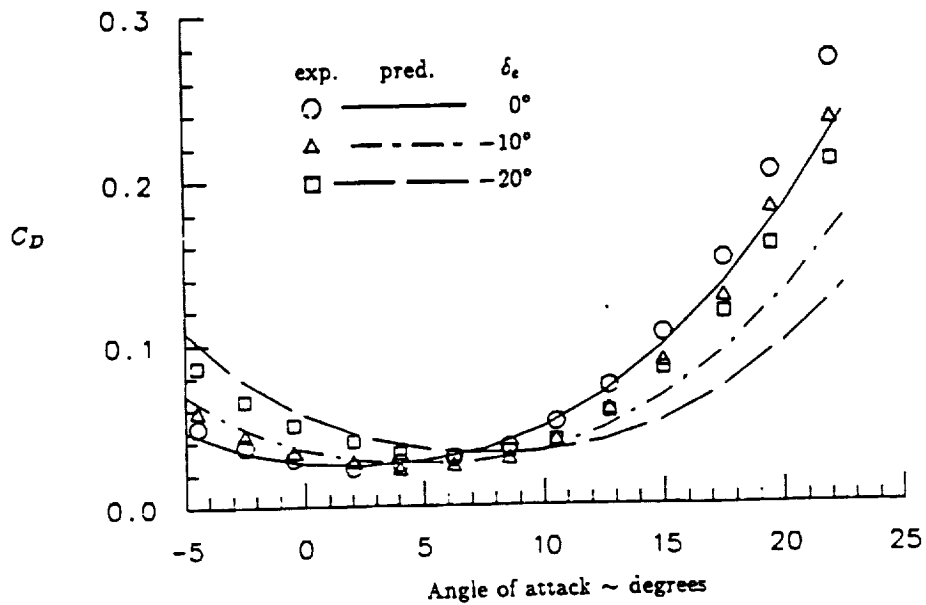


Fig. 83 Comparison Between Predicted and Experimentally Measured Drag on Hypersonic Research Airplane at High Subsonic Speed Including the Effect of Elevator Deflection.
HRA ; C_D vs. α ; $M = 0.8$; $\delta_e = 0^\circ, -10^\circ, \text{ and } -20^\circ$

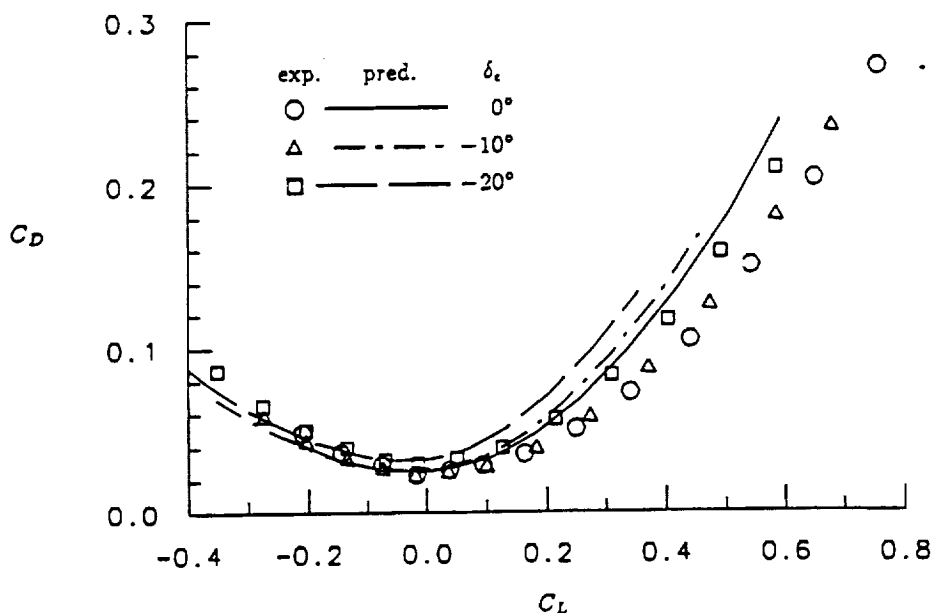


Fig. 84 Comparison Between Predicted and Experimentally Measured Drag as a Function of Lift on the Hypersonic Research Airplane at High Subsonic Speed Including the Effect of Elevator Deflection. HRA ; C_D vs. C_L ; $M = 0.8$; $\delta_e = 0^\circ, -10^\circ, \text{ and } -20^\circ$

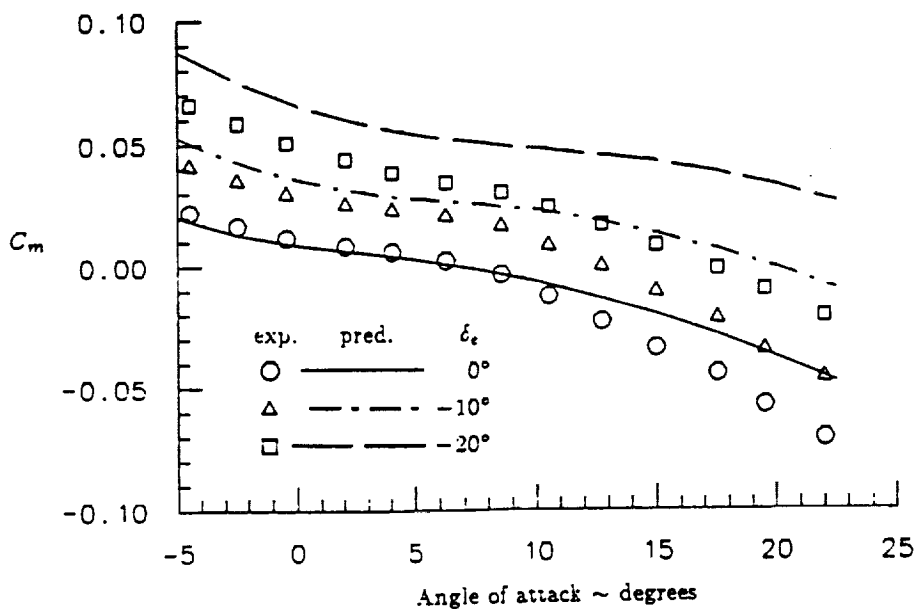


Fig. 85 Comparison Between Predicted and Experimentally Measured Moment on Hypersonic Research Airplane at High Subsonic Speed Including the Effect of Elevator Deflection. HRA ; C_m vs. α ; $M = 0.8$; $\delta_e = 0^\circ, -10^\circ, \text{ and } -20^\circ$

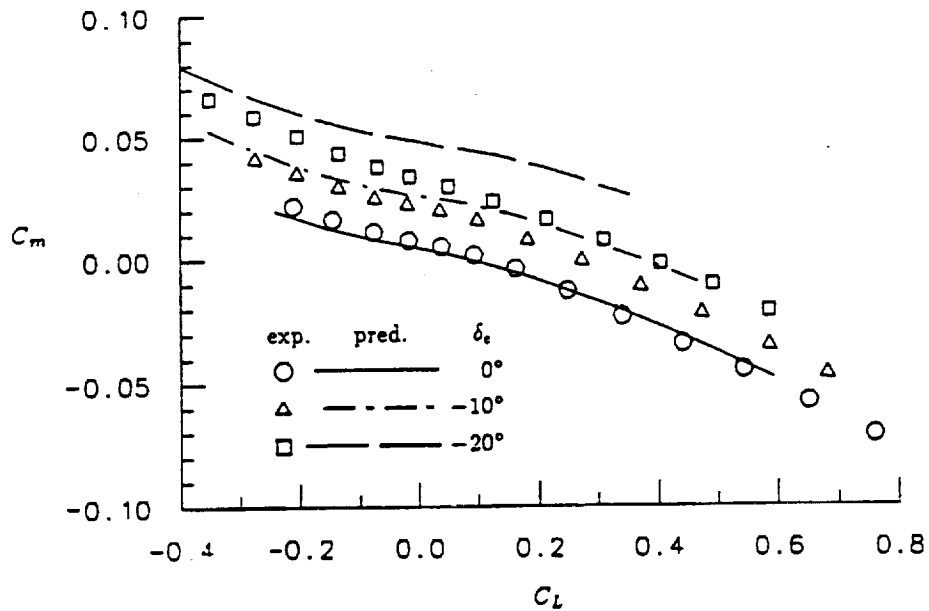


Fig. 86 Comparison Between Predicted and Experimentally Measured Moment as a Function of Lift on the Hypersonic Research Airplane at High Subsonic Speed Including the Effect of Elevator Deflection. HRA ; C_m vs. C_L ; $M = 0.8$; $\delta_e = 0^\circ, -10^\circ, \text{ and } -20^\circ$

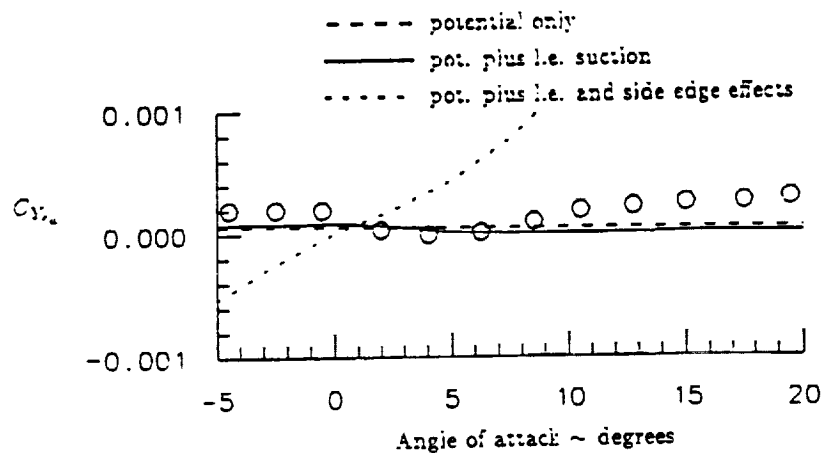


Fig. 87 Comparison Between Predicted and Experimentally Measured Side Force Due to Aileron Deflection on the Hypersonic Research Airplane at High Subsonic Speed Including the Effect of Different Modelling Techniques. HRA ; C_{Y_a} vs. α ; $M = 0.8$

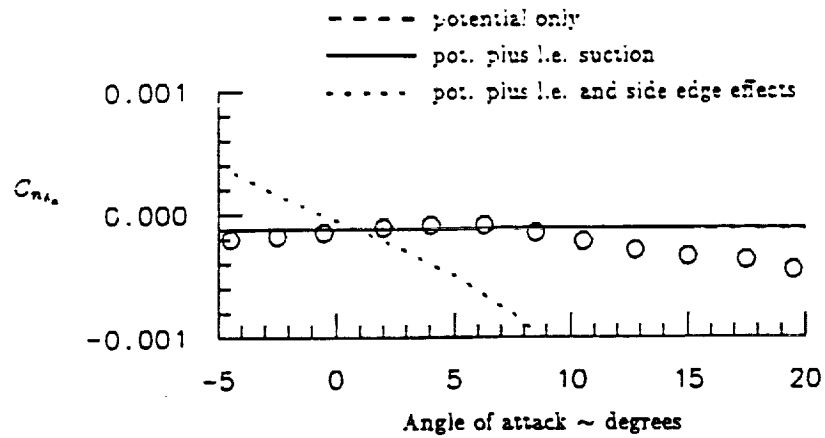


Fig. 88 Comparison Between Predicted and Experimentally Measured Yawing Moment Due to Aileron Deflection on the Hypersonic Research Airplane at High Subsonic Speed Including the Effect of Different Modelling Techniques.
HRA ; $C_{n_{\dot{\alpha}}}$ vs. α ; $M = 0.8$

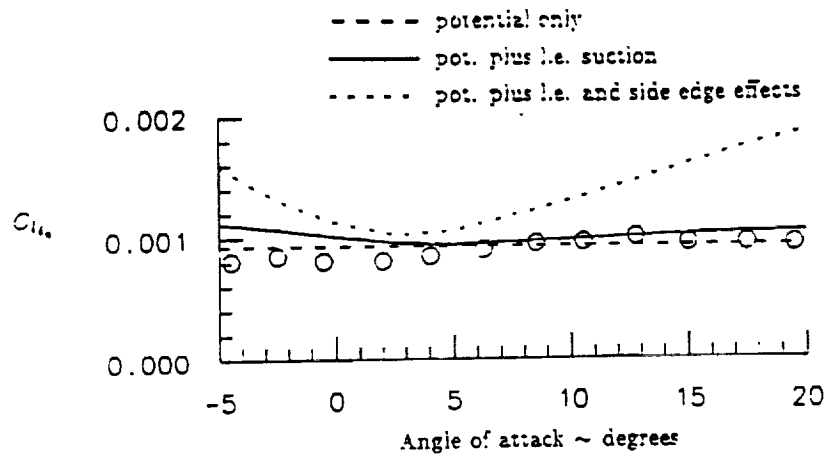


Fig. 89 Comparison Between Predicted and Experimentally Measured Rolling Moment Due to Aileron Deflection on the Hypersonic Research Airplane at High Subsonic Speed Including the Effect of Different Modelling Techniques.
HRA ; $C_{l_{\dot{\alpha}}}$ vs. α ; $M = 0.8$

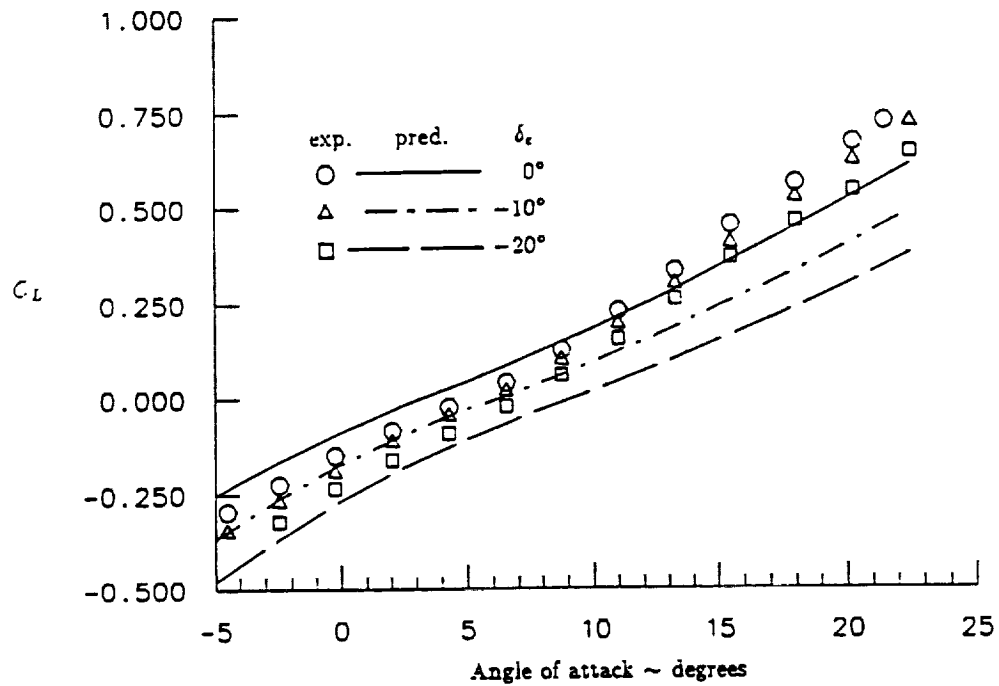


Fig. 90 Comparison Between Predicted and Experimentally Measured Lift on Hypersonic Research Airplane at Transonic Speed Including the Effect of Elevator Deflection.
HRA ; C_L vs. α ; $M = 0.98$; $\delta_e = 0^\circ, -10^\circ, \text{ and } -20^\circ$

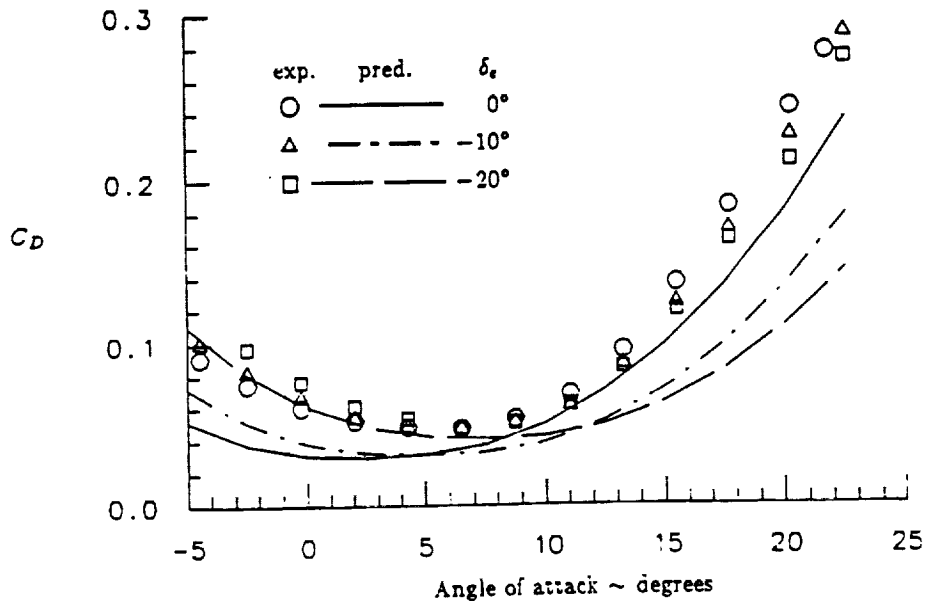


Fig. 91 Comparison Between Predicted and Experimentally Measured Drag on Hypersonic Research Airplane at Transonic Speed Including the Effect of Elevator Deflection.
HRA ; C_D vs. α ; $M = 0.98$; $\delta_e = 0^\circ, -10^\circ, \text{ and } -20^\circ$

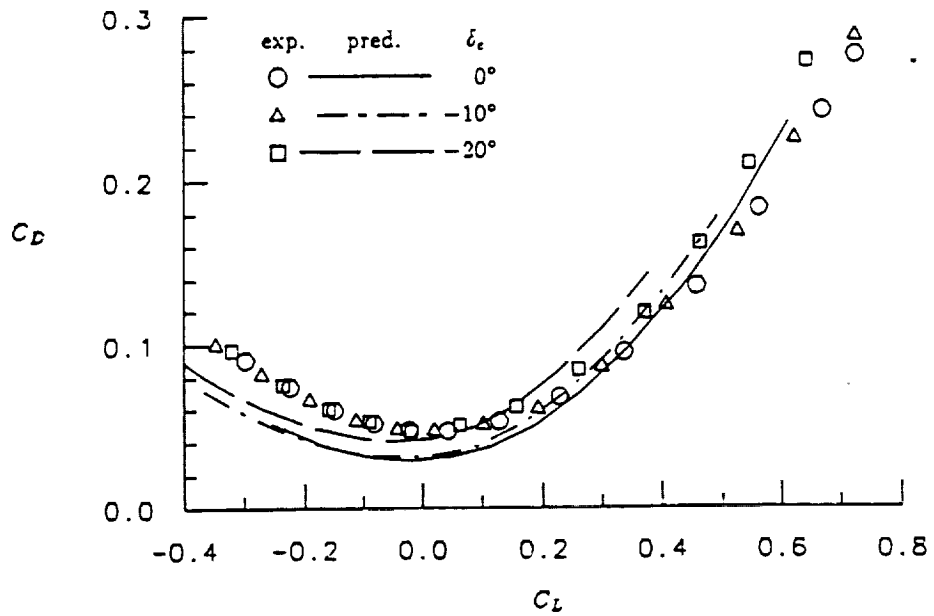


Fig. 92 Comparison Between Predicted and Experimentally Measured Drag as a Function of Lift on the Hypersonic Research Airplane at Transonic Speed Including the Effect of Elevator Deflection. HRA ; C_D vs. C_L ; $M = 0.98$; $\delta_e = 0^\circ, -10^\circ, \text{ and } -20^\circ$

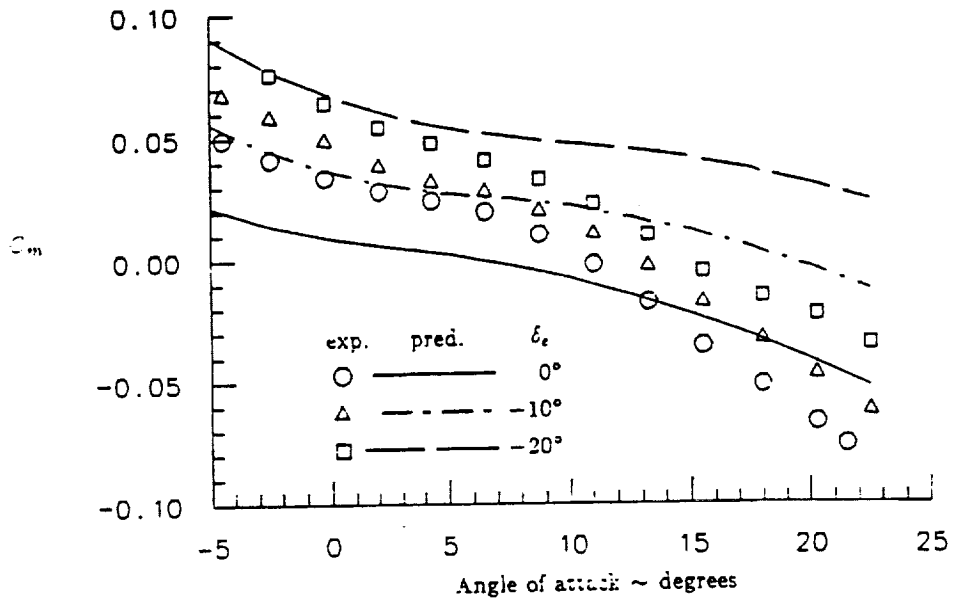


Fig. 93 Comparison Between Predicted and Experimentally Measured Moment on Hypersonic Research Airplane at Transonic Speed Including the Effect of Elevator Deflection. HRA ; C_m vs. α ; $M = 0.98$; $\delta_e = 0^\circ, -10^\circ, \text{ and } -20^\circ$

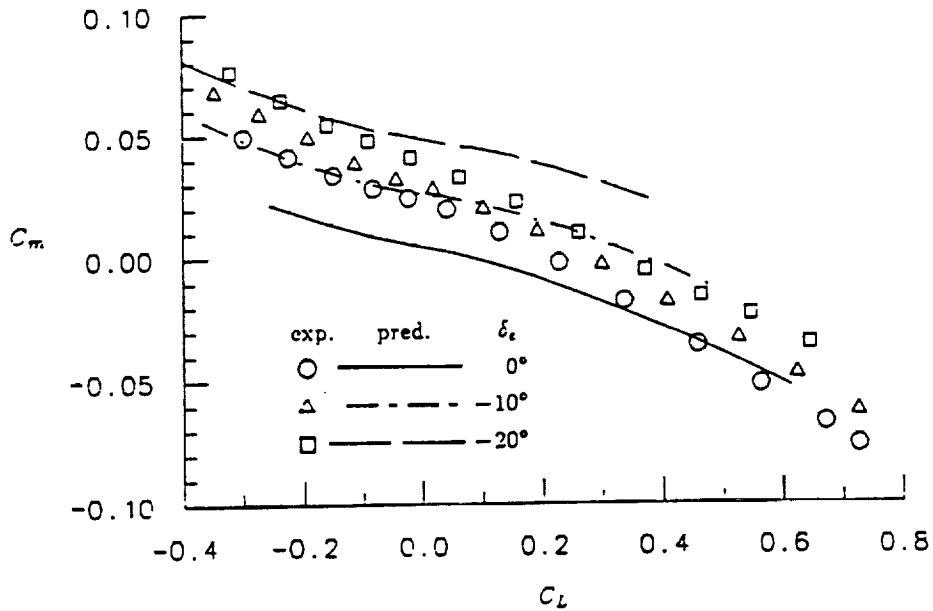


Fig. 94 Comparison Between Predicted and Experimentally Measured Moment as a Function of Lift on the Hypersonic Research Airplane at Transonic Speed Including the Effect of Elevator Deflection. HRA ; C_m vs. C_L ; $M = 0.98$; $\delta_e = 0^\circ, -10^\circ, \text{ and } -20^\circ$

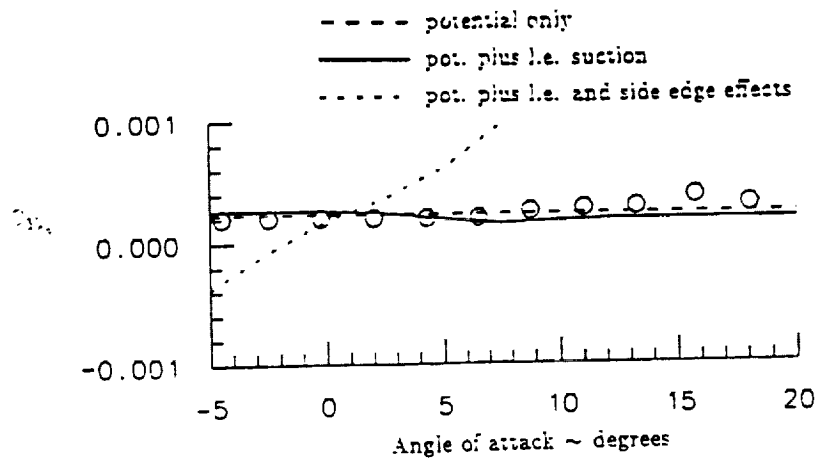


Fig. 95 Comparison Between Predicted and Experimentally Measured Side Force Due to Aileron Deflection on the Hypersonic Research Airplane at Transonic Speed Including the Effect of Different Modelling Techniques. HRA ; C_{Y_a} vs. α ; $M = 0.98$

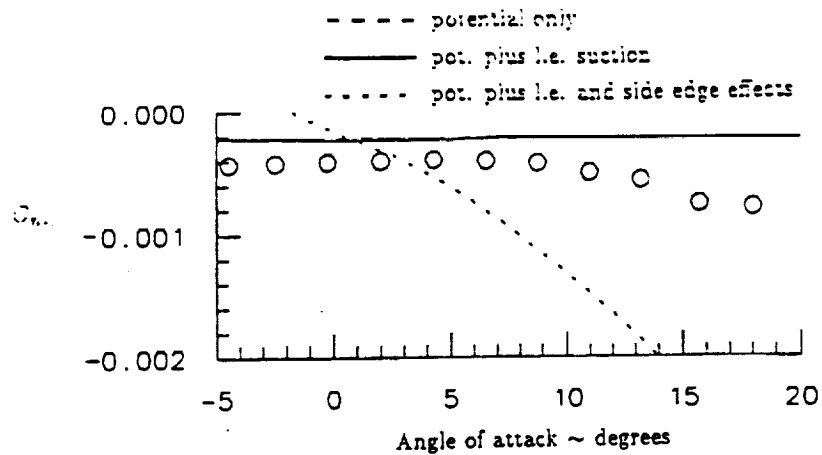


Fig. 96 Comparison Between Predicted and Experimentally Measured Yawing Moment Due to Aileron Deflection on the Hypersonic Research Airplane at Transonic Speed Including the Effect of Different Modelling Techniques.
HRA ; $C_{n_{\delta_a}}$ vs. α ; $M = 0.98$

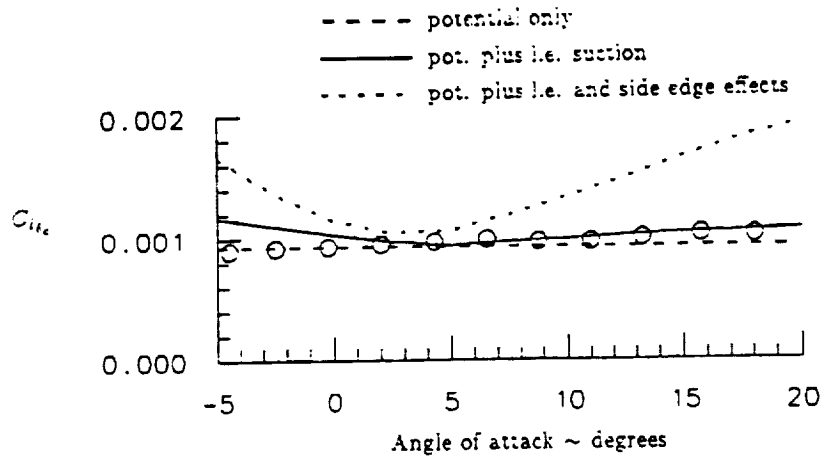


Fig. 97 Comparison Between Predicted and Experimentally Measured Rolling Moment Due to Aileron Deflection on the Hypersonic Research Airplane at Transonic Speed Including the Effect of Different Modelling Techniques.
HRA ; $C_{l_{\delta_a}}$ vs. α ; $M = 0.98$

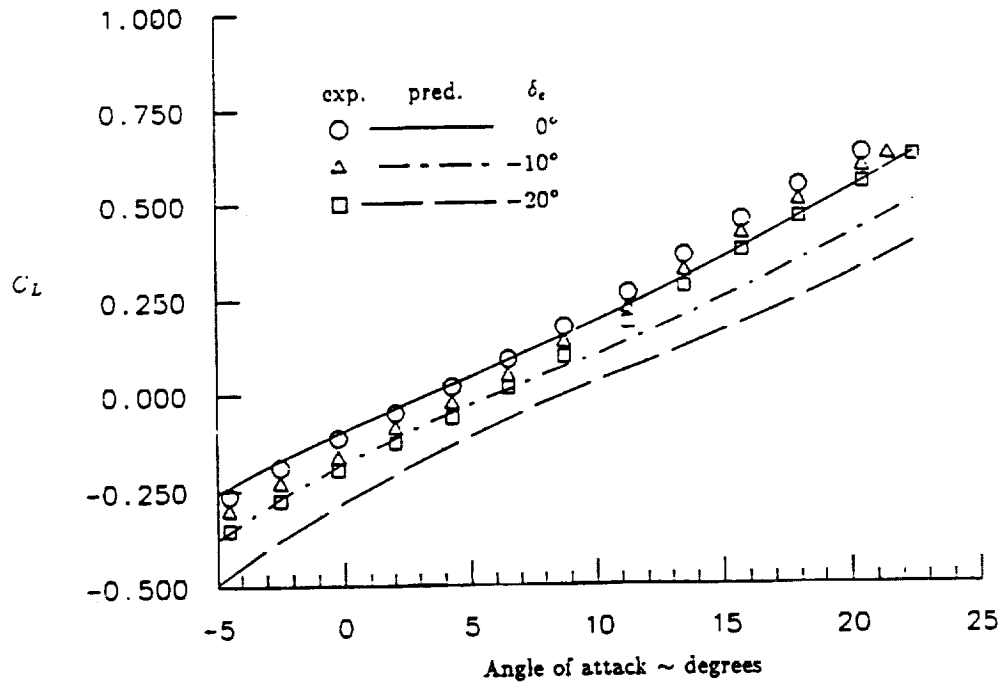


Fig. 98 Comparison Between Predicted and Experimentally Measured Lift on Hypersonic Research Airplane at Supersonic Speed Including the Effect of Elevator Deflection.
HRA ; C_L vs. α ; $M = 1.20$; $\delta_e = 0^\circ, -10^\circ, \text{ and } -20^\circ$

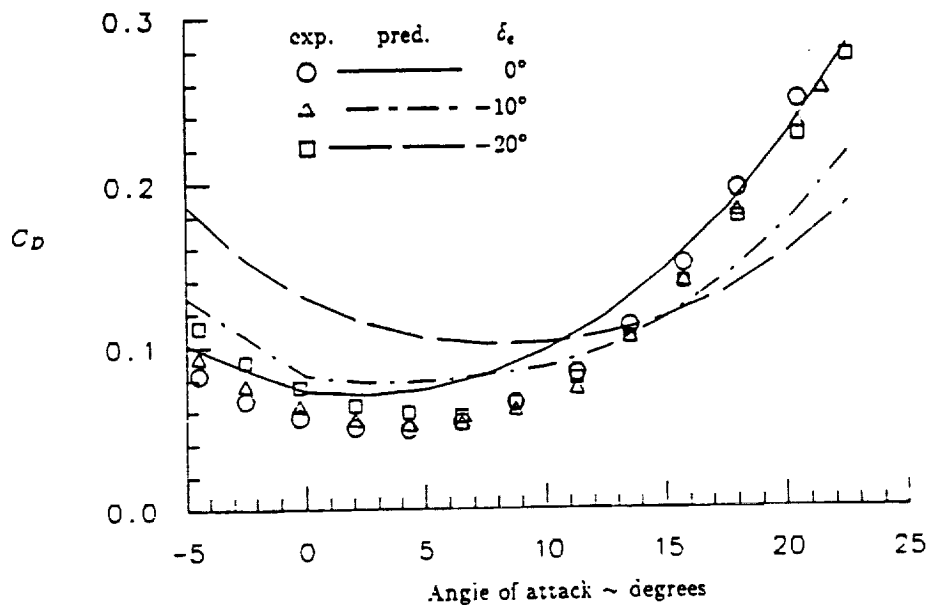


Fig. 99 Comparison Between Predicted and Experimentally Measured Drag on Hypersonic Research Airplane at Supersonic Speed Including the Effect of Elevator Deflection.
HRA ; C_D vs. α ; $M = 1.20$; $\delta_e = 0^\circ, -10^\circ, \text{ and } -20^\circ$

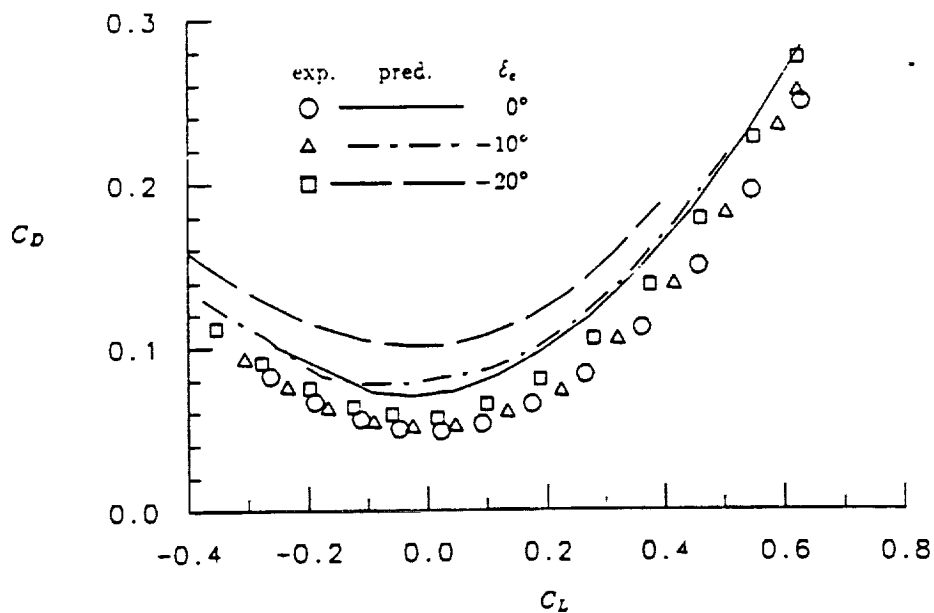


Fig. 100 Comparison Between Predicted and Experimentally Measured Drag as a Function of Lift on the Hypersonic Research Airplane at Supersonic Speed Including the Effect of Elevator Deflection.
HRA ; C_D vs. C_L ; $M = 1.20$; $\delta_e = 0^\circ, -10^\circ, \text{ and } -20^\circ$

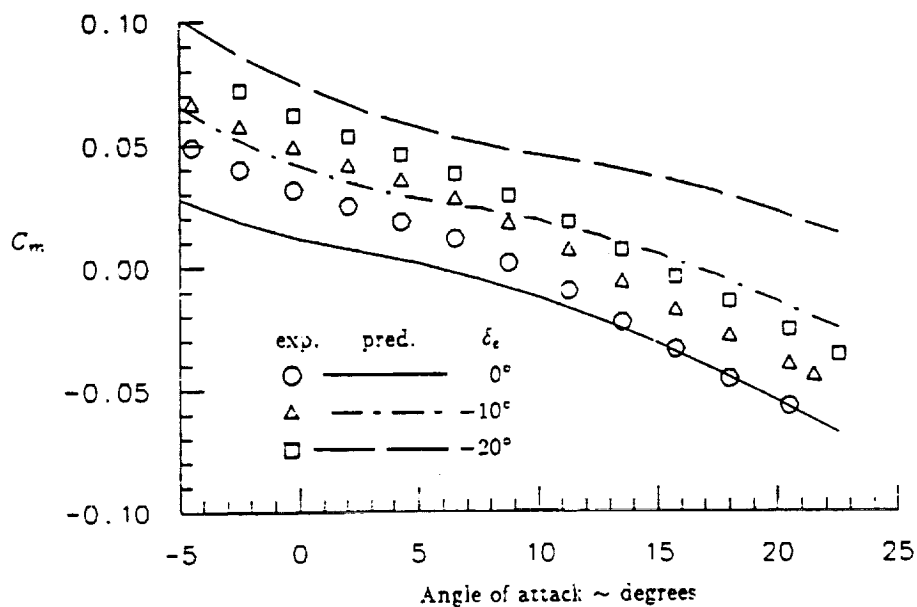


Fig. 101 Comparison Between Predicted and Experimentally Measured Moment on Hypersonic Research Airplane at Supersonic Speed Including the Effect of Elevator Deflection.
HRA ; C_m vs. α ; $M = 1.20$; $\delta_e = 0^\circ, -10^\circ, \text{ and } -20^\circ$

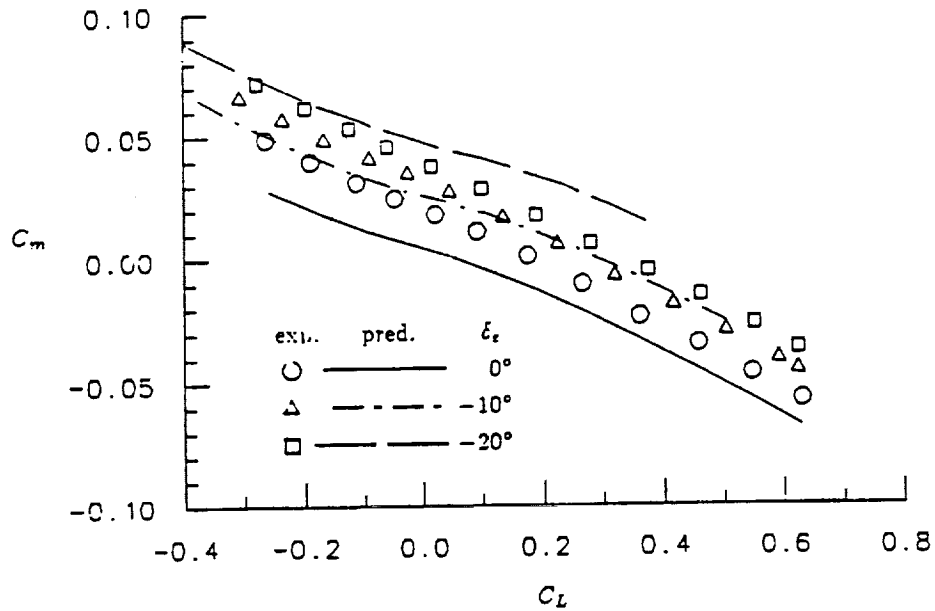


Fig. 102 Comparison Between Predicted and Experimentally Measured Moment as a Function of Lift on the Hypersonic Research Airplane at Supersonic Speed Including the Effect of Elevator Deflection. HRA ; C_m vs. C_L ; $M = 1.20$; $\delta_e = 0^\circ, -10^\circ, \text{ and } -20^\circ$

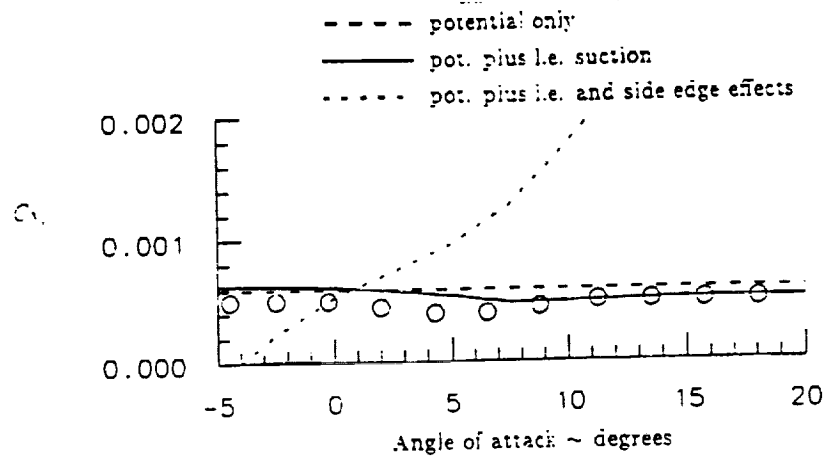


Fig. 103 Comparison Between Predicted and Experimentally Measured Side Force Due to Aileron Deflection on the Hypersonic Research Airplane at Supersonic Speed Including the Effect of Different Modelling Techniques. HRA ; C_{Y_a} vs. α ; $M = 1.20$

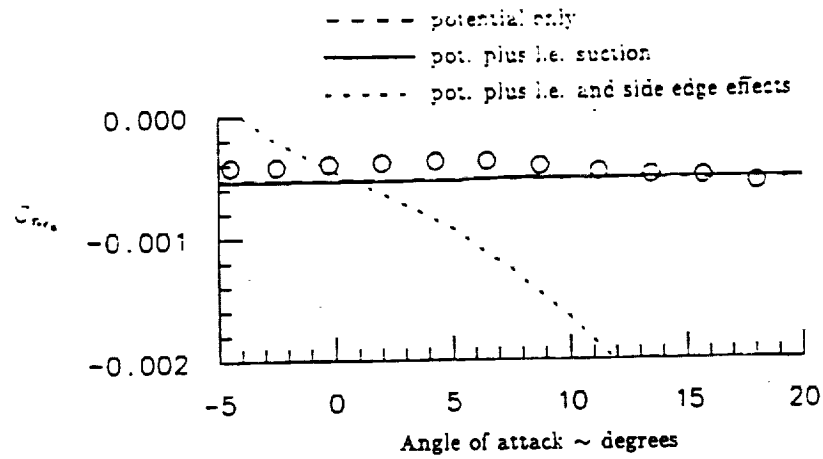


Fig. 104 Comparison Between Predicted and Experimentally Measured Yawing Moment Due to Aileron Deflection on the Hypersonic Research Airplane at Supersonic Speed Including the Effect of Different Modelling Techniques.
HRA ; $C_{n\delta_a}$ vs. α ; $M = 1.20$

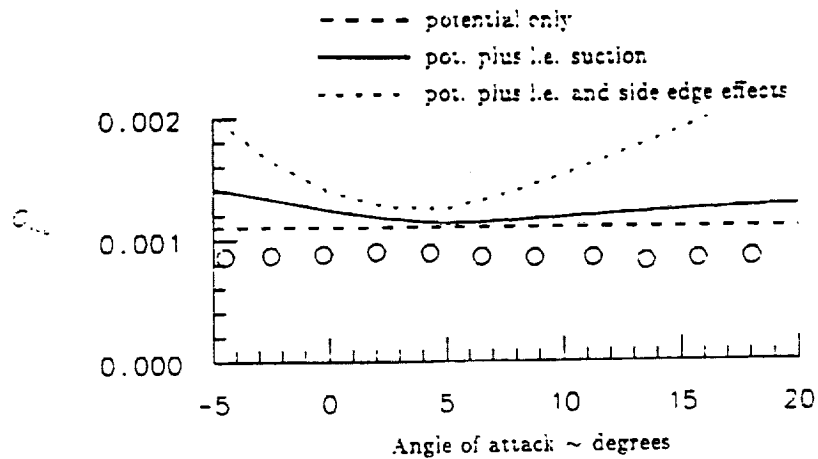


Fig. 105 Comparison Between Predicted and Experimentally Measured Rolling Moment Due to Aileron Deflection on the Hypersonic Research Airplane at Supersonic Speed Including the Effect of Different Modelling Techniques.
HRA ; $C_{l\delta_a}$ vs. α ; $M = 1.20$

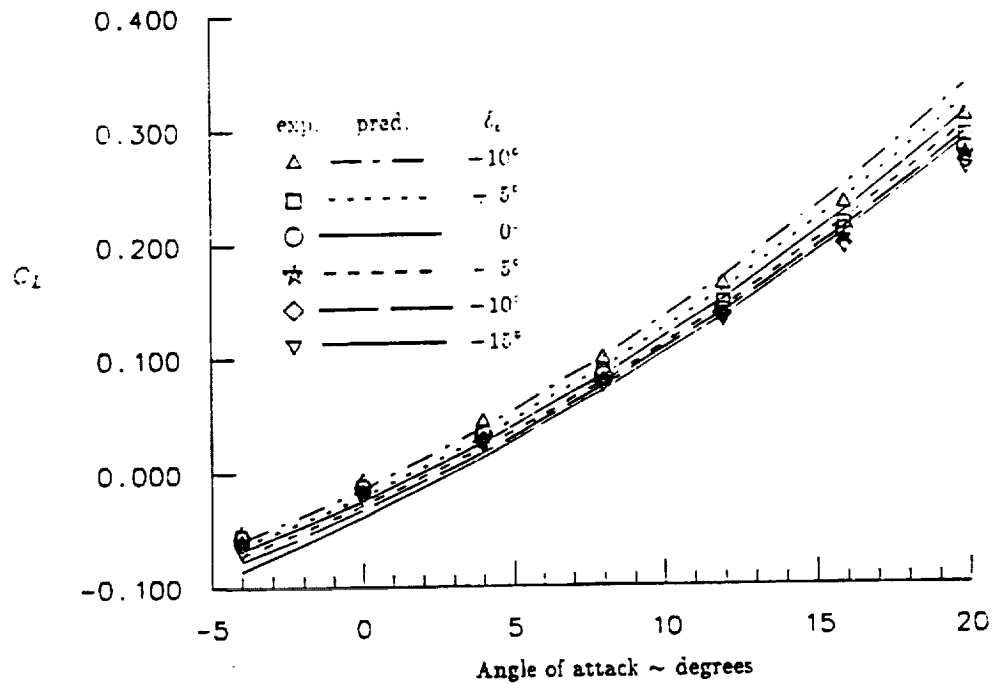


Fig. 106 Comparison Between Prediction Without Shielding and Experimentally Measured Lift on the Hypersonic Research Airplane at Hypersonic Speed Including the Effect of Elevator Deflection.
HRA ; C_L vs. α ; $M = 6.0$; $\delta_e = +10^\circ, 5^\circ, 0^\circ, -5^\circ, -10^\circ, \text{ and } -15^\circ$;
without shielding

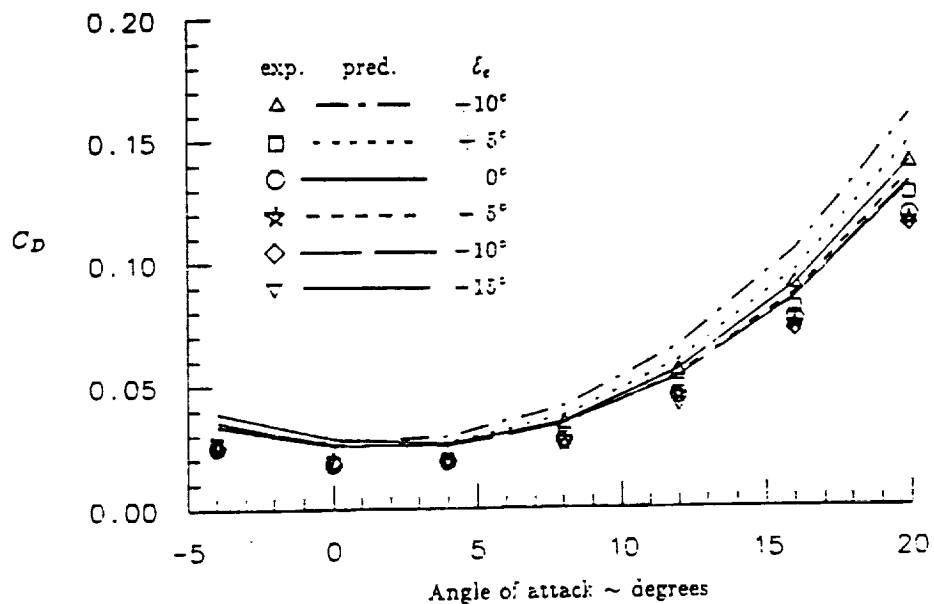


Fig. 107 Comparison Between Prediction Without Shielding and Experimentally Measured Drag on the Hypersonic Research Airplane at Hypersonic Speed Including the Effect of Elevator Deflection.
HRA ; C_D vs. α ; $M = 6.0$; $\delta_e = +10^\circ, 5^\circ, 0^\circ, -5^\circ, -10^\circ, \text{ and } -15^\circ$;
without shielding

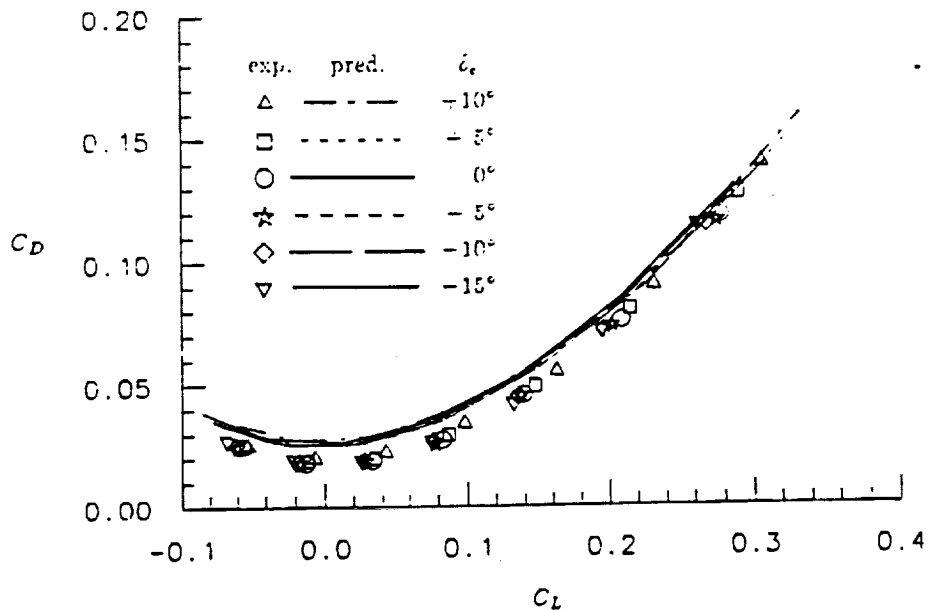


Fig. 108 Comparison Between Prediction Without Shielding and Experimentally Measured Drag as a Function of Lift on the Hypersonic Research Airplane at Hypersonic Speed Including the Effect of Elevator Deflection. HRA ; C_D vs. C_L ; $M = 6.0$; $\delta_e = +10^\circ, 5^\circ, 0^\circ, -5^\circ, -10^\circ,$ and -15° ; without shielding

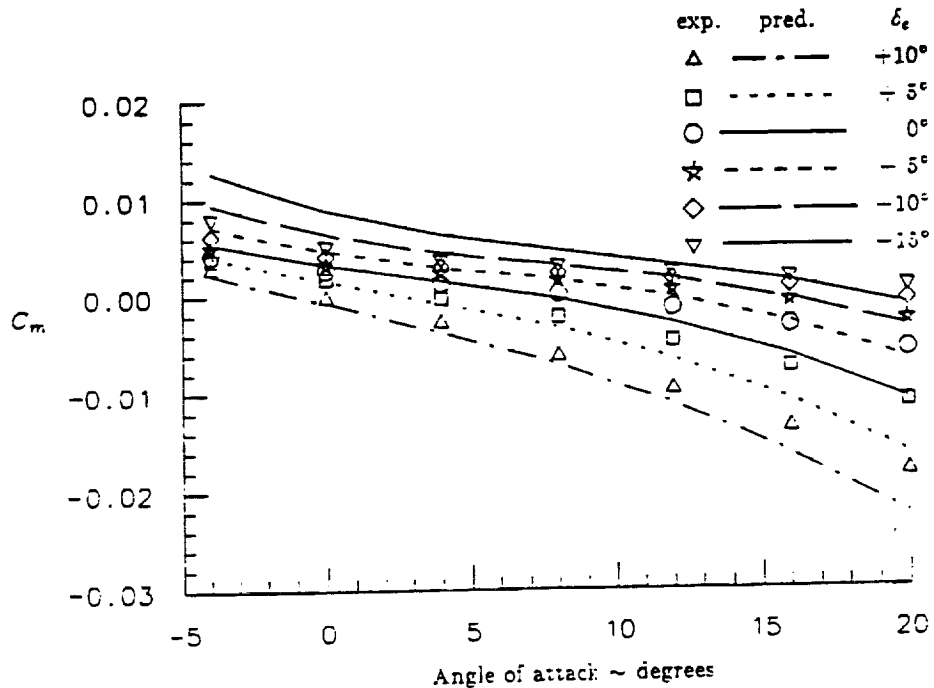


Fig. 109 Comparison Between Prediction Without Shielding and Experimentally Measured Moment on the Hypersonic Research Airplane at Hypersonic Speed Including the Effect of Elevator Deflection. HRA ; C_m vs. α ; $M = 6.0$; $\delta_e = +10^\circ, +5^\circ, 0^\circ, -5^\circ, -10^\circ,$ and -15° ; without shielding

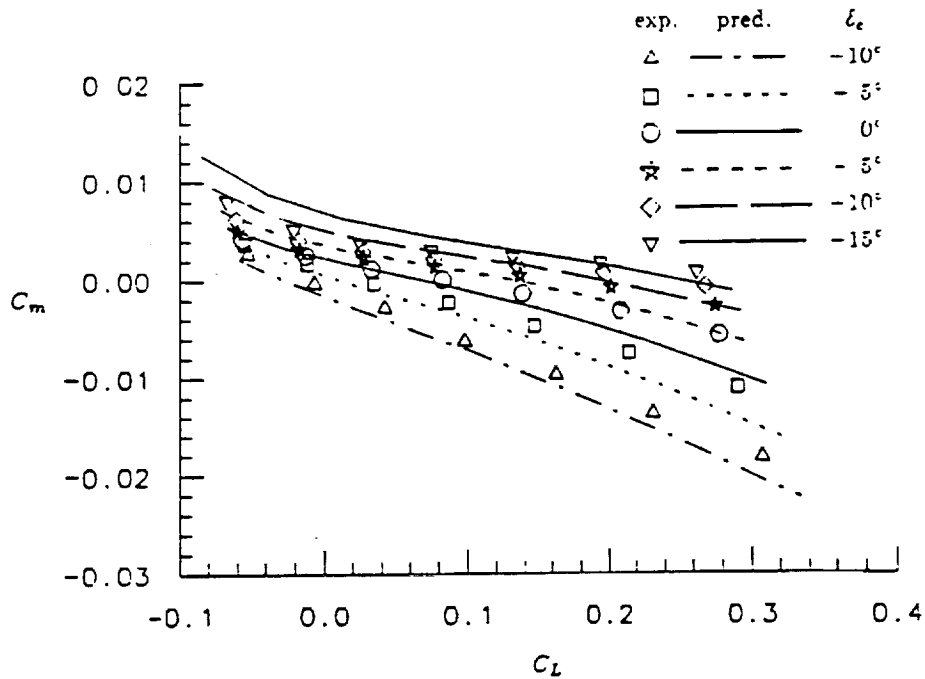


Fig. 110 Comparison Between Prediction Without Shielding and Experimentally Measured Moment as a Function of Lift on the Hypersonic Research Airplane at Hypersonic Speed Including the Effect of Elevator Deflection. HRA ; C_m vs. C_L ; $M = 6.0$; $\delta_e = +10^\circ, 5^\circ, 0^\circ, -5^\circ, -10^\circ,$ and -15° ; without shielding

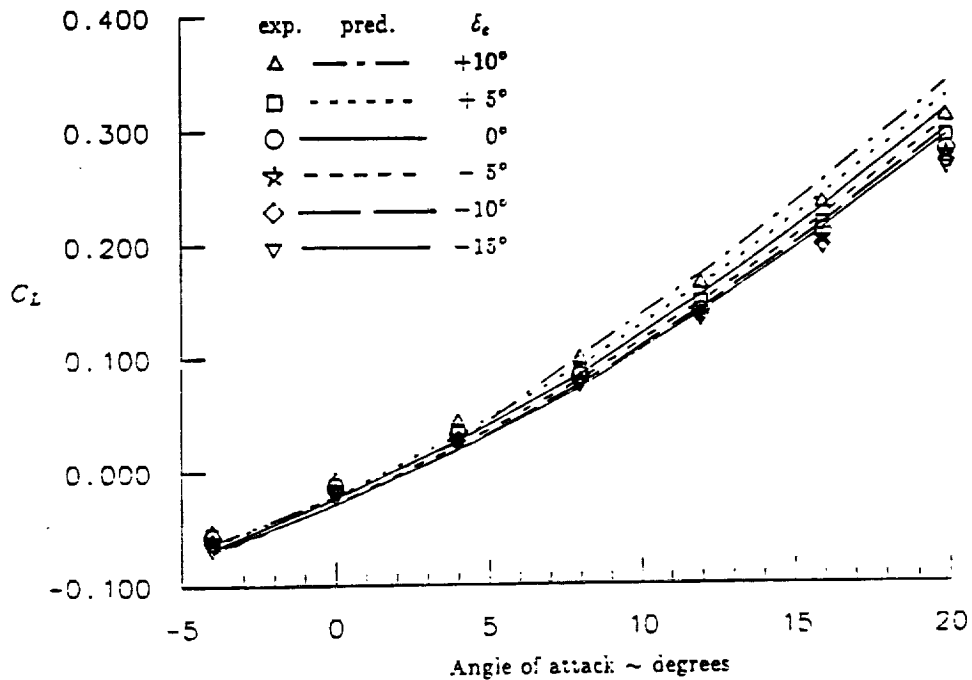


Fig. 111 Comparison Between Prediction With Shielding and Experimentally Measured Lift on the Hypersonic Research Airplane at Hypersonic Speed Including the Effect of Elevator Deflection. HRA ; C_L vs. α ; $M = 6.0$; $\delta_e = +10^\circ, 5^\circ, 0^\circ, -5^\circ, -10^\circ,$ and -15° ; with shielding

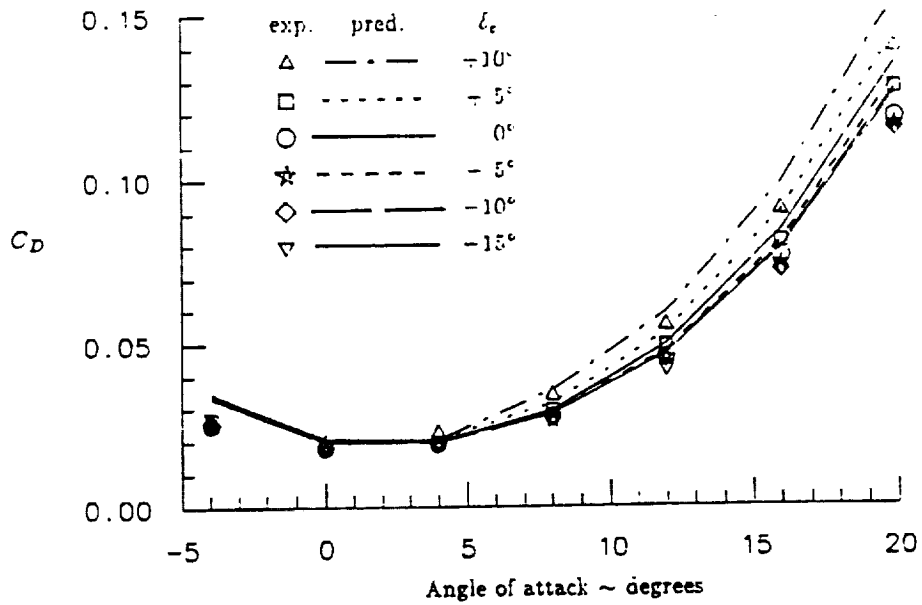


Fig. 112 Comparison Between Prediction With Shielding and Experimentally Measured Drag on the Hypersonic Research Airplane at Hypersonic Speed Including the Effect of Elevator Deflection. HRA ; C_D vs. α ; $M = 6.0$; $\delta_e = +10^\circ, 5^\circ, 0^\circ, -5^\circ, -10^\circ,$ and -15° ; with shielding

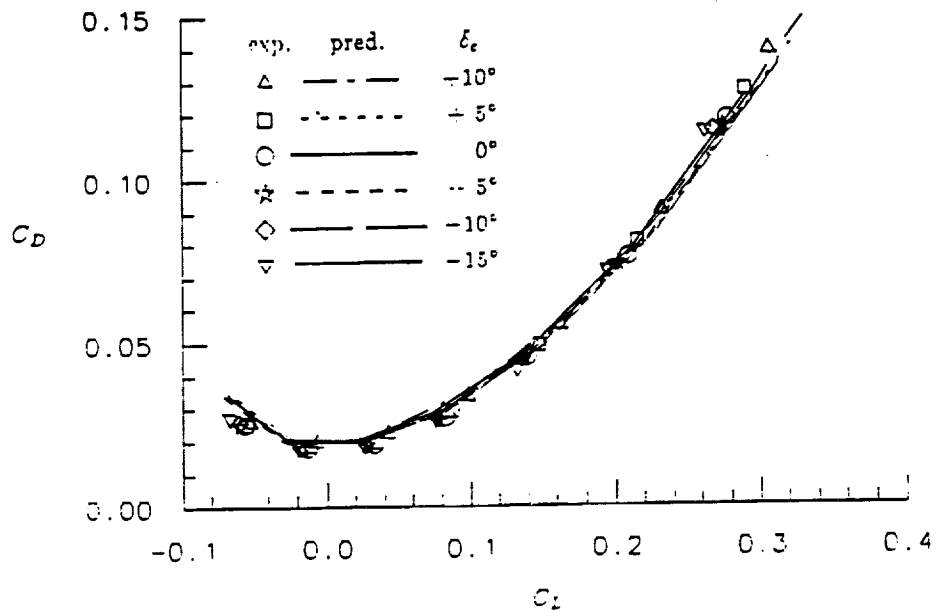


Fig. 113 Comparison Between Prediction With Shielding and Experimentally Measured Drag as a Function of Lift on the Hypersonic Research Airplane at Hypersonic Speed Including the Effect of Elevator Deflection. HRA ; C_D vs. C_L ; $M = 6.0$; $\delta_e = +10^\circ, 5^\circ, 0^\circ, -5^\circ, -10^\circ,$ and -15° ; with shielding

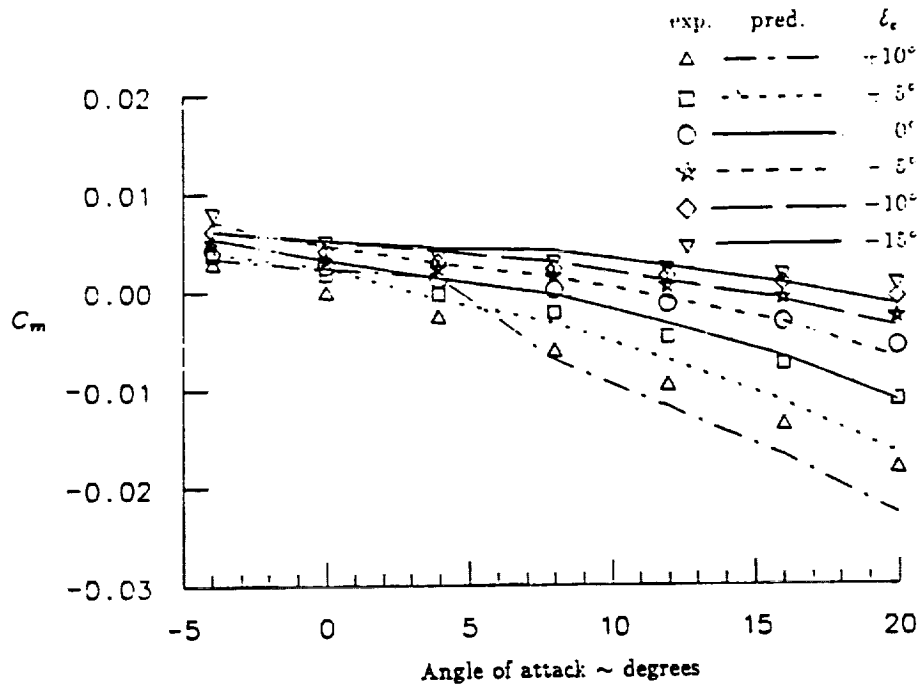


Fig. 114 Comparison Between Prediction With Shielding and Experimentally Measured Moment on the Hypersonic Research Airplane at Hypersonic Speed Including the Effect of Elevator Deflection.
 HRA ; C_m vs. α ; $M = 6.0$; $\delta_e = +10^\circ, 5^\circ, 0^\circ, -5^\circ, -10^\circ, \text{ and } -15^\circ$;
 with shielding

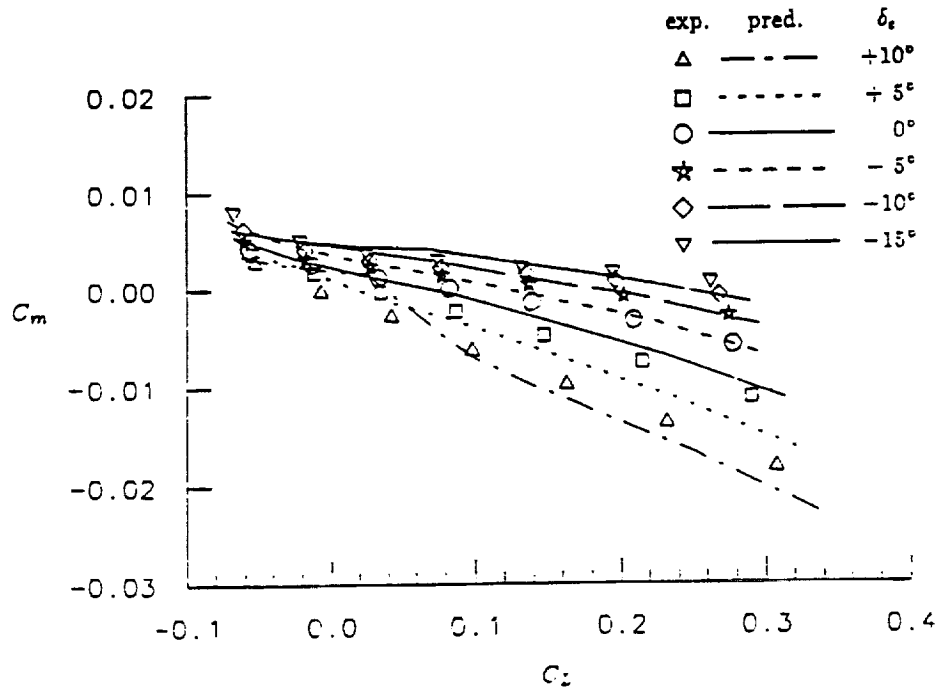


Fig. 115 Comparison Between Prediction With Shielding and Experimentally Measured Moment as a Function of Lift on the Hypersonic Research Airplane at Hypersonic Speed Including the Effect of Elevator Deflection.
 HRA ; C_m vs. C_L ; $M = 6.0$; $\delta_e = +10^\circ, 5^\circ, 0^\circ, -5^\circ, -10^\circ, \text{ and } -15^\circ$;
 with shielding

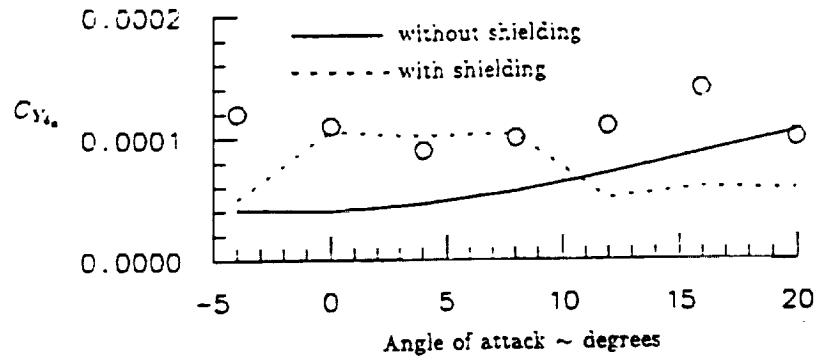


Fig. 116 Comparison Between Prediction With and Without Shielding and Experimentally Measured Side Force Due to Aileron Deflection on the Hypersonic Research Airplane at Hypersonic Speed.
HRA ; $C_{Y_{\delta_a}}$ vs. α ; $M = 6.0$; with and without shielding

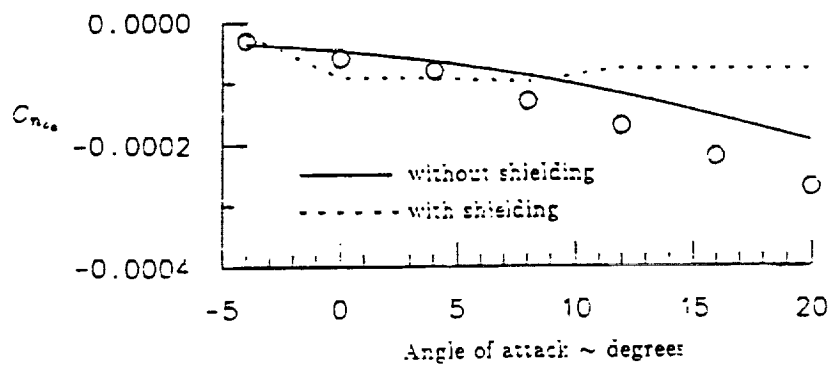


Fig. 117 Comparison Between Prediction With and Without Shielding and Experimentally Measured Yawing Moment Due to Aileron Deflection on the Hypersonic Research Airplane at Hypersonic Speed.
HRA ; $C_{n_{\delta_a}}$ vs. α ; $M = 6.0$; with and without shielding

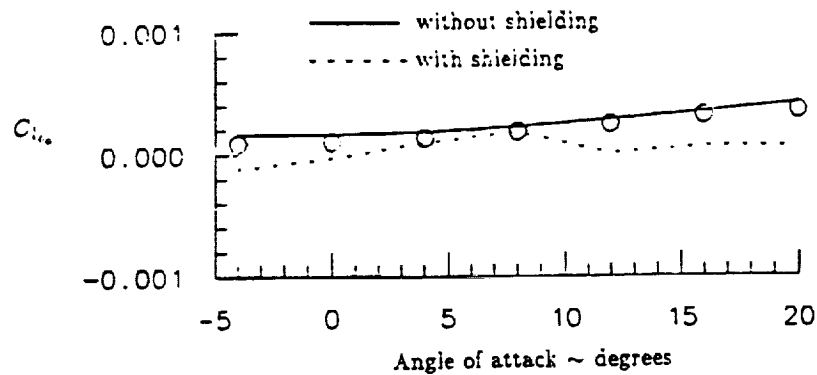


Fig. 118 Comparison Between Prediction With and Without Shielding and Experimentally Measured Rolling Moment Due to Aileron Deflection on the Hypersonic Research Airplane at Hypersonic Speed.
HRA ; $C_{l_{\delta_a}}$ vs. α ; $M = 6.0$; with and without shielding

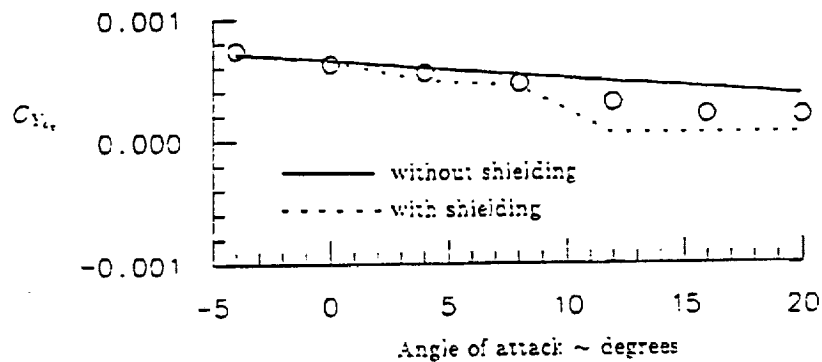


Fig. 119 Comparison Between Prediction With and Without Shielding and Experimentally Measured Side Force Due to Rudder Deflection on the Hypersonic Research Airplane at Hypersonic Speed.
HRA ; $C_{Y_{\delta_r}}$ vs. α ; $M = 6.0$; with and without shielding

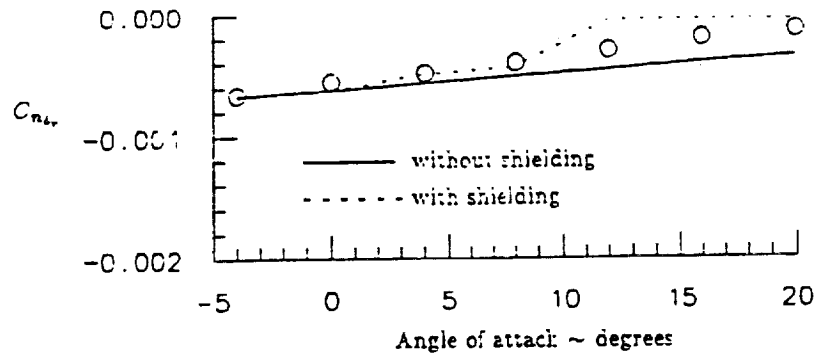


Fig. 120 Comparison Between Prediction With and Without Shielding and Experimentally Measured Yawing Moment Due to Rudder Deflection on the Hypersonic Research Airplane at Hypersonic Speed.
HRA ; $C_{n_{\dot{\alpha}}}$ vs. α ; $M = 6.0$; with and without shielding

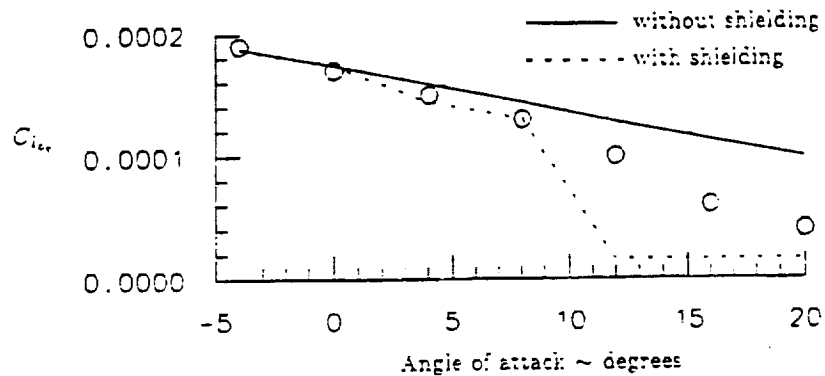


Fig. 121 Comparison Between Prediction With and Without Shielding and Experimentally Measured Rolling Moment Due to Rudder Deflection on the Hypersonic Research Airplane at Hypersonic Speed.
HRA ; $C_{l_{\dot{\alpha}}}$ vs. α ; $M = 6.0$; with and without shielding

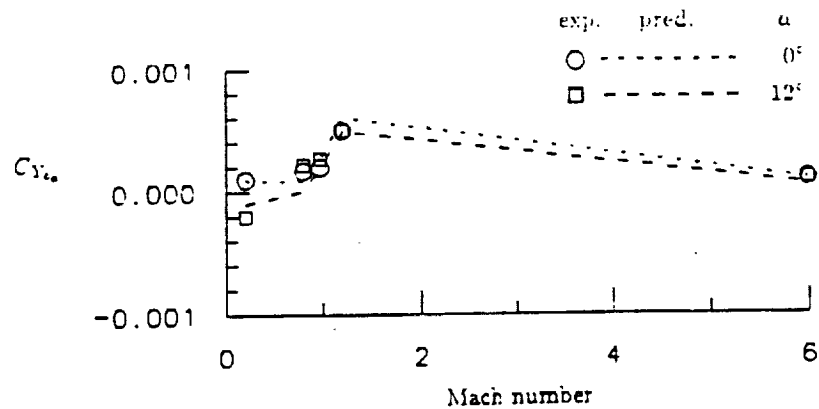


Fig. 122 Comparison Between Predicted and Experimentally Measured Side Force Due to Aileron Deflection on the Hypersonic Research Airplane as a Function of Mach Number at Two Angles of Attack.
HRA ; $C_{Y_{\delta_a}}$ vs. M ; $\alpha = 0^\circ$ and 12°

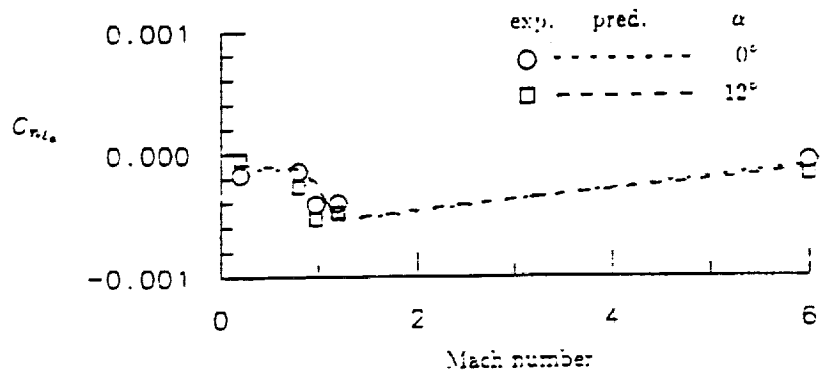


Fig. 123 Comparison Between Predicted and Experimentally Measured Yawing Moment Due to Aileron Deflection on the Hypersonic Research Airplane as a Function of Mach Number at Two Angles of Attack.
HRA ; $C_{n_{\delta_a}}$ vs. M ; $\alpha = 0^\circ$ and 12°

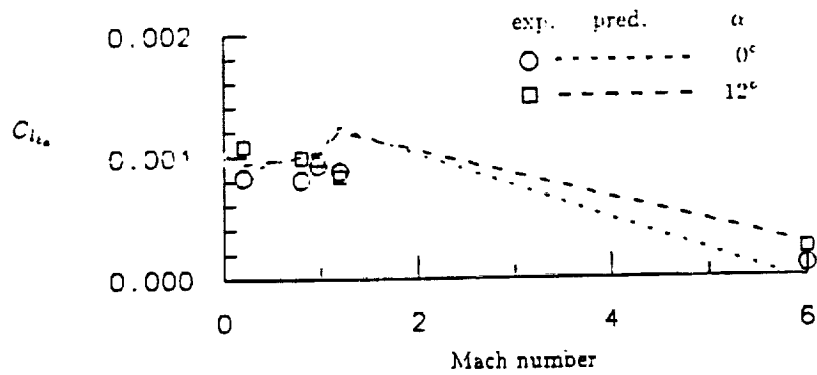


Fig. 124 Comparison Between Predicted and Experimentally Measured Rolling Moment Due to Aileron Deflection on the Hypersonic Research Airplane as a Function of Mach Number at Two Angles of Attack. HRA ; $C_{l_{\delta_a}}$ vs. M ; $\alpha = 0^\circ$ and 12°

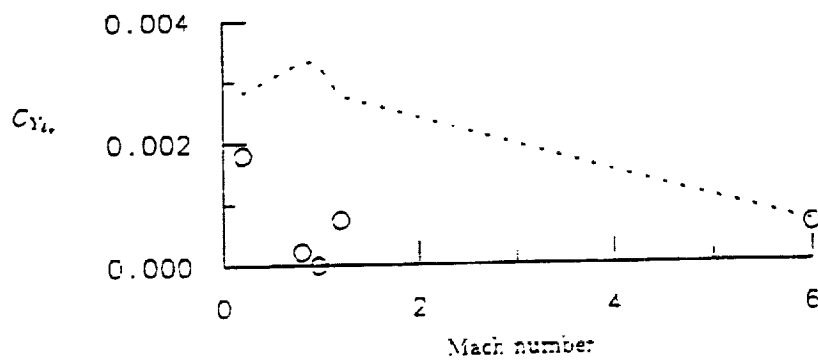


Fig. 125 Comparison Between Predicted and Experimentally Measured Side Force Due to Rudder Deflection on the Hypersonic Research Airplane as a Function of Mach Number. HRA ; $C_{Y_{\delta_r}}$ vs. M ; $\alpha = 0^\circ$

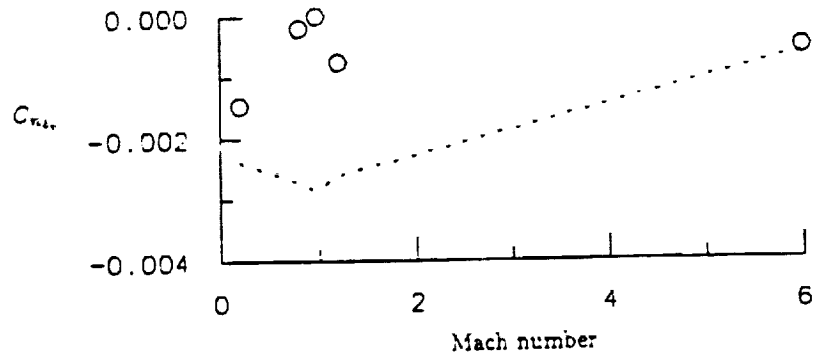


Fig. 126 Comparison Between Predicted and Experimentally Measured Yawing Moment Due to Rudder Deflection on the Hypersonic Research Airplane as a Function of Mach Number.
HRA ; $C_{n_{\delta_r}}$ vs. M ; $\alpha = 0^\circ$

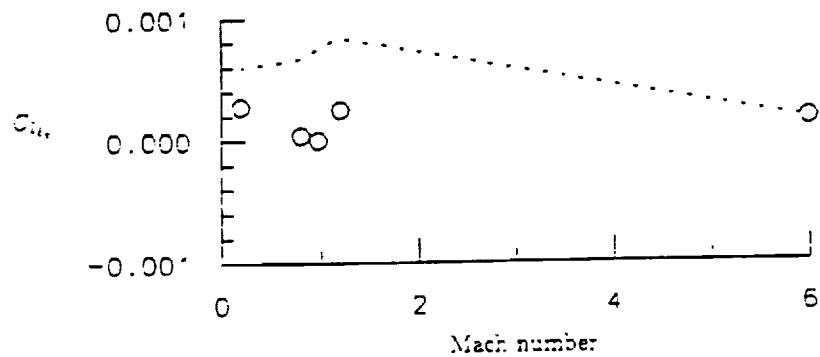


Fig. 127 Comparison Between Predicted and Experimentally Measured Rolling Moment Due to Rudder Deflection on the Hypersonic Research Airplane as a Function of Mach Number.
HRA ; $C_{l_{\delta_r}}$ vs. M ; $\alpha = 0^\circ$

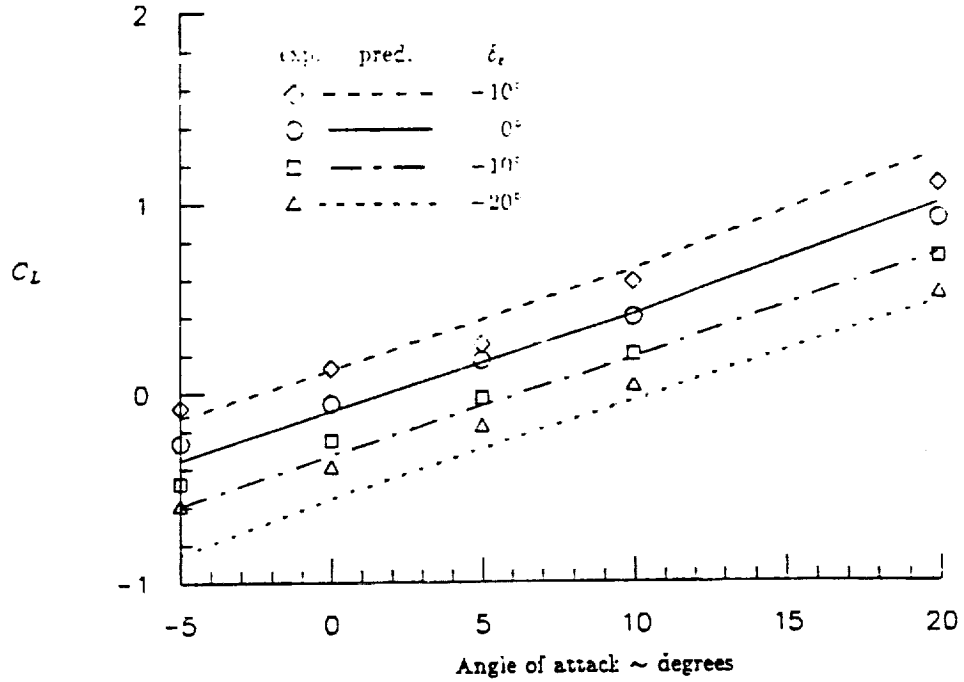


Fig. 128 Comparison Between Predicted and Experimentally Measured Lift on Shuttle Orbiter at Low Speed Including the Effect of Elevator Deflection. Shuttle ; C_L vs. α ; $M = 0.25$; $\delta_e = +10^\circ, 0^\circ, -10^\circ, \text{ and } -20^\circ$

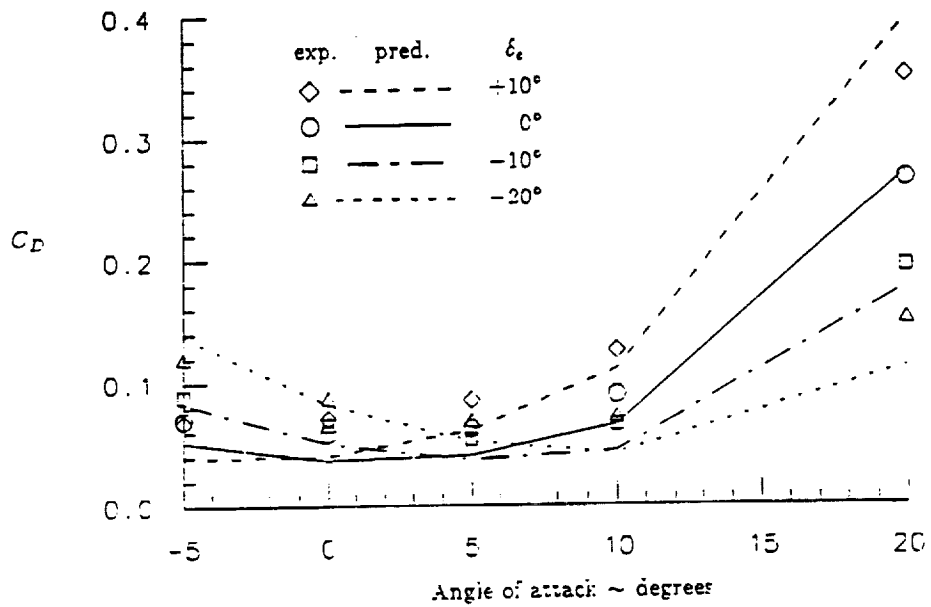


Fig. 129 Comparison Between Predicted and Experimentally Measured Drag on Shuttle Orbiter at Low Speed Including the Effect of Elevator Deflection. Shuttle ; C_D vs. α ; $M = 0.25$; $\delta_e = +10^\circ, 0^\circ, -10^\circ, \text{ and } -20^\circ$

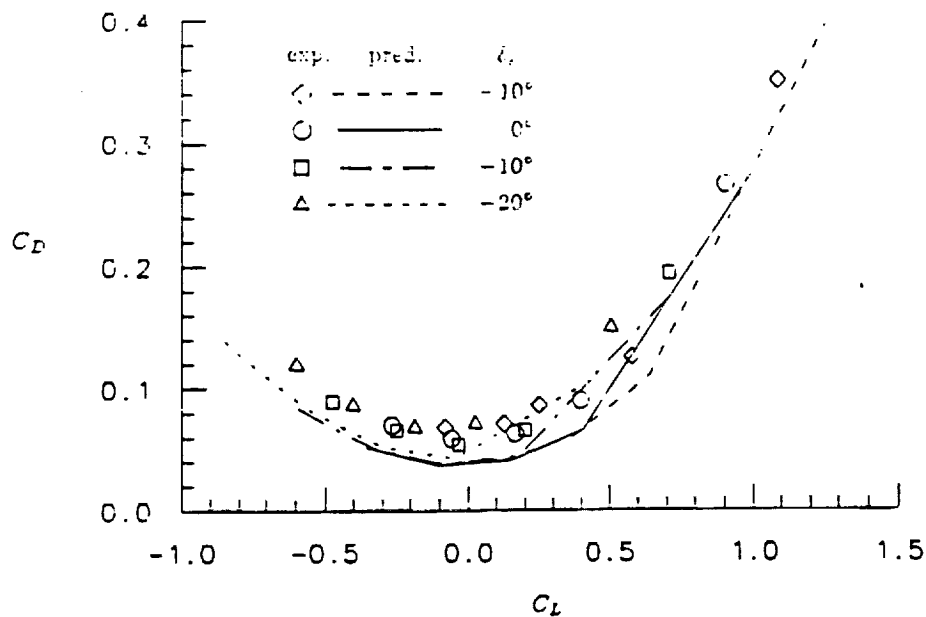


Fig. 130 Comparison Between Predicted and Experimentally Measured Drag as a Function of Lift on the Shuttle Orbiter at Low Speed Including the Effect of Elevator Deflection.
Shuttle ; C_D vs. C_L ; $M = 0.25$; $\delta_e = +10^\circ, 0^\circ, -10^\circ, \text{ and } -20^\circ$

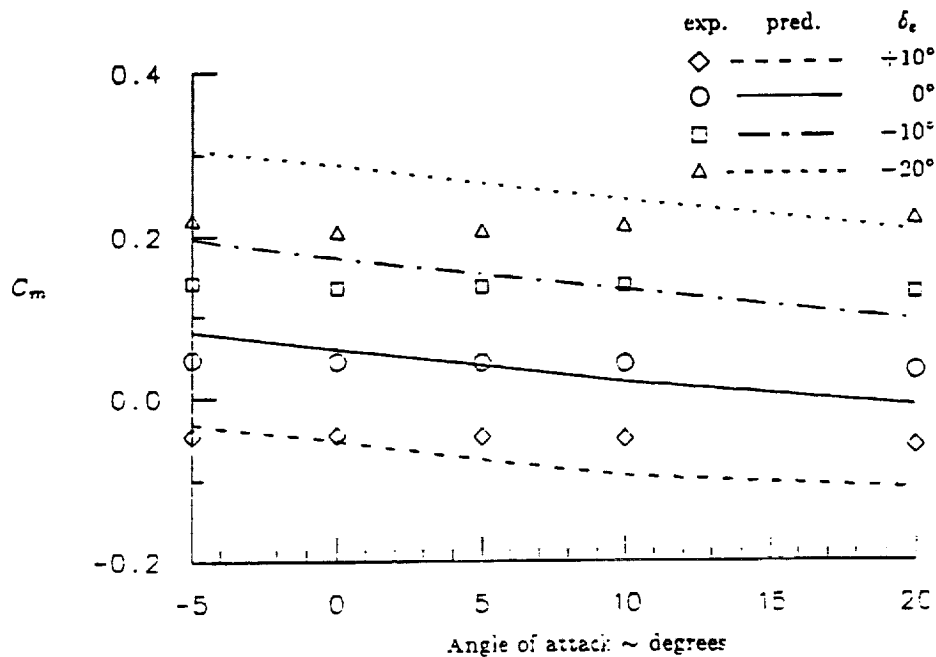


Fig. 131 Comparison Between Predicted and Experimentally Measured Moment on Shuttle Orbiter at Low Speed Including the Effect of Elevator Deflection.
Shuttle ; C_m vs. α ; $M = 0.25$; $\delta_e = +10^\circ, 0^\circ, -10^\circ, \text{ and } -20^\circ$

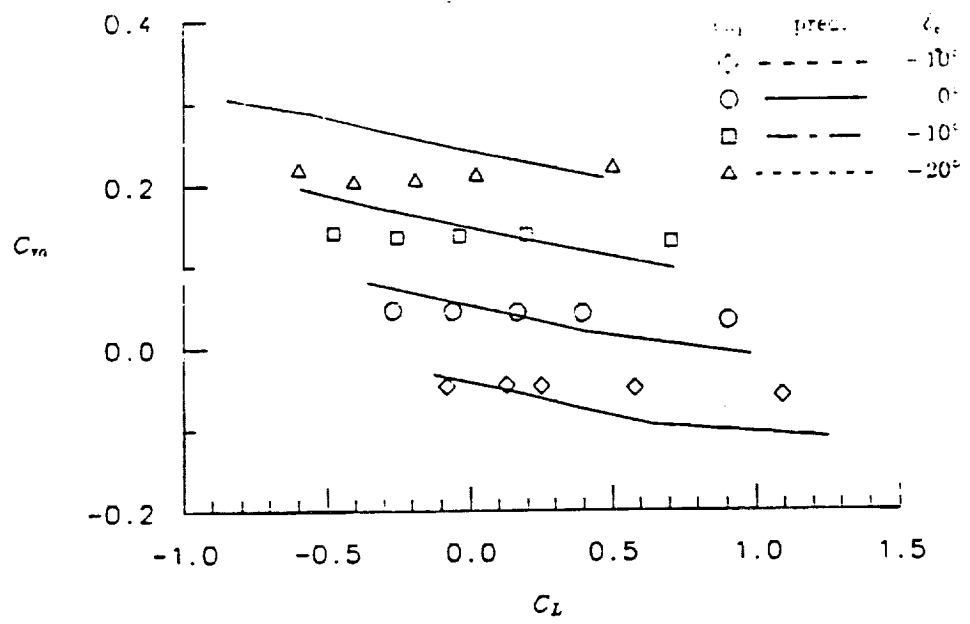


Fig. 132 Comparison Between Predicted and Experimentally Measured Moment as a Function of Lift on the Shuttle Orbiter at Low Speed Including the Effect of Elevator Deflection. Shuttle ; C_m vs. C_L ; $M = 0.25$; $\delta_e = +10^\circ, 0^\circ, -10^\circ, \text{ and } -20^\circ$

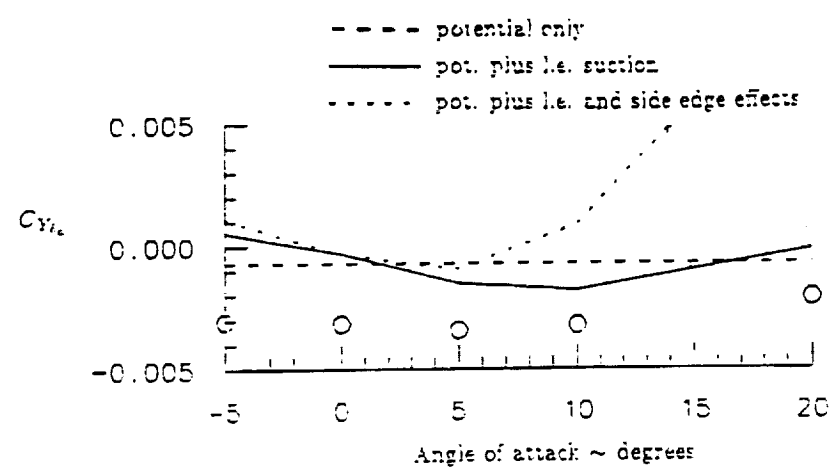


Fig. 133 Comparison Between Predicted and Experimentally Measured Side Force Due to Aileron Deflection on the Shuttle Orbiter at Low Speed Including the Effect of Different Modelling Techniques. Shuttle ; $C_{Y_{\delta_a}}$ vs. α ; $M = 0.25$

ORIGINAL PAGE IS
OF POOR QUALITY

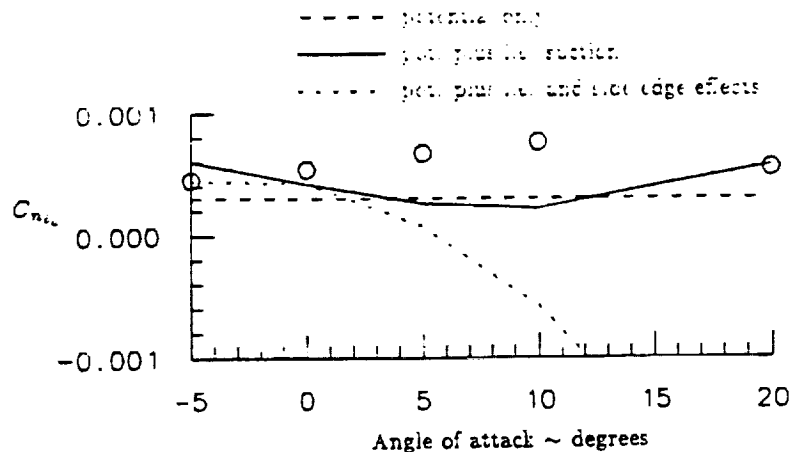


Fig. 134 Comparison Between Predicted and Experimentally Measured Yawing Moment Due to Aileron Deflection on the Shuttle Orbiter at Low Speed Including the Effect of Different Modelling Techniques. Shuttle ; $C_{n\delta_a}$ vs. α ; $M = 0.25$

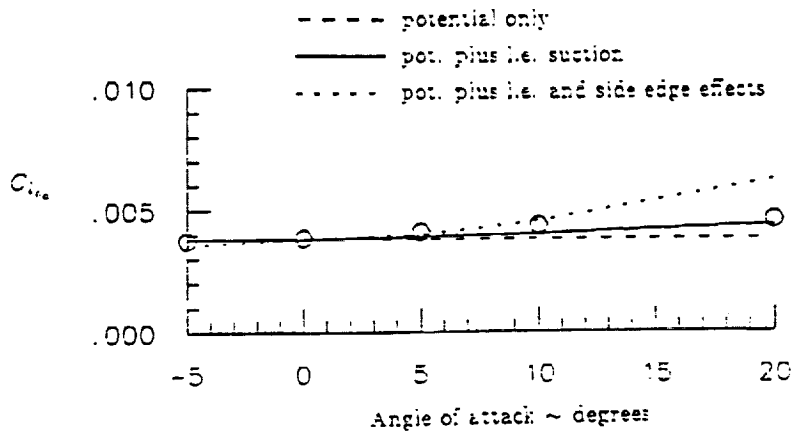


Fig. 135 Comparison Between Predicted and Experimentally Measured Rolling Moment Due to Aileron Deflection on the Shuttle Orbiter at Low Speed Including the Effect of Different Modelling Techniques. Shuttle ; $C_{l\delta_a}$ vs. α ; $M = 0.25$

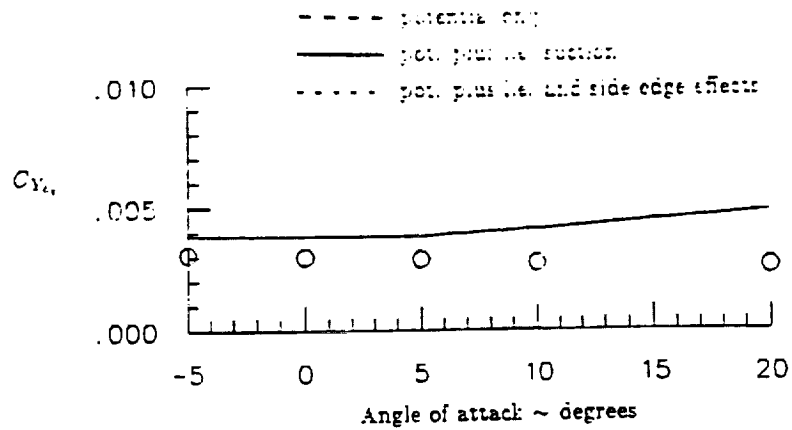


Fig. 136 Comparison Between Predicted and Experimentally Measured Side Force Due to Rudder Deflection on the Shuttle Orbiter at Low Speed. Shuttle ; $C_{Y\delta}$ vs. α ; $M = 0.25$

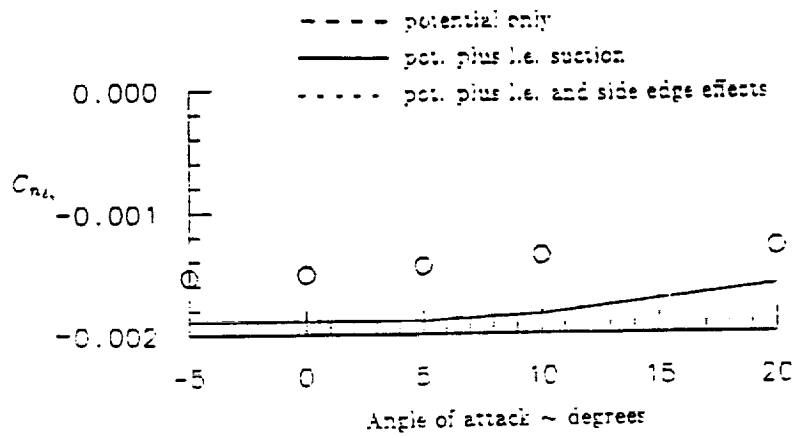


Fig. 137 Comparison Between Predicted and Experimentally Measured Yawing Moment Due to Rudder Deflection on the Shuttle Orbiter at Low Speed. Shuttle ; $C_{n\delta}$ vs. α ; $M = 0.25$

ORIGINAL PAGE IS
OF POOR QUALITY

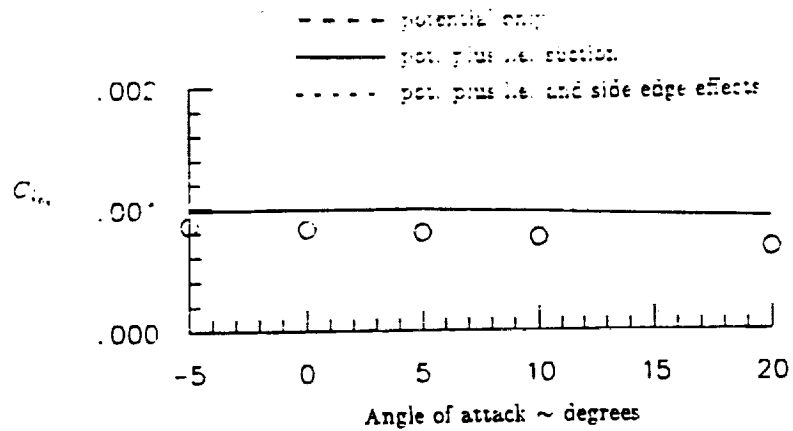


Fig. 138 Comparison Between Predicted and Experimentally Measured Rolling Moment Due to Rudder Deflection on the Shuttle Orbiter at Low Speed. Shuttle ; $C_{l_{\delta_e}}$ vs. α ; $M = 0.25$

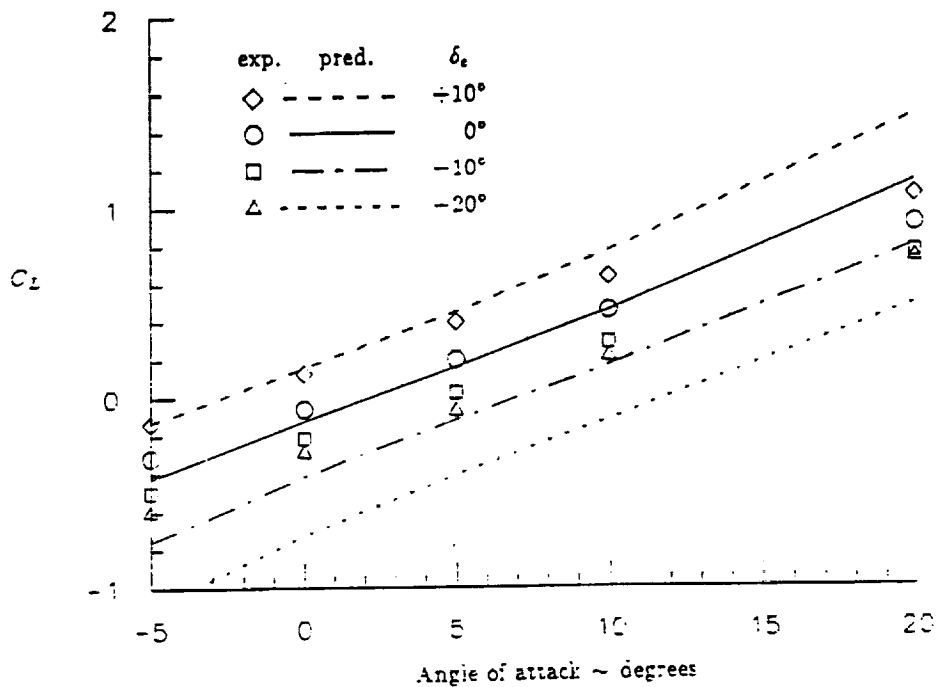


Fig. 139 Comparison Between Predicted and Experimentally Measured Lift on the Shuttle Orbiter at High Subsonic Speed Including the Effect of Elevator Deflection. Shuttle ; C_L vs. α ; $M = 0.8$; $\delta_e = +10^\circ, 0^\circ, -10^\circ, \text{ and } -20^\circ$

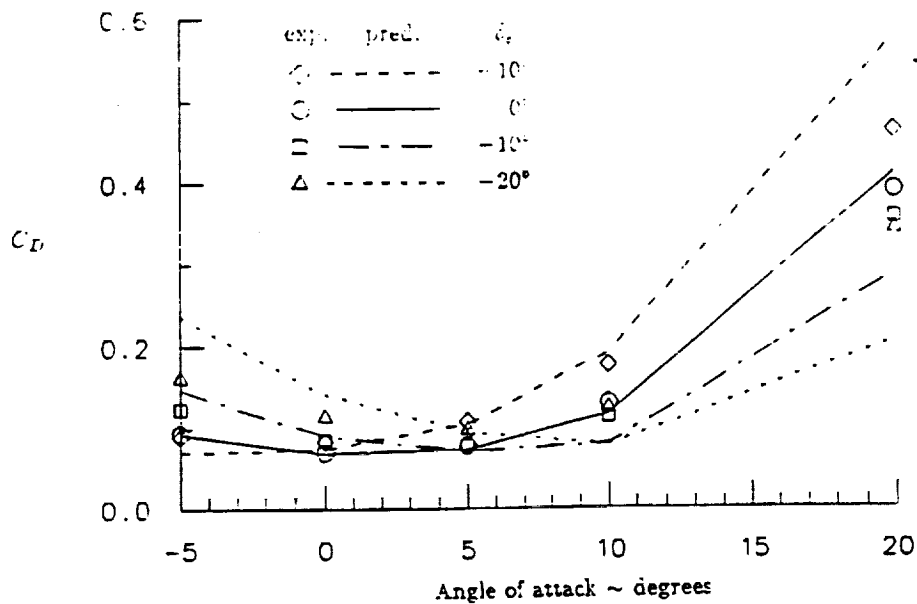


Fig. 140 Comparison Between Predicted and Experimentally Measured Drag on the Shuttle Orbiter at High Subsonic Speed Including the Effect of Elevator Deflection.
Shuttle ; C_D vs. α ; $M = 0.8$; $\delta_e = +10^\circ, 0^\circ, -10^\circ, \text{ and } -20^\circ$

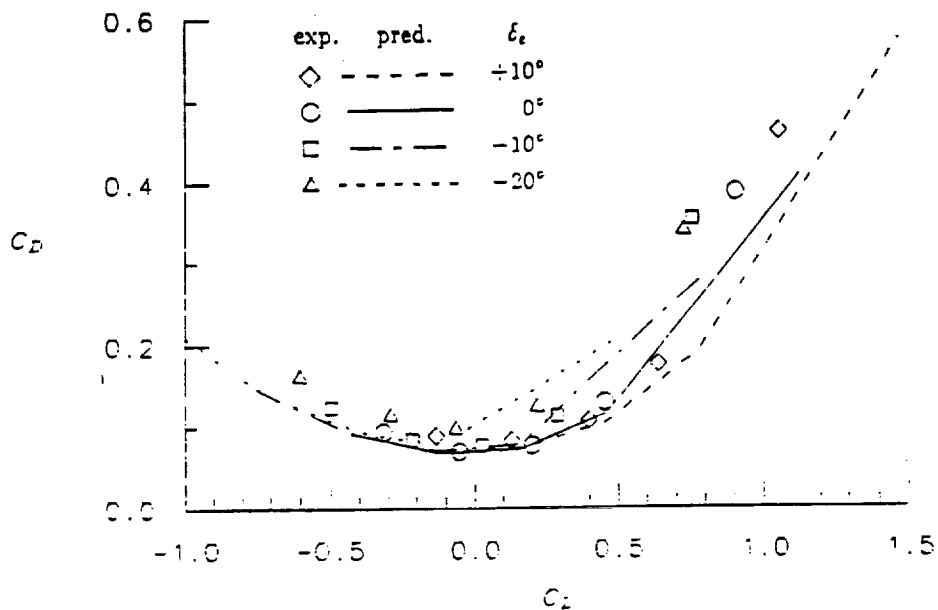


Fig. 141 Comparison Between Predicted and Experimentally Measured Drag as a Function of Lift on the Shuttle Orbiter at High Subsonic Speed Including the Effect of Elevator Deflection.
Shuttle ; C_D vs. C_L ; $M = 0.8$; $\delta_e = +10^\circ, 0^\circ, -10^\circ, \text{ and } -20^\circ$

ORIGINAL PAGE IS
OF POOR QUALITY

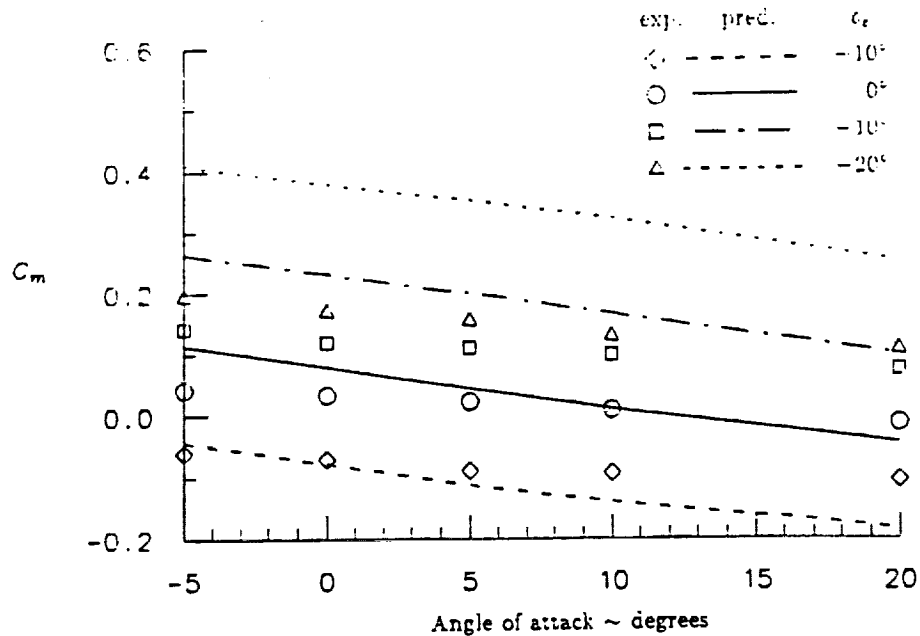


Fig. 142 Comparison Between Predicted and Experimentally Measured Moment on the Shuttle Orbiter at High Subsonic Speed Including the Effect of Elevator Deflection.
Shuttle ; C_m vs. α ; $M = 0.8$; $\delta_e = +10^\circ, 0^\circ, -10^\circ, \text{ and } -20^\circ$

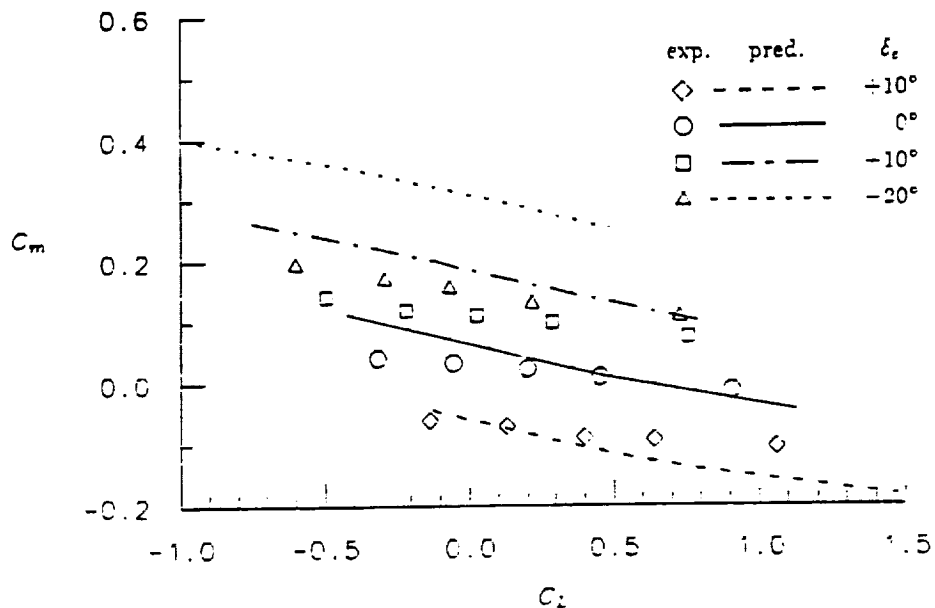


Fig. 143 Comparison Between Predicted and Experimentally Measured Moment as a Function of Lift on the Shuttle Orbiter at High Subsonic Speed Including the Effect of Elevator Deflection.
Shuttle ; C_m vs. C_L ; $M = 0.8$; $\delta_e = +10^\circ, 0^\circ, -10^\circ, \text{ and } -20^\circ$

ORIGINAL PAGE IS
OF POOR QUALITY

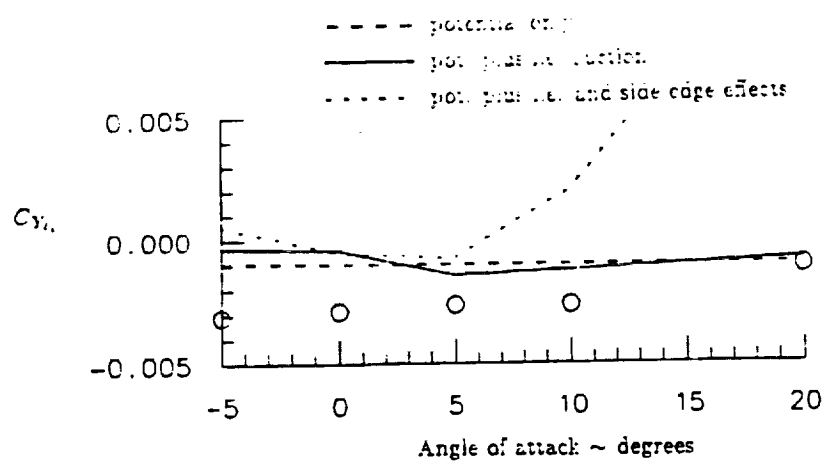


Fig. 144 Comparison Between Predicted and Experimentally Measured Side Force Due to Aileron Deflection on the Shuttle Orbiter at High Subsonic Speed Including the Effect of Different Modelling Techniques. Shuttle ; $C_{Y_{\delta_a}}$ vs. α ; $M = 0.8$

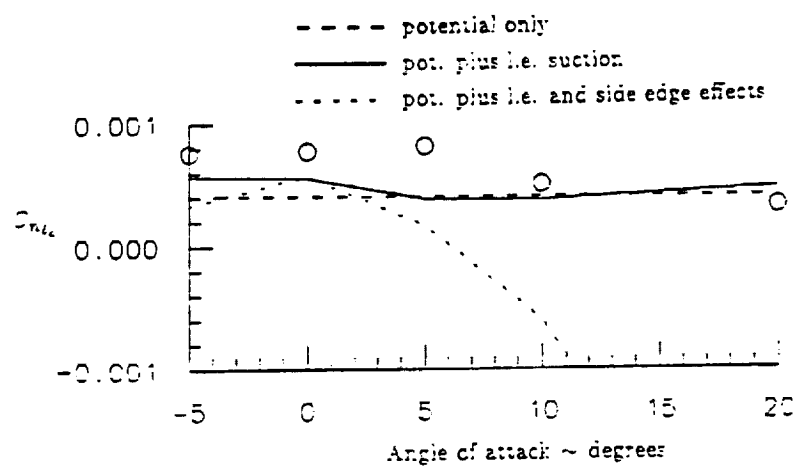


Fig. 145 Comparison Between Predicted and Experimentally Measured Yawing Moment Due to Aileron Deflection on the Shuttle Orbiter at High Subsonic Speed Including the Effect of Different Modelling Techniques. Shuttle ; $C_{n_{\delta_a}}$ vs. α ; $M = 0.8$

ORIGINAL PAGE IS
OF POOR QUALITY

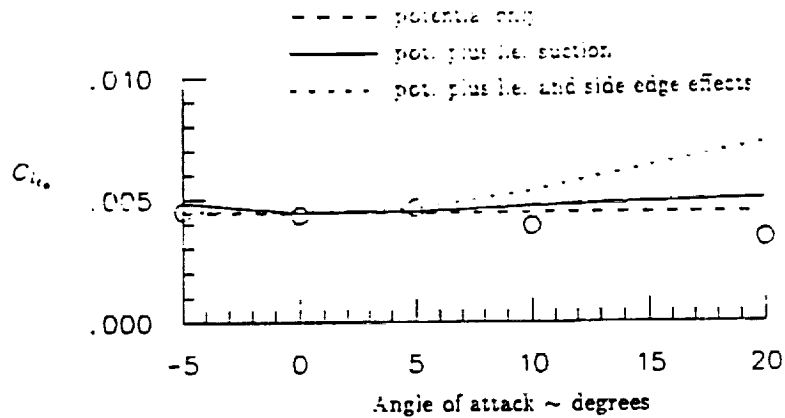


Fig. 146 Comparison Between Predicted and Experimentally Measured Rolling Moment Due to Aileron Deflection on the Shuttle Orbiter at High Subsonic Speed Including the Effect of Different Modelling Techniques. Shuttle ; C_{l_a} vs. α ; $M = 0.8$

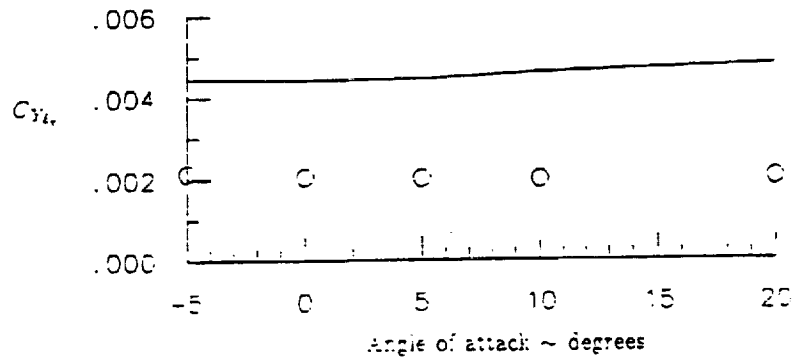


Fig. 147 Comparison Between Predicted and Experimentally Measured Side Force Due to Rudder Deflection on the Shuttle Orbiter at High Subsonic Speed. Shuttle ; C_{Y_a} vs. α ; $M = 0.8$

ORIGINAL PAGE IS
OF POOR QUALITY

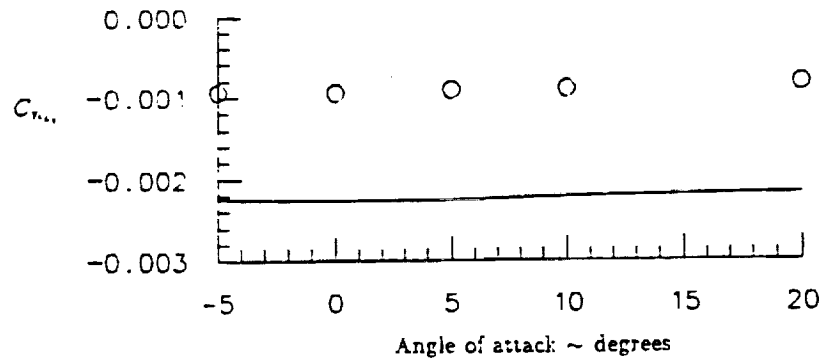


Fig. 148 Comparison Between Predicted and Experimentally Measured Yawing Moment Due to Rudder Deflection on the Shuttle Orbiter at High Subsonic Speed.
Shuttle ; $C_{n\delta_r}$ vs. α ; $M = 0.8$

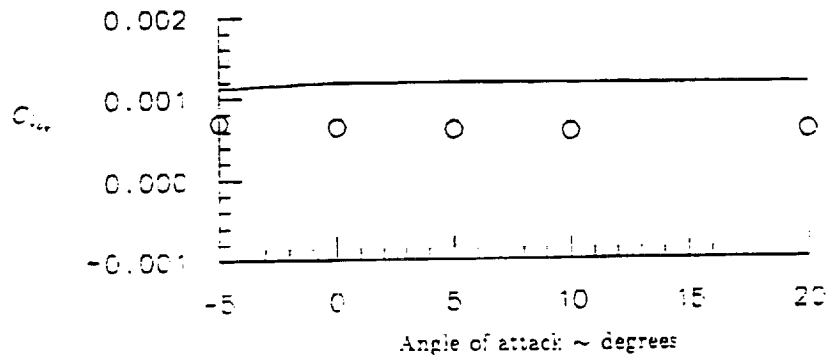


Fig. 149 Comparison Between Predicted and Experimentally Measured Rolling Moment Due to Rudder Deflection on the Shuttle Orbiter at High Subsonic Speed.
Shuttle ; $C_{l\delta_r}$ vs. α ; $M = 0.8$

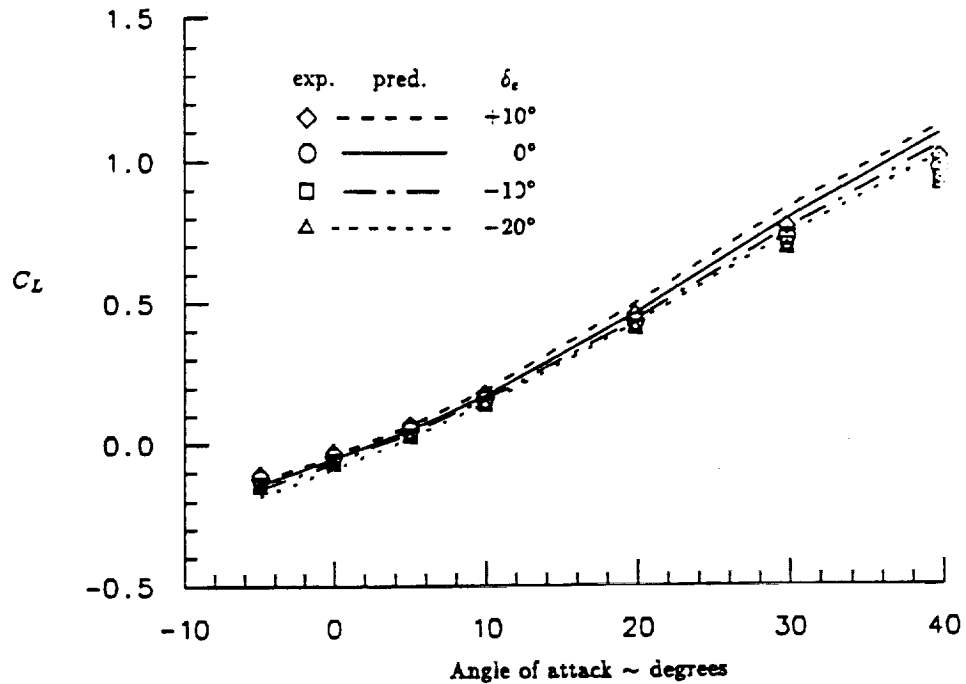


Fig. 150 Comparison Between Predicted and Experimentally Measured Lift on the Shuttle Orbiter at Hypersonic Speed Including the Effect of Elevator Deflection. Shuttle ; C_L vs. α ; $M = 5.0$; $\delta_e = +10^\circ, 0^\circ, -10^\circ, \text{ and } -20^\circ$

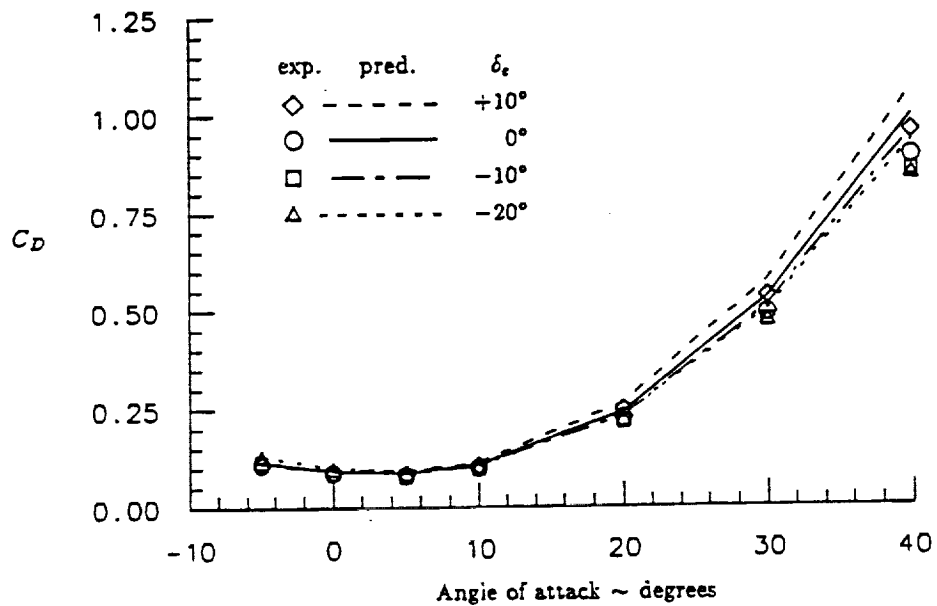


Fig. 151 Comparison Between Predicted and Experimentally Measured Drag on the Shuttle Orbiter at Hypersonic Speed Including the Effect of Elevator Deflection. Shuttle ; C_D vs. α ; $M = 5.0$; $\delta_e = +10^\circ, 0^\circ, -10^\circ, \text{ and } -20^\circ$

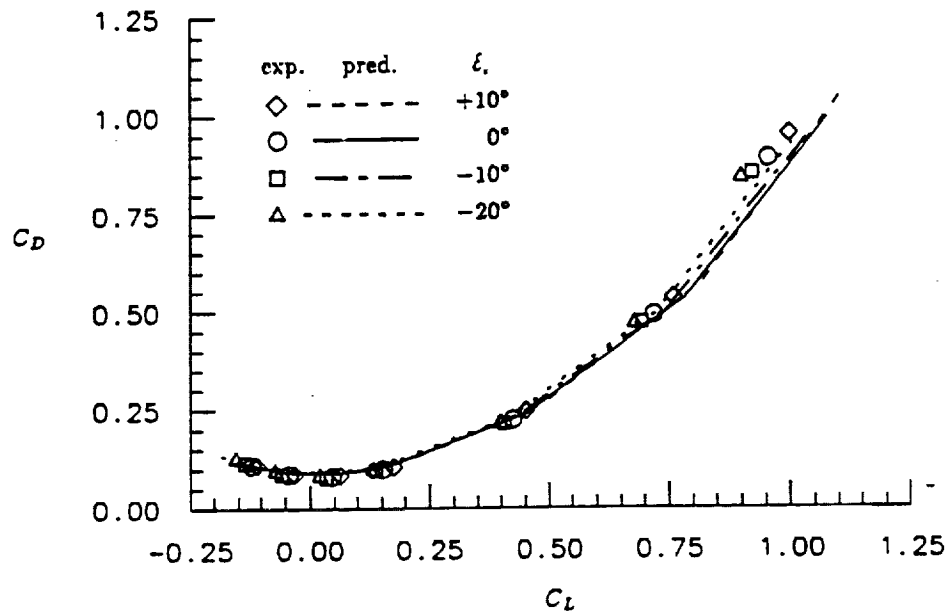


Fig. 152 Comparison Between Predicted and Experimentally Measured Drag as a Function of Lift on the Shuttle Orbiter at Hypersonic Speed Including the Effect of Elevator Deflection. Shuttle ; C_D vs. C_L ; $M = 5.0$; $\delta_e = +10^\circ, 0^\circ, -10^\circ, \text{ and } -20^\circ$

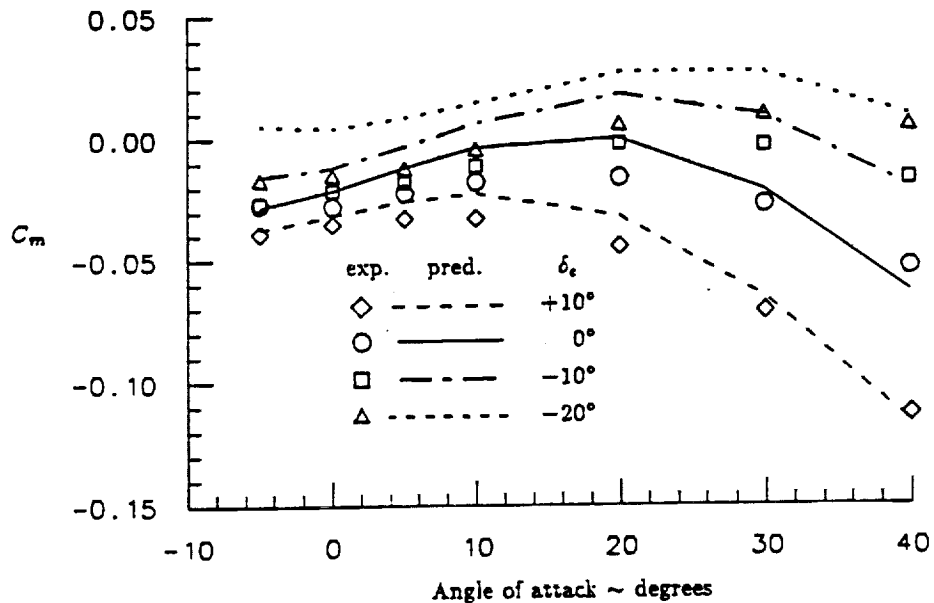


Fig. 153 Comparison Between Predicted and Experimentally Measured Moment on the Shuttle Orbiter at Hypersonic Speed Including the Effect of Elevator Deflection. Shuttle ; C_m vs. α ; $M = 5.0$; $\delta_e = +10^\circ, 0^\circ, -10^\circ, \text{ and } -20^\circ$

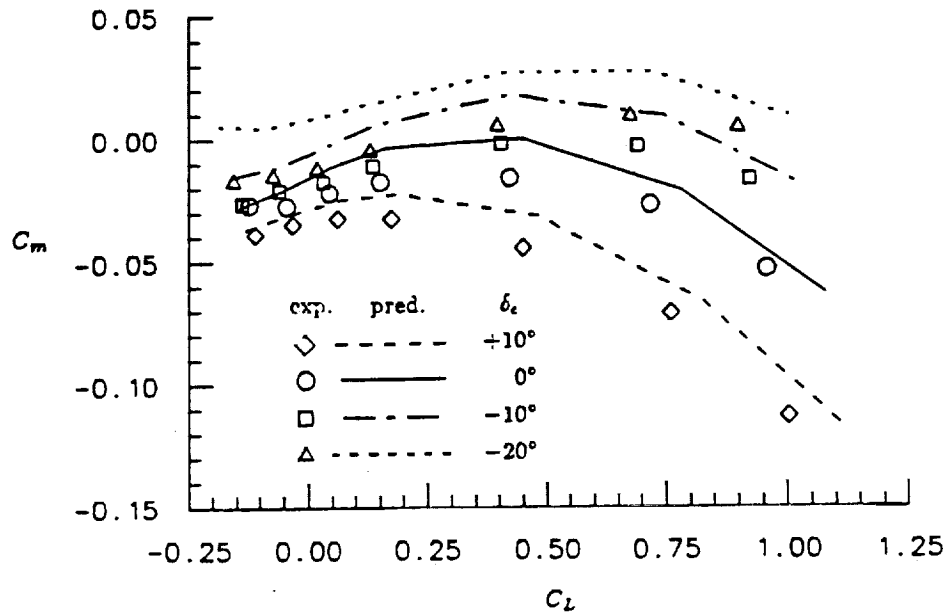


Fig. 154 Comparison Between Predicted and Experimentally Measured Moment as a Function of Lift on the Shuttle Orbiter at Hypersonic Speed Including the Effect of Elevator Deflection. Shuttle ; C_m vs. C_L ; $M = 5.0$; $\delta_e = +10^\circ, 0^\circ, -10^\circ, \text{ and } -20^\circ$

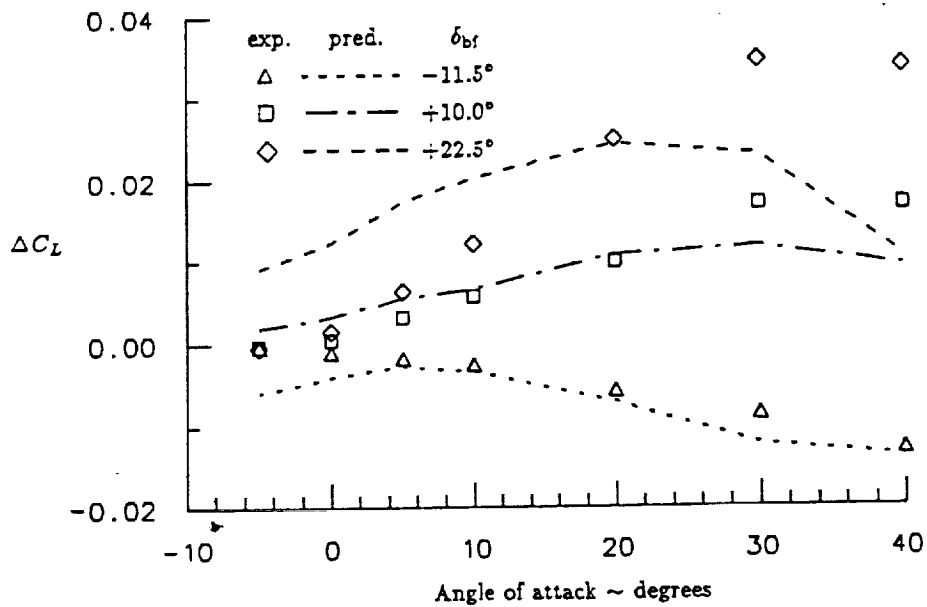


Fig. 155 Comparison Between Predicted and Experimentally Measured Lift on the Shuttle Orbiter at Hypersonic Speed Including the Effect of Body Flap Deflection. Shuttle ; ΔC_L vs. α ; $M = 5.0$; $\delta_{bf} = -11.5^\circ, +10.0^\circ, \text{ and } +22.5^\circ$

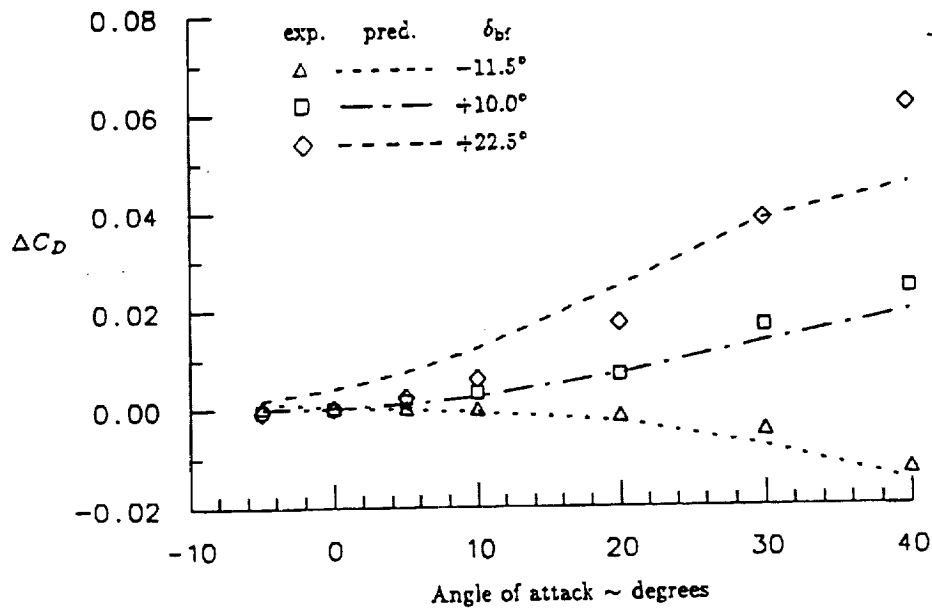


Fig. 156 Comparison Between Predicted and Experimentally Measured Drag on the Shuttle Orbiter at Hypersonic Speed Including the Effect of Body Flap Deflection.
Shuttle ; ΔC_D vs. α ; $M = 5.0$; $\delta_{bf} = -11.5^\circ, +10.0^\circ, \text{ and } +22.5^\circ$

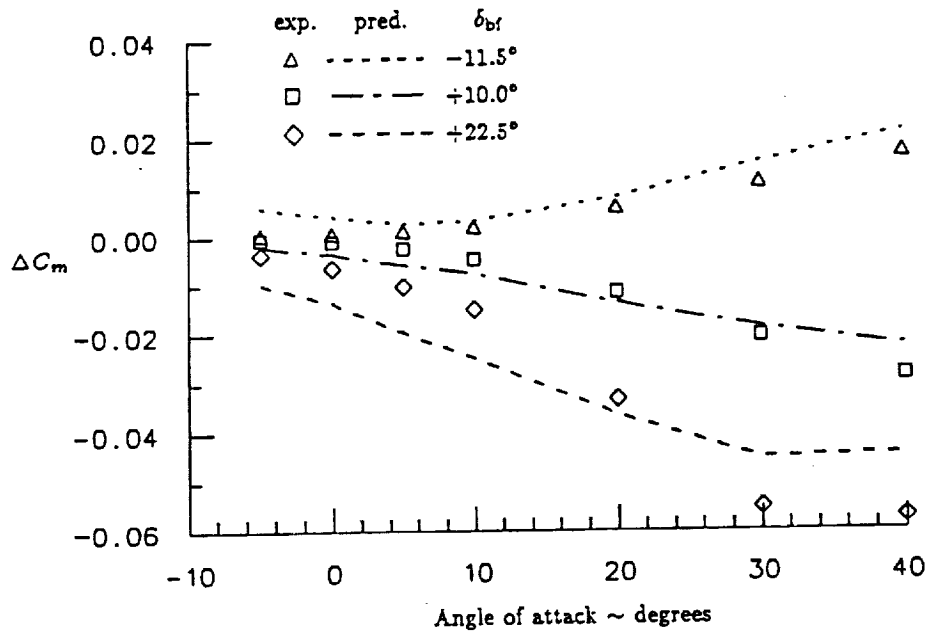


Fig. 157 Comparison Between Predicted and Experimentally Measured Moment on the Shuttle Orbiter at Hypersonic Speed Including the Effect of Body Flap Deflection.
Shuttle ; ΔC_m vs. α ; $M = 5.0$; $\delta_{bf} = -11.5^\circ, +10.0^\circ, \text{ and } +22.5^\circ$

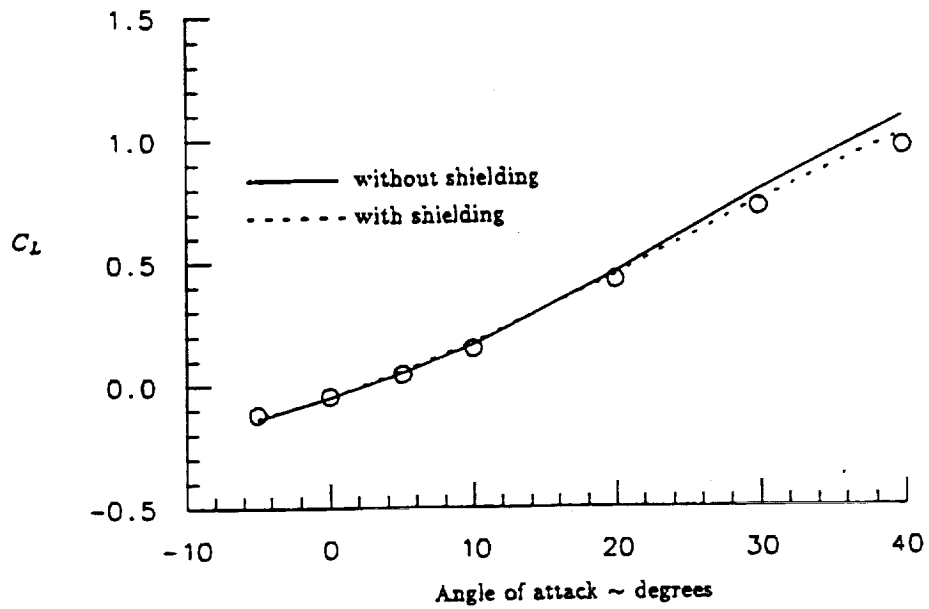


Fig. 158 The Effect of Shielding on the Predicted Lift on the Shuttle Vehicle at Hypersonic Speed.
 Shuttle ; C_L vs. α ; $M = 5.0$; with and without shielding

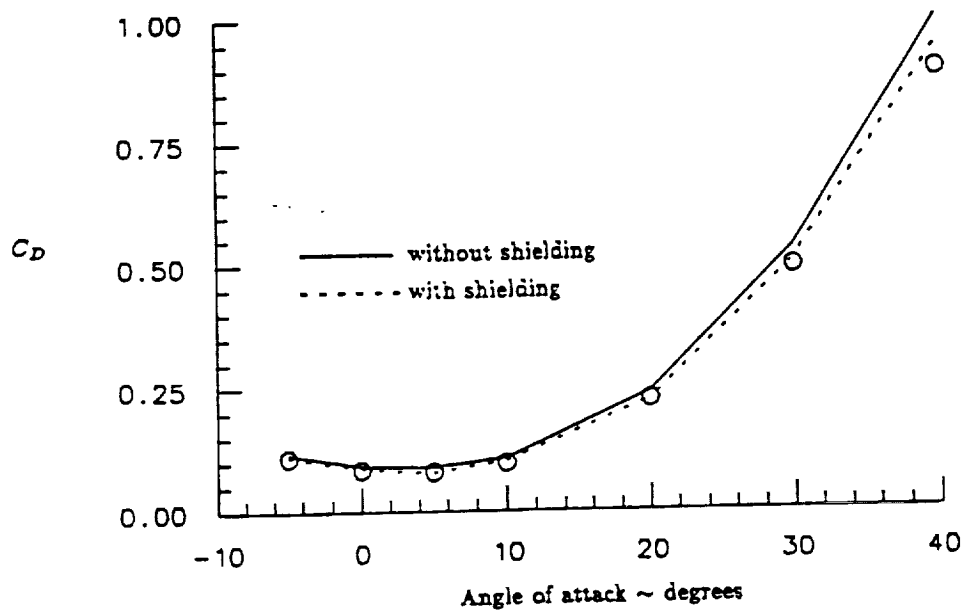


Fig. 159 The Effect of Shielding on the Predicted Drag on the Shuttle Vehicle at Hypersonic Speed.
 Shuttle ; C_D vs. α ; $M = 5.0$; with and without shielding

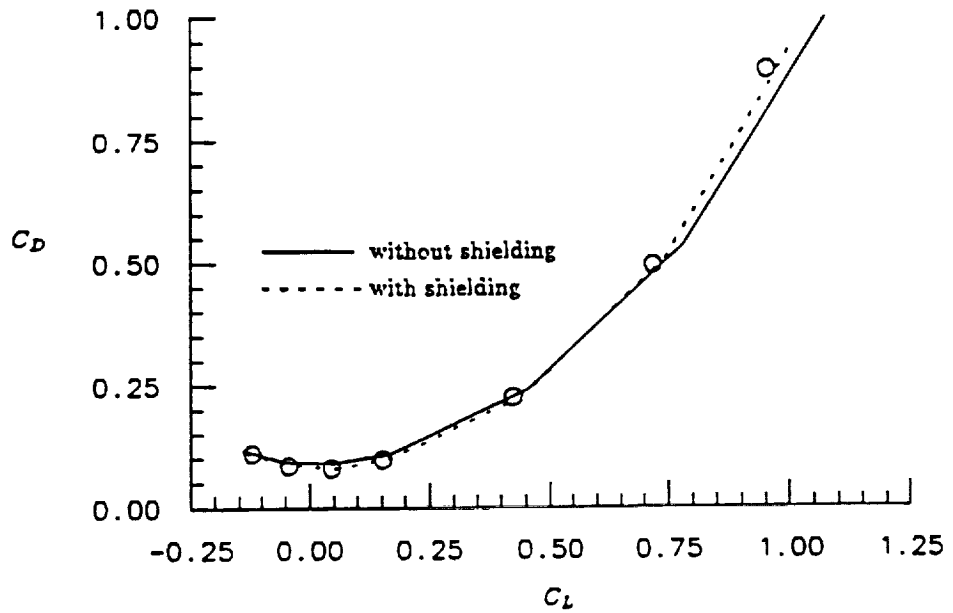


Fig. 160 The Effect of Shielding on the Predicted Drag as a Function of Lift on the Shuttle Vehicle at Hypersonic Speed.
 Shuttle ; C_D vs. C_L ; $M = 5.0$; with and without shielding

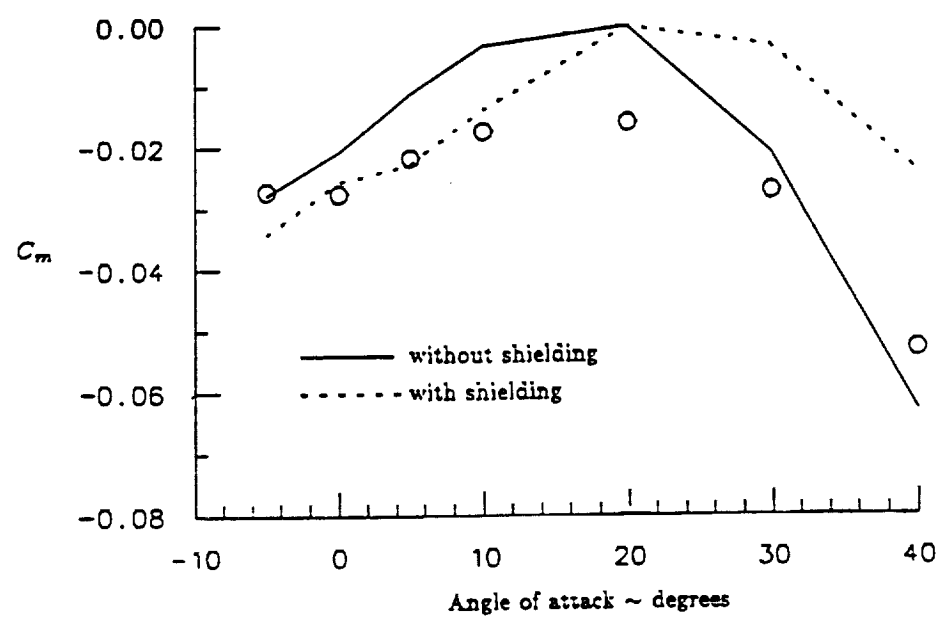


Fig. 161 The Effect of Shielding on the Predicted Moment on the Shuttle Orbiter at Hypersonic Speed.
 Shuttle ; C_m vs. α ; $M = 5.0$; with and without shielding

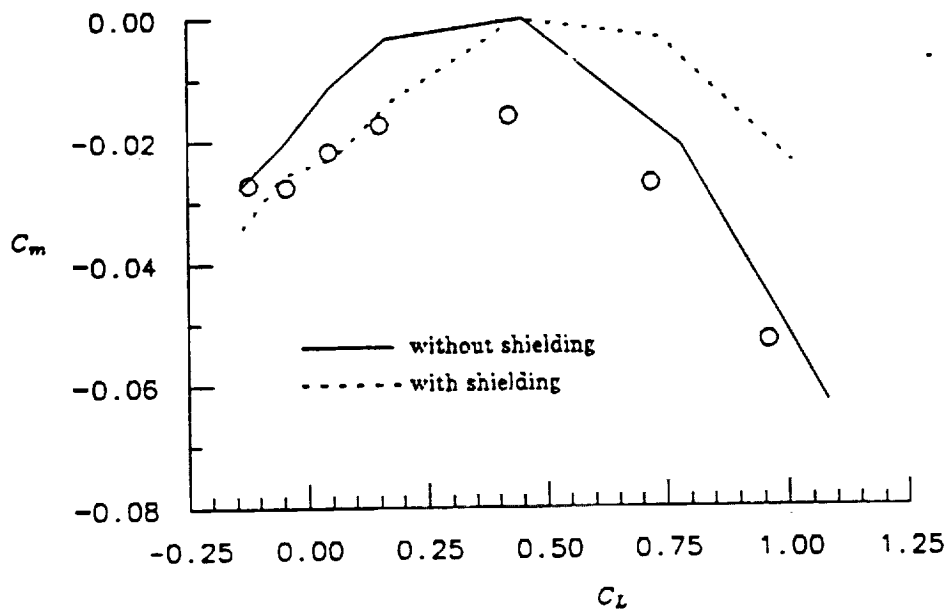


Fig. 162 The Effect of Shielding on the Predicted Moment as a Function of Lift on the Shuttle Orbiter at Hypersonic Speed. Shuttle ; C_m vs. C_L ; $M = 5.0$; with and without shielding

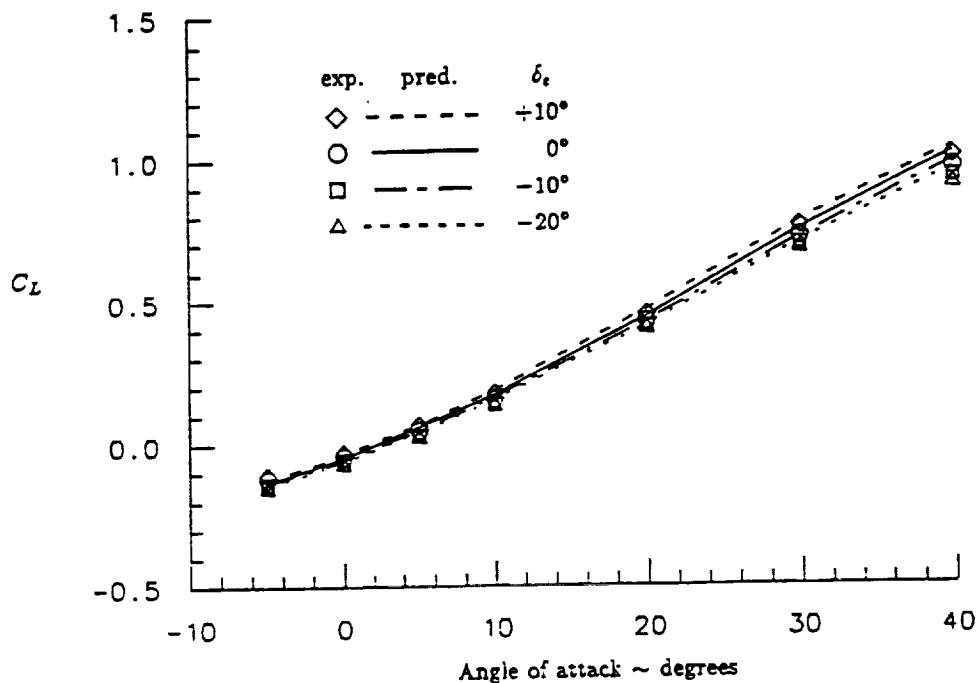


Fig. 163 Comparison Between Prediction With Shielding and Experimentally Measured Lift on the Shuttle Orbiter at Hypersonic Speed Including the Effect of Elevator Deflection. Shuttle ; C_L vs. α ; $M = 5.0$; $\delta_e = +10^\circ, 0^\circ, -10^\circ, \text{ and } -20^\circ$; with shielding

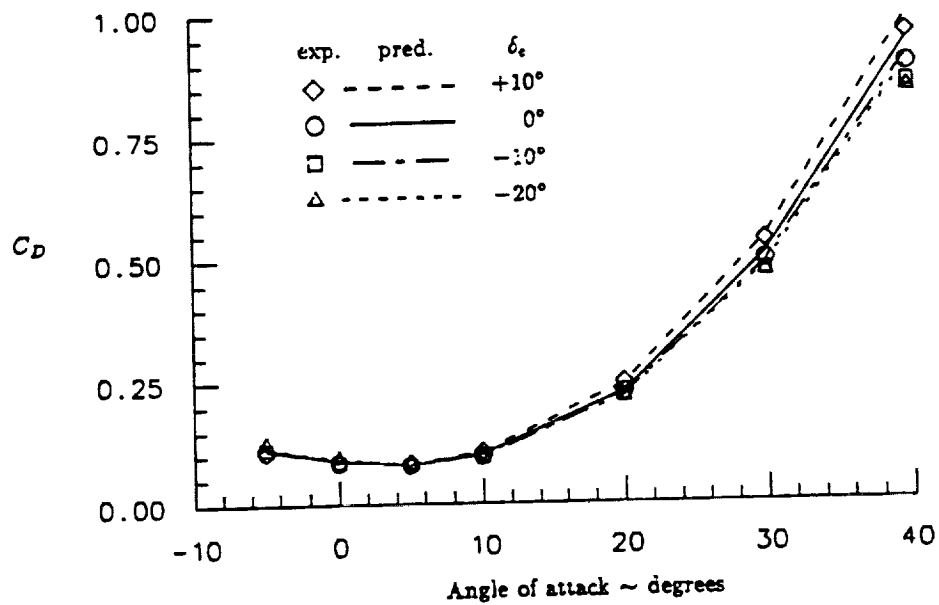


Fig. 164 Comparison Between Prediction With Shielding and Experimentally Measured Drag on the Shuttle Orbiter at Hypersonic Speed Including the Effect of Elevator Deflection. Shuttle ; C_D vs. α ; $M = 5.0$; $\delta_e = +10^\circ, 0^\circ, -10^\circ, \text{ and } -20^\circ$; with shielding

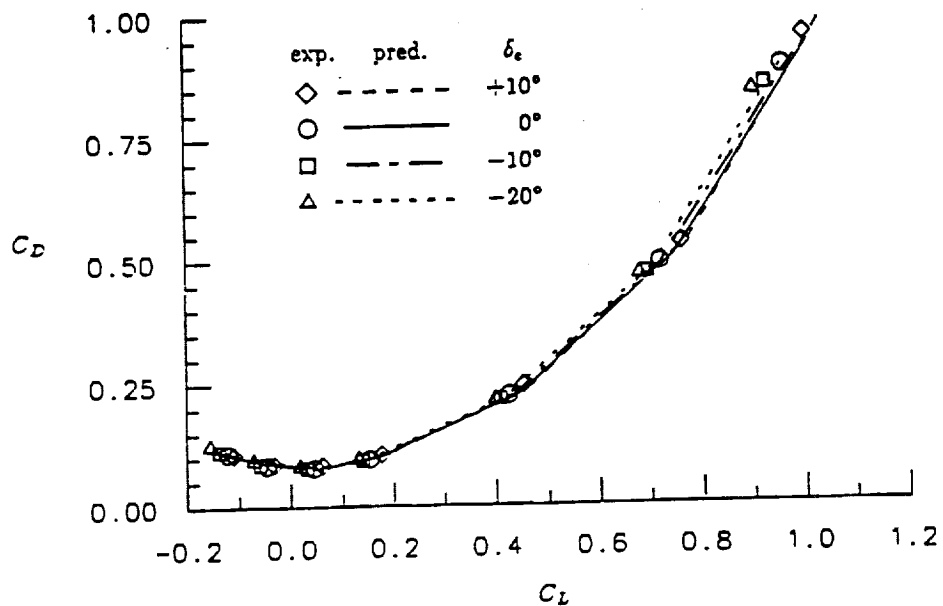


Fig. 165 Comparison Between Prediction With Shielding and Experimentally Measured Drag as a Function of Lift on the Shuttle Orbiter at Hypersonic Speed Including the Effect of Elevator Deflection. Shuttle ; C_D vs. C_L ; $M = 5.0$; $\delta_e = +10^\circ, 0^\circ, -10^\circ, \text{ and } -20^\circ$; with shielding

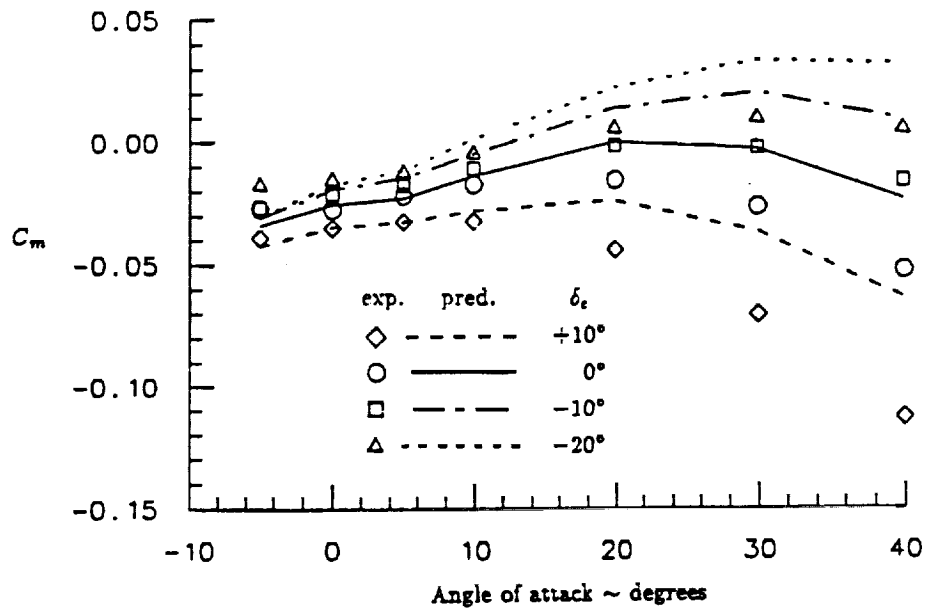


Fig. 166 Comparison Between Prediction With Shielding and Experimentally Measured Moment on the Shuttle Orbiter at Hypersonic Speed Including the Effect of Elevator Deflection. Shuttle ; C_m vs. α ; $M = 5.0$; $\delta_e = +10^\circ, 0^\circ, -10^\circ, \text{ and } -20^\circ$; with shielding

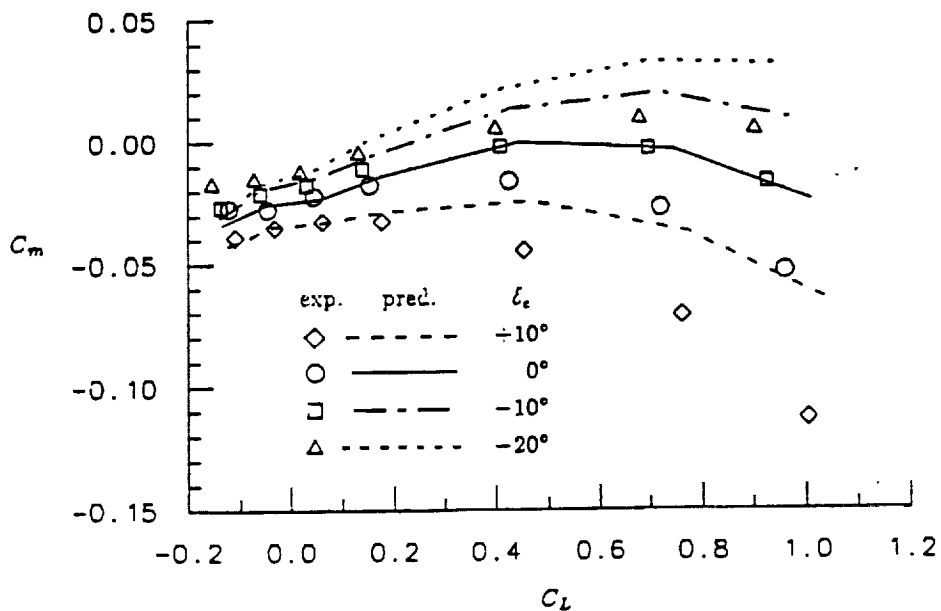


Fig. 167 Comparison Between Prediction With Shielding and Experimentally Measured Moment as a Function of Lift on the Shuttle Orbiter at Hypersonic Speed Including the Effect of Elevator Deflection. Shuttle ; C_m vs. C_L ; $M = 5.0$; $\delta_e = +10^\circ, 0^\circ, -10^\circ, \text{ and } -20^\circ$; with shielding

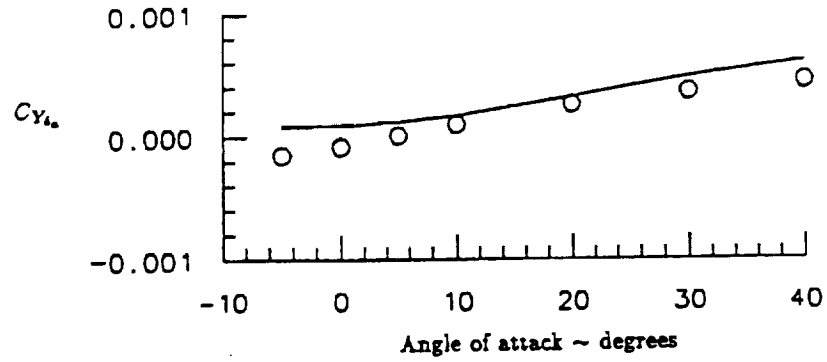


Fig. 168 Comparison Between Predicted and Experimentally Measured Side Force Due to Aileron Deflection on the Shuttle Orbiter at Hypersonic Speed. Shuttle ; $C_{Y\delta_a}$ vs. α ; $M = 5.0$

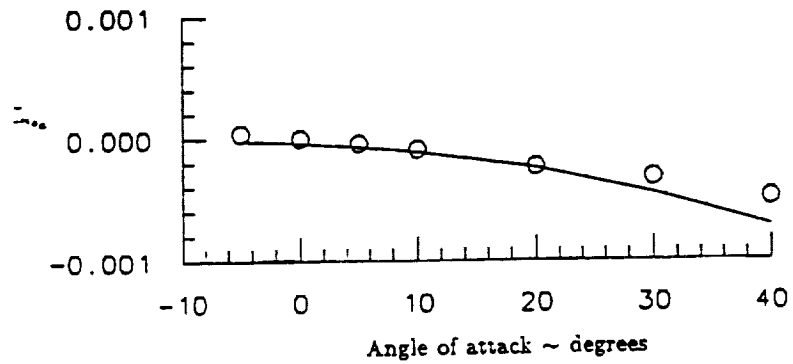


Fig. 169 Comparison Between Predicted and Experimentally Measured Yawing Moment Due to Aileron Deflection on the Shuttle Orbiter at Hypersonic Speed. Shuttle ; $C_{n\delta_a}$ vs. α ; $M = 5.0$

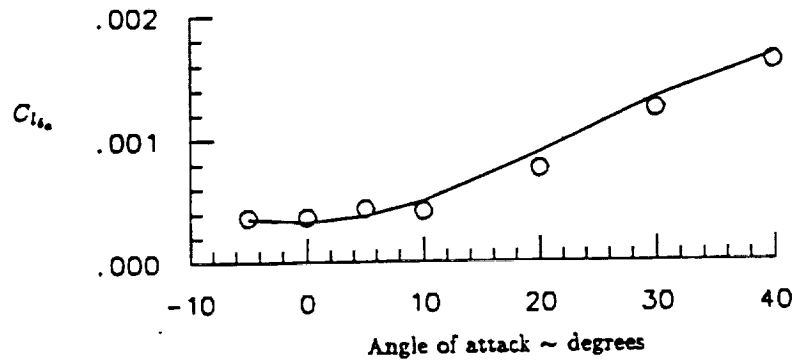


Fig. 170 Comparison Between Predicted and Experimentally Measured Rolling Moment Due to Aileron Deflection on the Shuttle Orbiter at Hypersonic Speed.
Shuttle ; $C_{l_{\delta_a}}$ vs. α ; $M = 5.0$

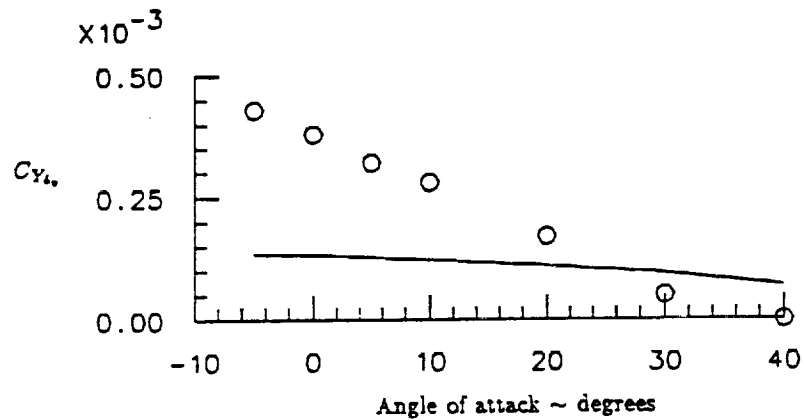


Fig. 171 Comparison Between Predicted and Experimentally Measured Side Force Due to Rudder Deflection on the Shuttle Orbiter at Hypersonic Speed.
Shuttle ; $C_{Y_{\delta_r}}$ vs. α ; $M = 5.0$

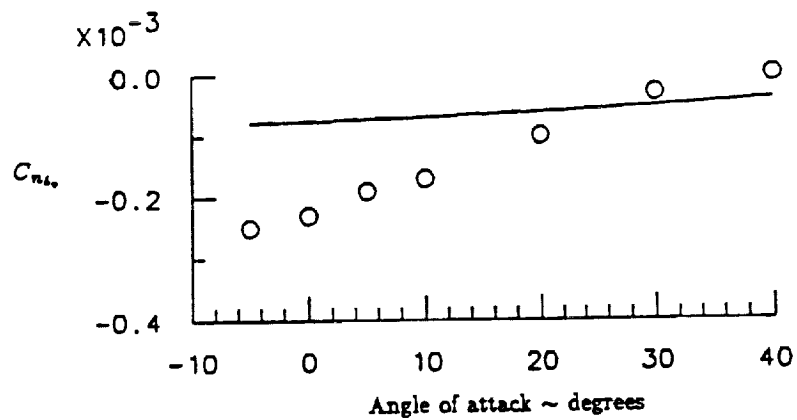


Fig. 172 Comparison Between Predicted and Experimentally Measured Yawing Moment Due to Rudder Deflection on the Shuttle Orbiter at Hypersonic Speed.
Shuttle ; $C_{n\delta}$ vs. α ; $M = 5.0$

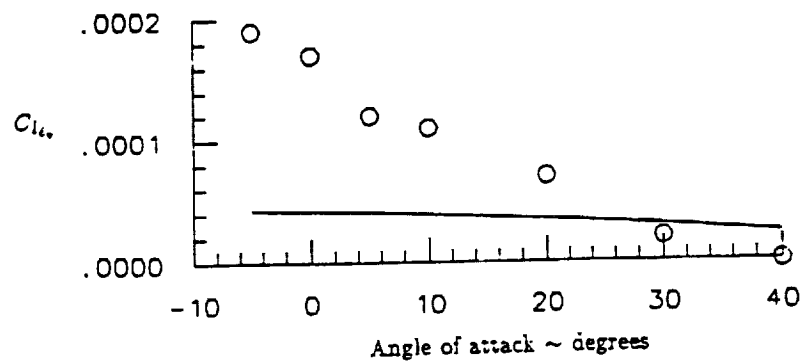


Fig. 173 Comparison Between Predicted and Experimentally Measured Rolling Moment Due to Rudder Deflection on the Shuttle Orbiter at Hypersonic Speed.
Shuttle ; $C_{l\delta}$ vs. α ; $M = 5.0$

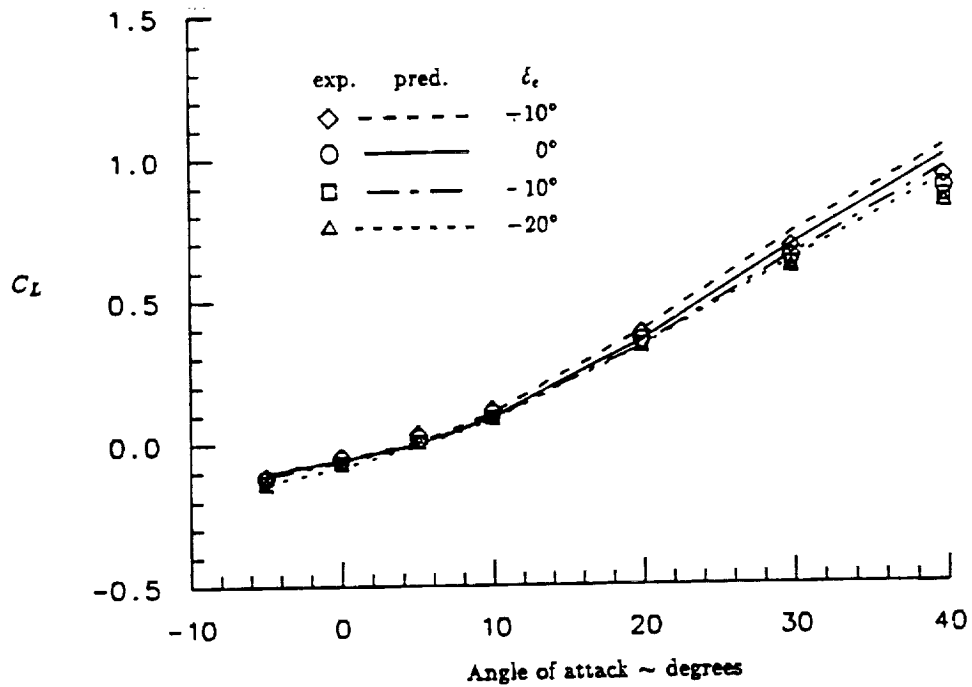


Fig. 174 Comparison Between Predicted and Experimentally Measured Lift on the Shuttle Orbiter at High Hypersonic Speed Including the Effect of Elevator Deflection.
Shuttle ; C_L vs. α ; $M = 20.0$; $\delta_e = +10^\circ, 0^\circ, -10^\circ, \text{ and } -20^\circ$

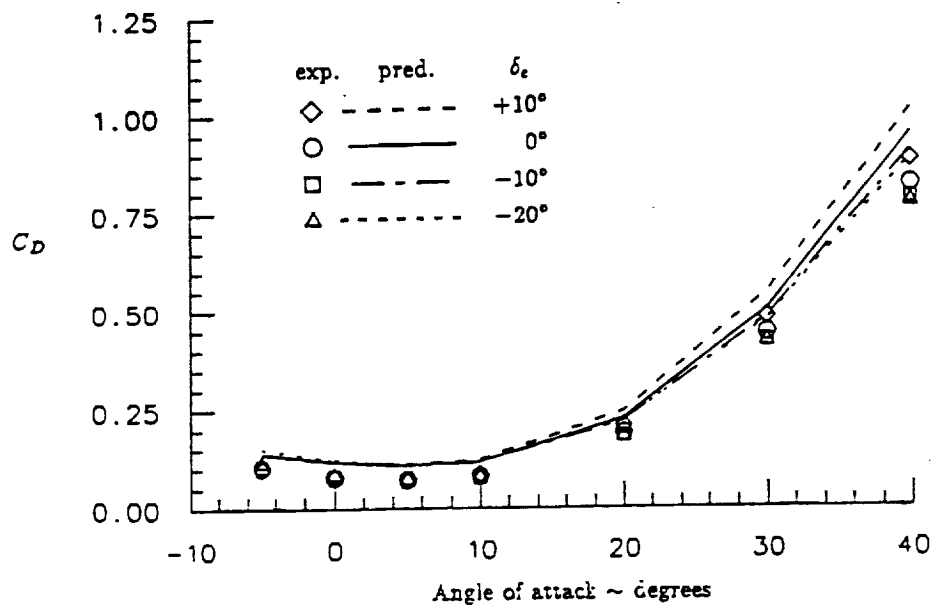


Fig. 175 Comparison Between Predicted and Experimentally Measured Drag on the Shuttle Orbiter at High Hypersonic Speed Including the Effect of Elevator Deflection.
Shuttle ; C_D vs. α ; $M = 20.0$; $\delta_e = +10^\circ, 0^\circ, -10^\circ, \text{ and } -20^\circ$

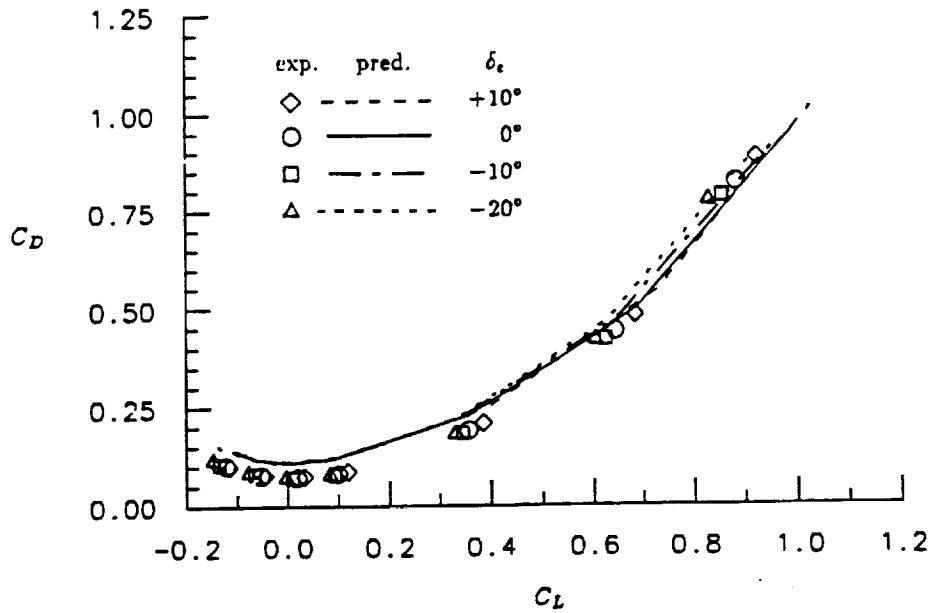


Fig. 176 Comparison Between Predicted and Experimentally Measured Drag as a Function of Lift on the Shuttle Orbiter at High Hypersonic Speed Including the Effect of Elevator Deflection. Shuttle ; C_D vs. C_L ; $M = 20.0$; $\delta_e = +10^\circ, 0^\circ, -10^\circ, \text{ and } -20^\circ$

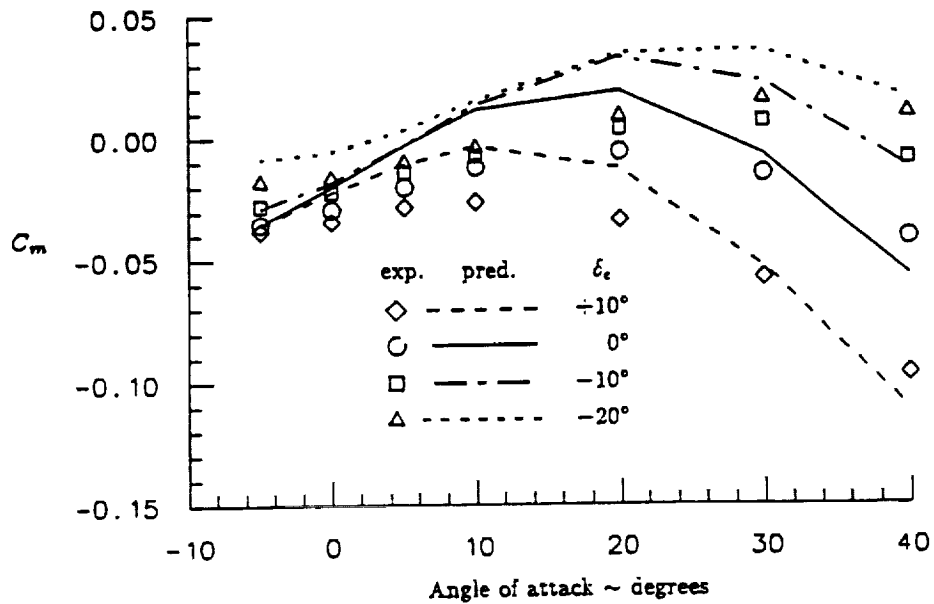


Fig. 177 Comparison Between Predicted and Experimentally Measured Moment on the Shuttle Orbiter at High Hypersonic Speed Including the Effect of Elevator Deflection. Shuttle ; C_m vs. α ; $M = 20.0$; $\delta_e = +10^\circ, 0^\circ, -10^\circ, \text{ and } -20^\circ$

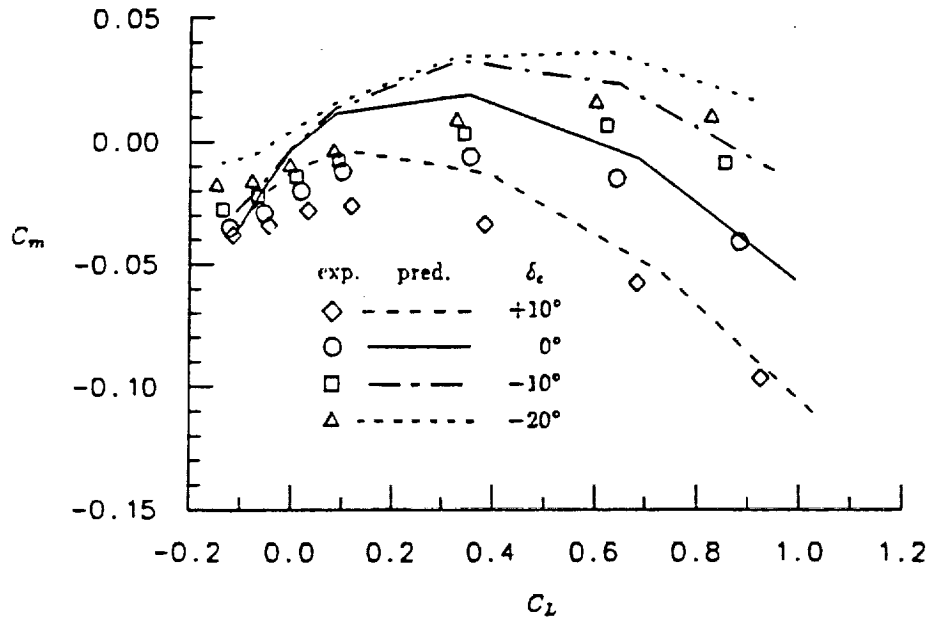


Fig. 178 Comparison Between Predicted and Experimentally Measured Moment as a Function of Lift on the Shuttle Orbiter at High Hypersonic Speed Including the Effect of Elevator Deflection. Shuttle ; C_m vs. C_L ; $M = 20.0$; $\delta_e = +10^\circ, 0^\circ, -10^\circ, \text{ and } -20^\circ$

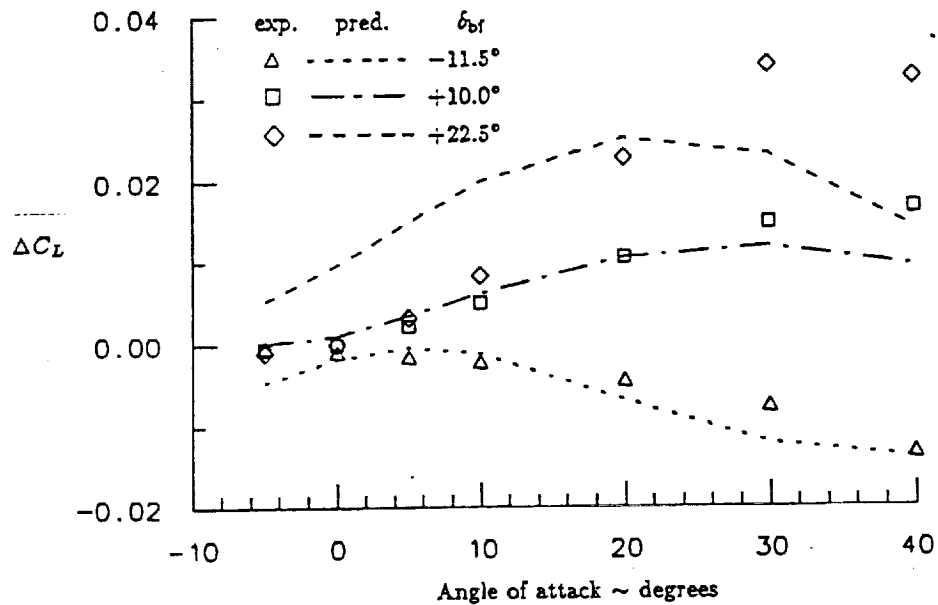


Fig. 179 Comparison Between Predicted and Experimentally Measured Lift on the Shuttle Orbiter at High Hypersonic Speed Including the Effect of Body Flap Deflection. Shuttle ; ΔC_L vs. α ; $M = 20.0$; $\delta_{bf} = -11.5^\circ, +10.0^\circ, \text{ and } +22.5^\circ$

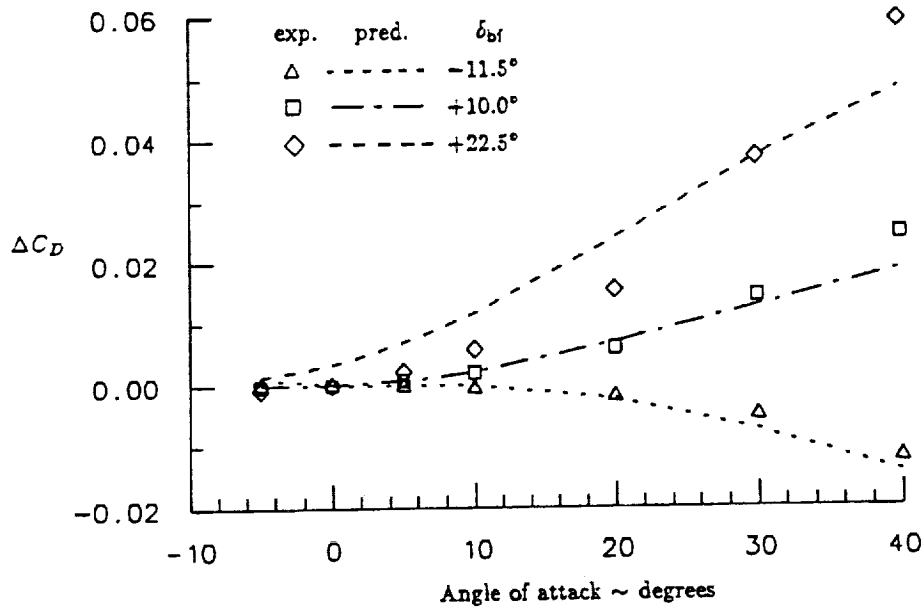


Fig. 180 Comparison Between Predicted and Experimentally Measured Drag on the Shuttle Orbiter at High Hypersonic Speed Including the Effect of Body Flap Deflection.
Shuttle ; ΔC_D vs. α ; $M = 20.0$; $\delta_{bf} = -11.5^\circ, +10.0^\circ, \text{ and } +22.5^\circ$

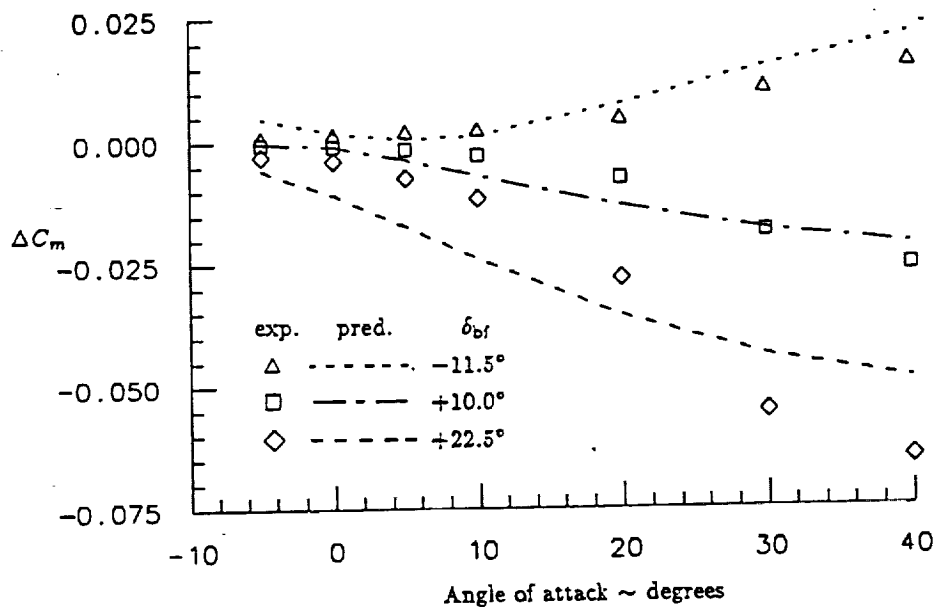


Fig. 181 Comparison Between Predicted and Experimentally Measured Moment on the Shuttle Orbiter at High Hypersonic Speed Including the Effect of Body Flap Deflection.
Shuttle ; ΔC_m vs. α ; $M = 20.0$; $\delta_{bf} = -11.5^\circ, +10.0^\circ, \text{ and } +22.5^\circ$

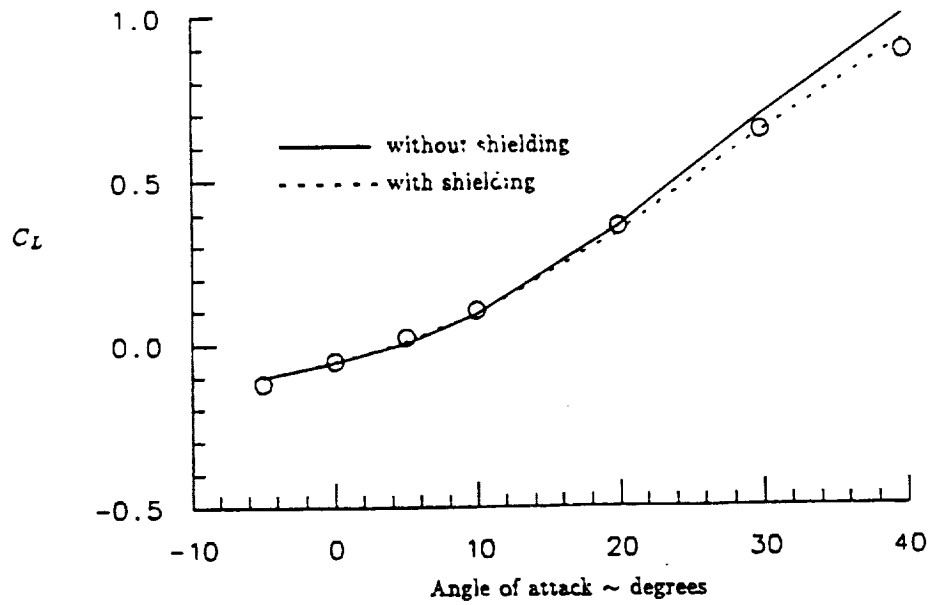


Fig. 182 The Effect of Shielding on the Predicted Lift on the Shuttle Vehicle at High Hypersonic Speed.
Shuttle ; C_L vs. α ; $M = 20.0$; with and without shielding

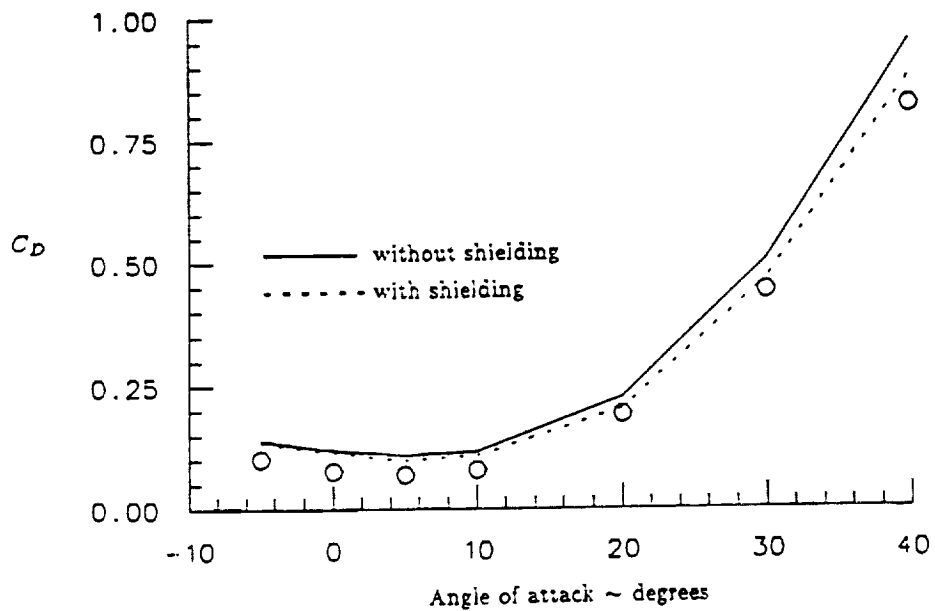


Fig. 183 The Effect of Shielding on the Predicted Drag on the Shuttle Vehicle at High Hypersonic Speed.
Shuttle ; C_D vs. α ; $M = 20.0$; with and without shielding

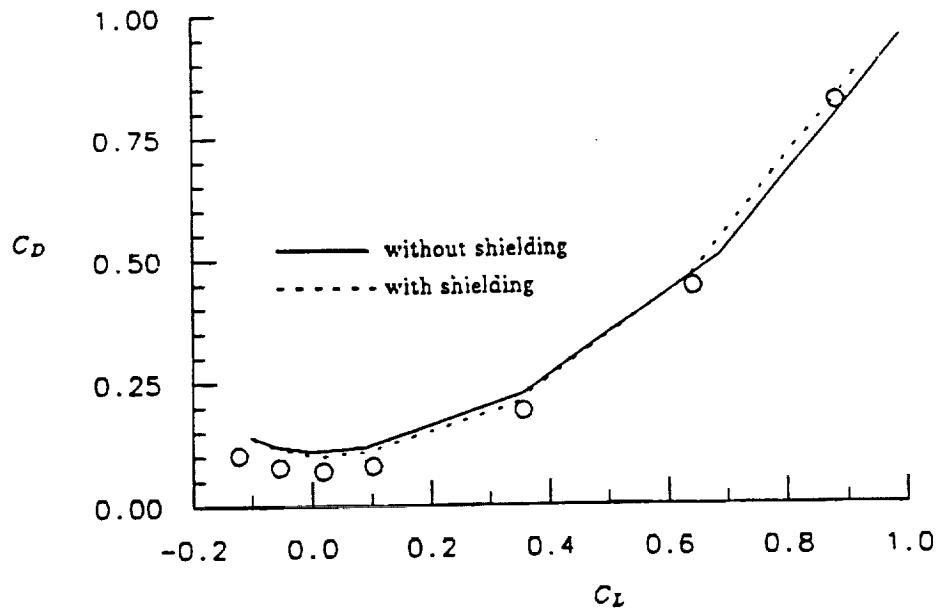


Fig. 184 The Effect of Shielding on the Predicted Drag as a Function of Lift on the Shuttle Vehicle at High Hypersonic Speed.
Shuttle ; C_D vs. C_L ; $M = 20.0$; with and without shielding

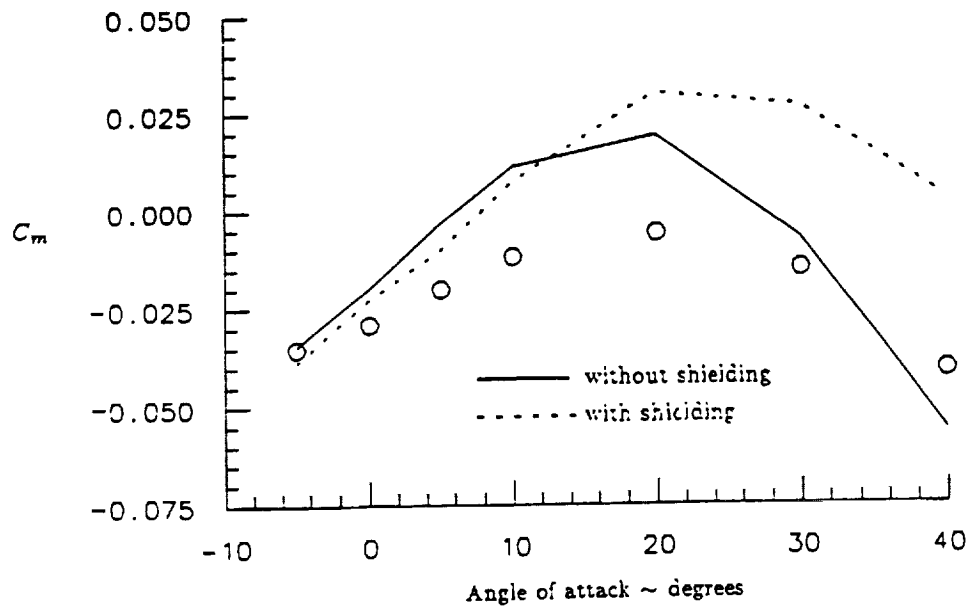


Fig. 185 The Effect of Shielding on the Predicted Moment on the Shuttle Orbiter at High Hypersonic Speed.
Shuttle ; C_m vs. α ; $M = 20.0$; with and without shielding

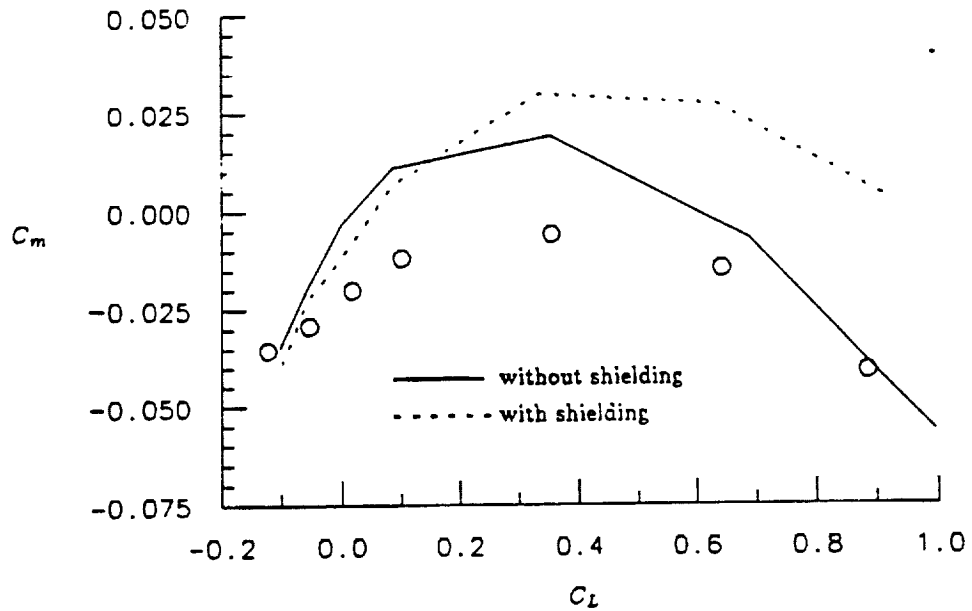


Fig. 186 The Effect of Shielding on the Predicted Moment as a Function of Lift on the Shuttle Orbiter at High Hypersonic Speed. Shuttle ; C_m vs. C_L ; $M = 20.0$; with and without shielding

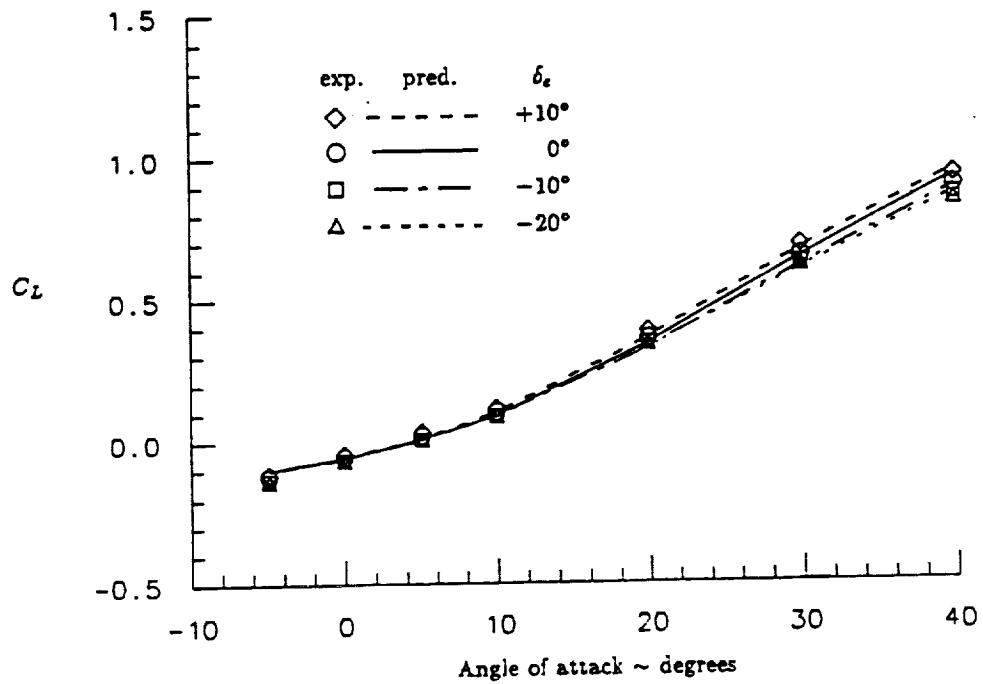


Fig. 187 Comparison Between Prediction With Shielding and Experimentally Measured Lift on the Shuttle Orbiter at High Hypersonic Speed Including the Effect of Elevator Deflection. Shuttle ; C_L vs. α ; $M = 20.0$; $\delta_e = +10^\circ, 0^\circ, -10^\circ, \text{ and } -20^\circ$; with shielding

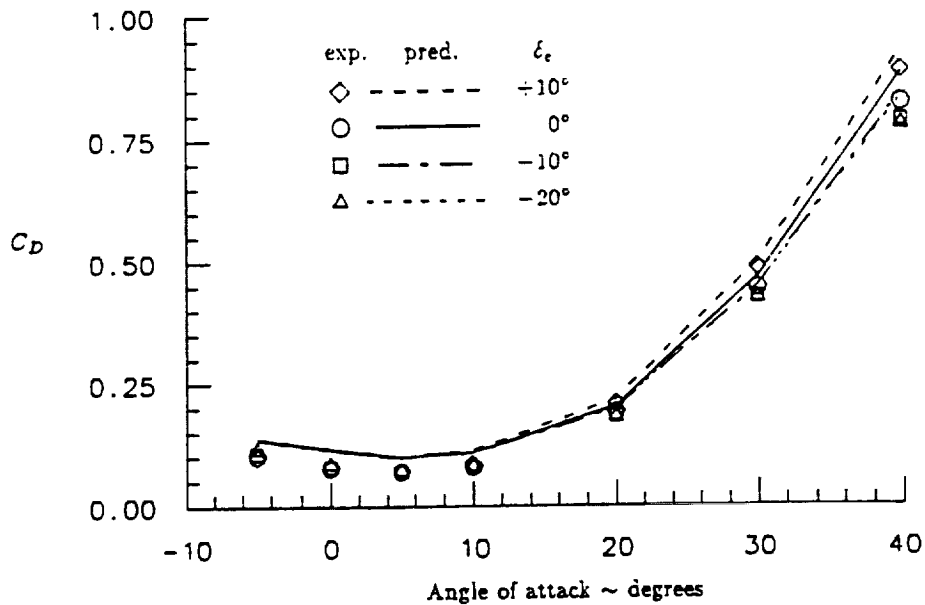


Fig. 188 Comparison Between Prediction With Shielding and Experimentally Measured Drag on the Shuttle Orbiter at High Hypersonic Speed Including the Effect of Elevator Deflection. Shuttle ; C_D vs. α ; $M = 20.0$; $\delta_e = +10^\circ, 0^\circ, -10^\circ, \text{ and } -20^\circ$; with shielding

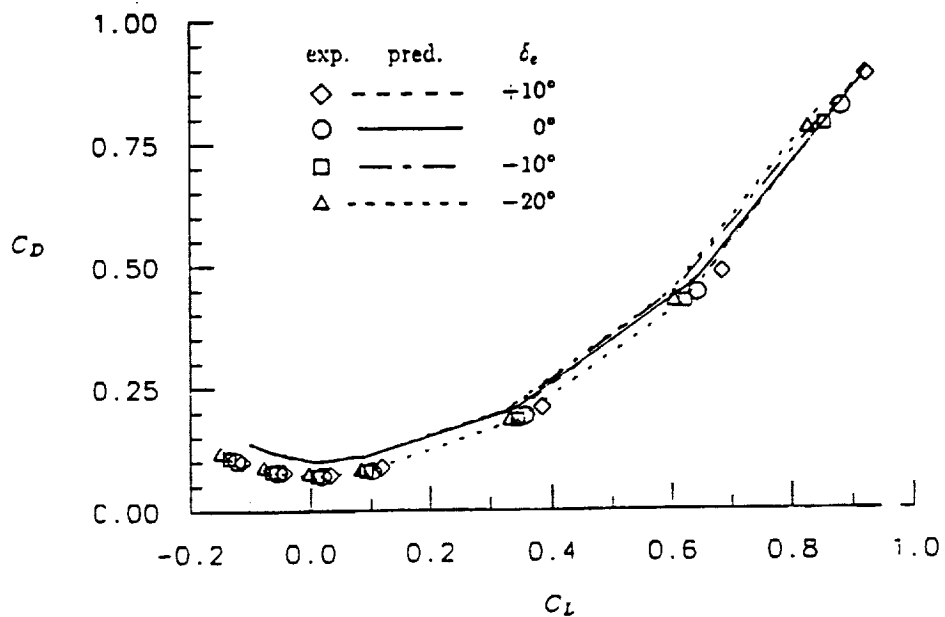


Fig. 189 Comparison Between Prediction With Shielding and Experimentally Measured Drag as a Function of Lift on the Shuttle Orbiter at High Hypersonic Speed Including the Effect of Elevator Deflection. Shuttle ; C_D vs. C_L ; $M = 20.0$; $\delta_e = +10^\circ, 0^\circ, -10^\circ, \text{ and } -20^\circ$; with shielding

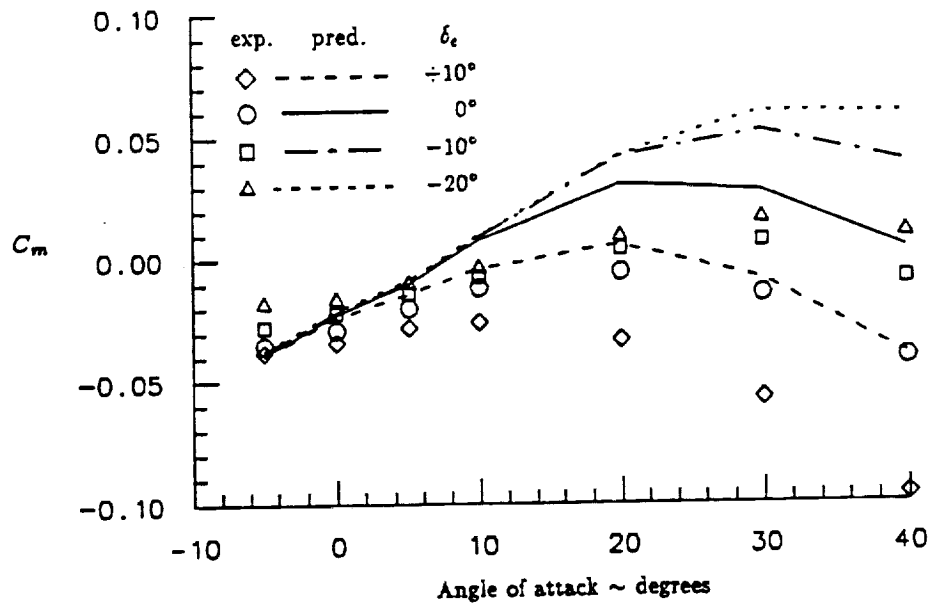


Fig. 190 Comparison Between Prediction With Shielding and Experimentally Measured Moment on the Shuttle Orbiter at High Hypersonic Speed Including the Effect of Elevator Deflection. Shuttle ; C_m vs. α ; $M = 20.0$; $\delta_e = +10^\circ, 0^\circ, -10^\circ, \text{ and } -20^\circ$; with shielding

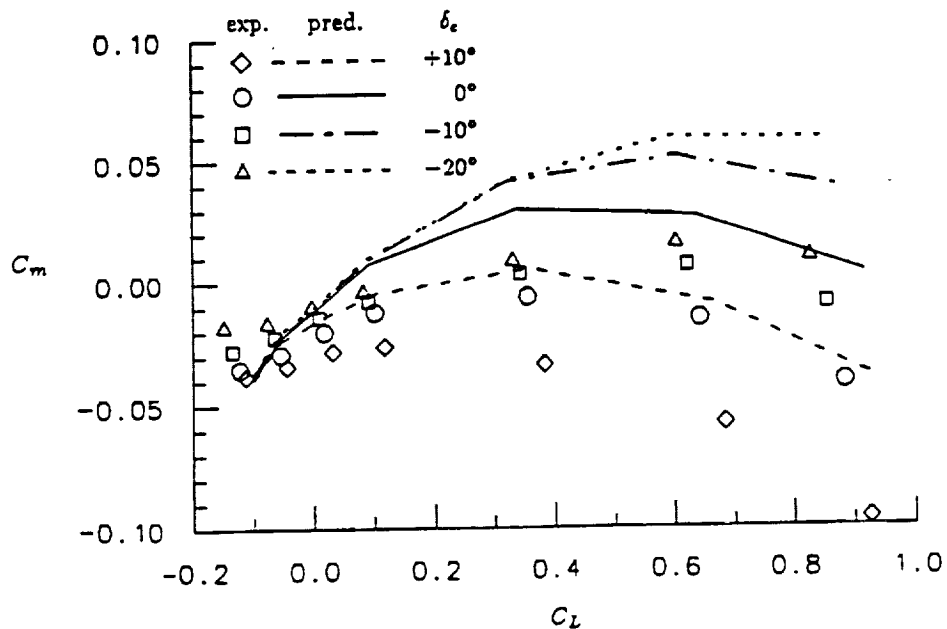


Fig. 191 Comparison Between Prediction With Shielding and Experimentally Measured Moment as a Function of Lift on the Shuttle Orbiter at High Hypersonic Speed Including the Effect of Elevator Deflection. Shuttle ; C_m vs. C_L ; $M = 20.0$; $\delta_e = +10^\circ, 0^\circ, -10^\circ, \text{ and } -20^\circ$; with shielding

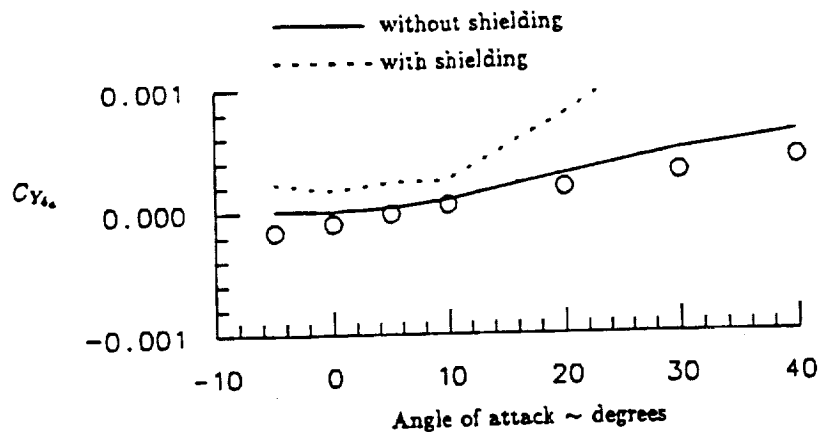


Fig. 192 Comparison Between Prediction With and Without Shielding and Experimentally Measured Side Force Due to Aileron Deflection on the Shuttle Orbiter at High Hypersonic Speed.
Shuttle ; $C_{Y_{\delta_a}}$ vs. α ; $M = 20.0$; with and without shielding

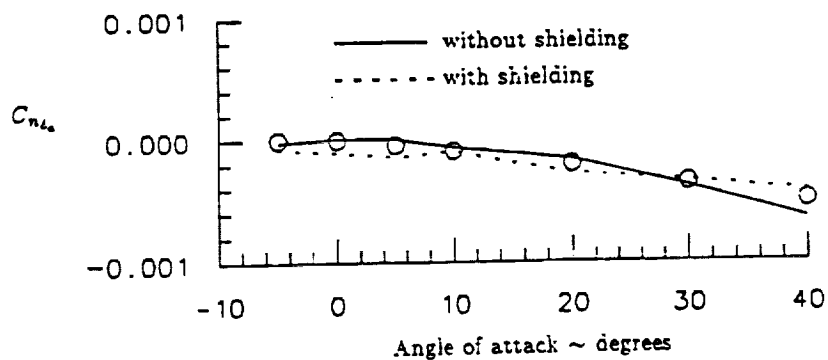


Fig. 193 Comparison Between Prediction With and Without Shielding and Experimentally Measured Yawing Moment Due to Aileron Deflection on the Shuttle Orbiter at High Hypersonic Speed.
Shuttle ; $C_{n_{\delta_a}}$ vs. α ; $M = 20.0$; with and without shielding

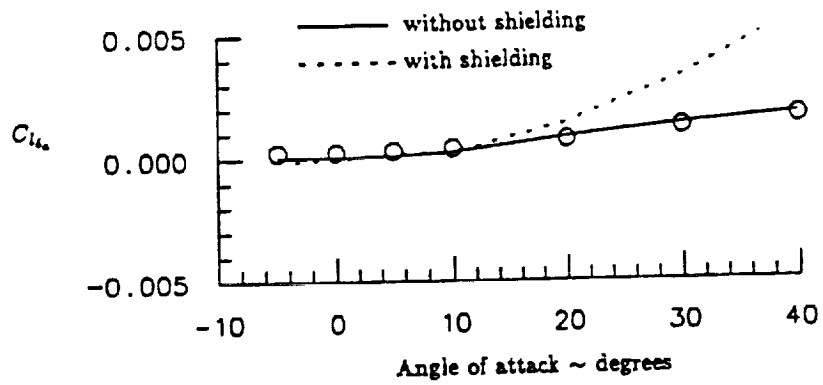


Fig. 194 Comparison Between Prediction With and Without Shielding and Experimentally Measured Rolling Moment Due to Aileron Deflection on the Shuttle Orbiter at High Hypersonic Speed.
Shuttle ; $C_{l_{\alpha}}$ vs. α ; $M = 20.0$; with and without shielding

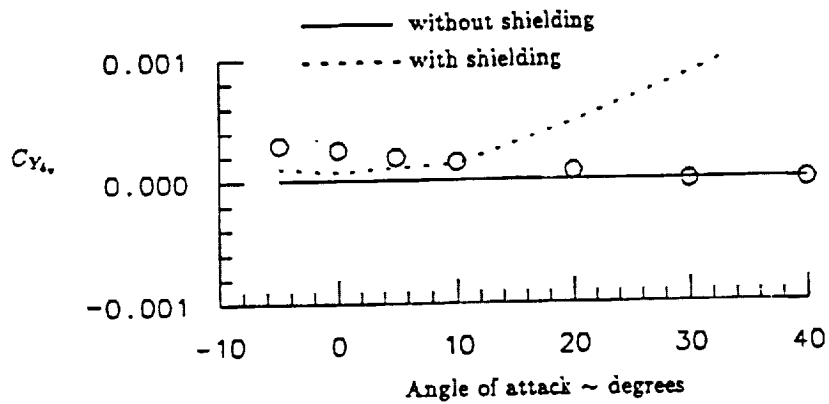


Fig. 195 Comparison Between Prediction With and Without Shielding and Experimentally Measured Side Force Due to Rudder Deflection on the Shuttle Orbiter at High Hypersonic Speed.
Shuttle ; $C_{Y_{\alpha}}$ vs. α ; $M = 20.0$; with and without shielding

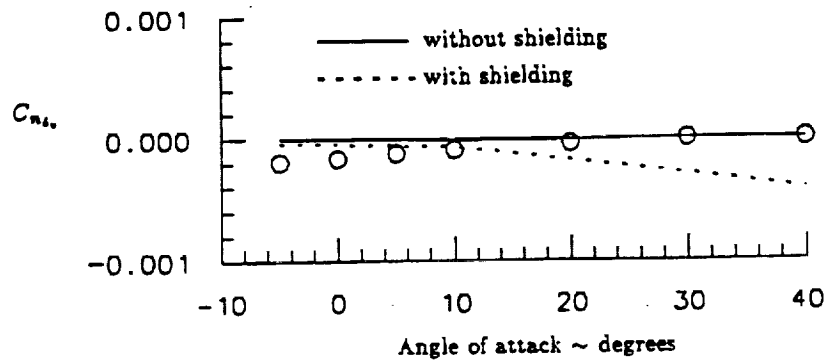


Fig. 196 Comparison Between Prediction With and Without Shielding and Experimentally Measured Yawing Moment Due to Rudder Deflection on the Shuttle Orbiter at High Hypersonic Speed. Shuttle ; $C_{n\delta_r}$ vs. α ; $M = 20.0$; with and without shielding

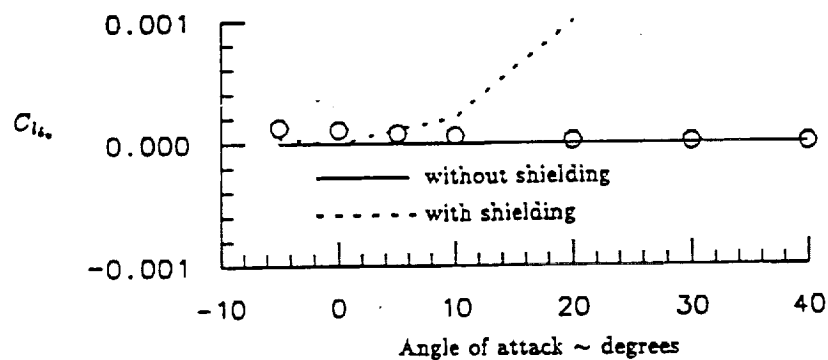


Fig. 197 Comparison Between Prediction With and Without Shielding and Experimentally Measured Rolling Moment Due to Rudder Deflection on the Shuttle Orbiter at High Hypersonic Speed. Shuttle ; $C_{l\delta_r}$ vs. α ; $M = 20.0$; with and without shielding

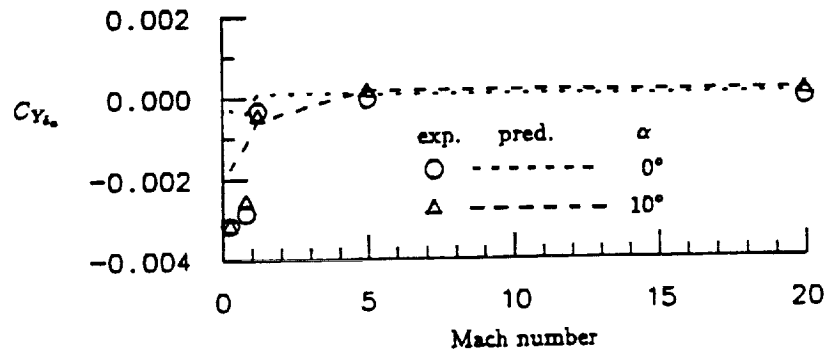


Fig. 198 Comparison Between Predicted and Experimentally Measured Side Force Due to Aileron Deflection on the Shuttle Orbiter as a Function of Mach Number at Two Angles of Attack.
Shuttle ; $C_{Y_{\delta_a}}$ vs. M ; $\alpha = 0^\circ$ and 10°

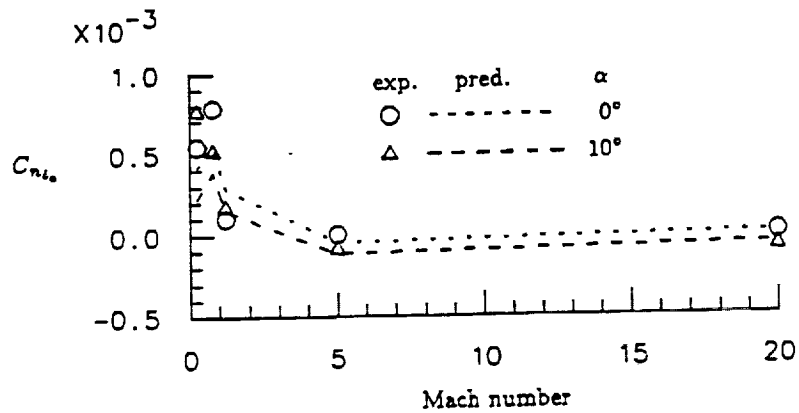


Fig. 199 Comparison Between Predicted and Experimentally Measured Yawing Moment Due to Aileron Deflection on the Shuttle Orbiter as a Function of Mach Number at Two Angles of Attack.
Shuttle ; $C_{n_{\delta_a}}$ vs. M ; $\alpha = 0^\circ$ and 10°

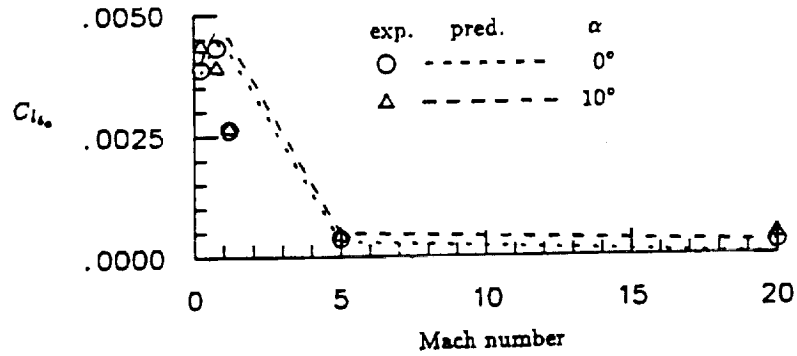


Fig. 200 Comparison Between Predicted and Experimentally Measured Rolling Moment Due to Aileron Deflection on the Shuttle Orbiter as a Function of Mach Number at Two Angles of Attack. Shuttle ; $C_{l_{\delta_a}}$ vs. M ; $\alpha = 0^\circ$ and 10°

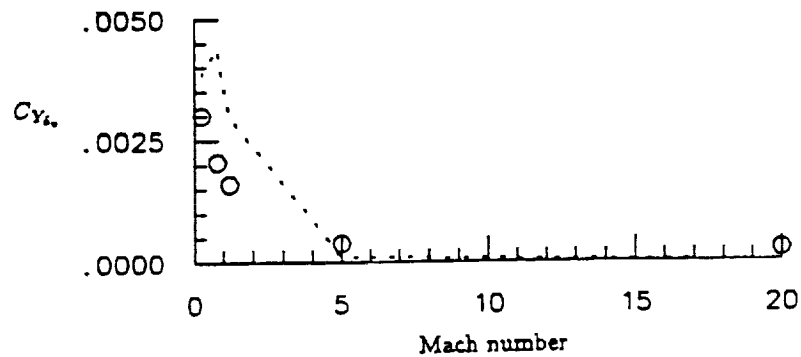


Fig. 201 Comparison Between Predicted and Experimentally Measured Side Force Due to Rudder Deflection on the Shuttle Orbiter as a Function of Mach Number. Shuttle ; $C_{Y_{\delta_r}}$ vs. M ; $\alpha = 0^\circ$

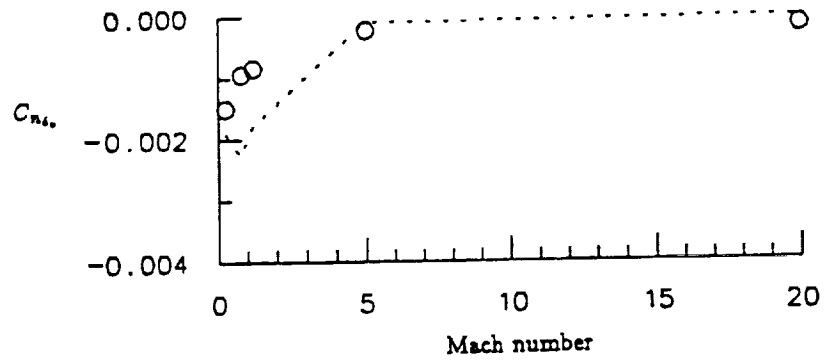


Fig. 202 Comparison Between Predicted and Experimentally Measured Yawing Moment Due to Rudder Deflection on the Shuttle Orbiter as a Function of Mach Number.
Shuttle ; $C_{n\delta}$ vs. M ; $\alpha = 0^\circ$

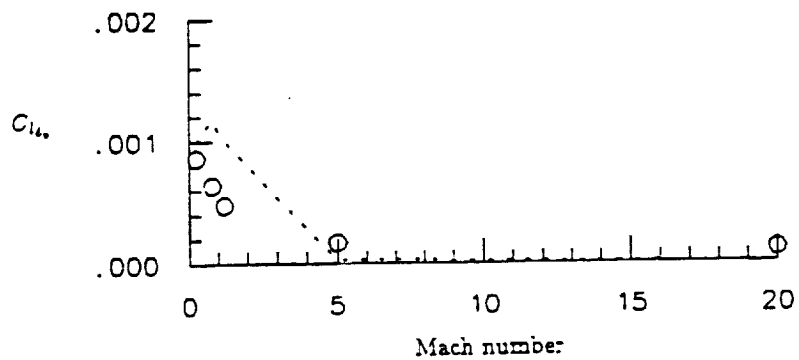


Fig. 203 Comparison Between Predicted and Experimentally Measured Rolling Moment Due to Rudder Deflection on the Shuttle Orbiter as a Function of Mach Number.
Shuttle ; $C_{l\delta}$ vs. M ; $\alpha = 0^\circ$

Appendix: Bibliography of Experimental Force and Moment Data For Hypersonic Vehicle Configurations

1. Beeler, D.E., "The X-15 Research Program," AGARD Report 289, October 1960.
Brief description of the X-15 research program. Comparison of wind tunnel tests and flight measured values of stability derivatives at Mach numbers from 0.0 to 8.0. Variation of control effectiveness with Mach number including horizontal tail, vertical tail and ailerons.
2. Bernot, P.T., "Effect of Modifications on Aerodynamic Characteristics of a Single-Stage-to Orbit Vehicle at Mach 5.9," NASA TM 84565, January 1983.
The model was based on control-configured stability concepts. Results are presented for elevons, body flap, and wing tip fin controllers. Model similar to that in NASA TM X-3550 (item 3).
3. Bernot, P.T., "Aerodynamic Characteristics of Two Single-Stage-to-Orbit Vehicles at Mach 20.3," NASA TM X-3550, August 1977.
Control deflection data are for elevons and a body flap. Most results are for high angles of attack (between 16° and 50°).
4. Boisseau, Peter C., "Investigation of the Low-speed Stability and Control Characteristics of a 1/7-Scale Model of the North American X-15 Airplane," NACA RM L57D09, 1957.
Early X-15 data from free flying model tests. Purpose was to evaluate the use of the horizontal tail for roll control. Control deflection results are presented for the wing trailing edge flap, all moving vertical tail, and symmetrical and differential horizontal tail deflections.
5. Boyden, R.P. and Freeman, D.C. Jr., "Subsonic and Transonic Dynamic Stability Characteristics of a Space Shuttle Orbiter," NASA TN D-8042, November 1975.
Dynamic and static stability are investigated. Dynamic results are presented to show the effect of rudder flare in combination with body flap deflection. The static lateral stability data show the effect of the vertical tail, combination body flap and rudder flare, and body flap alone.
6. Brooks, C.W. Jr. and Cone, C.D. Jr., "Hypersonic Aerodynamic Characteristics of Aircraft Configurations with Canard Controls," NASA TN D-3374, April 1966.
The investigation was done on a wing-body configuration with a 70° swept delta wing at a Mach number of 10.03. Four different canards were each tested on various configurations. Results include canard effectiveness on longitudinal, lateral, and directional characteristics.
7. Brooks, C.W. Jr., "Interference Effects of Canard Controls on the Longitudinal Aerodynamic Characteristics of a Winged Body at Mach 10," NASA TN D-4436, April 1968.
Effect of canard interference is studied by comparing body alone data with canard deflection data which appeared in NASA TN D-3374 (item 6) and TN D-3728 (item 44).

8. Clark, L.D., "Hypersonic Aerodynamic Characteristics of an All-Body Research Aircraft Configuration," NASA TN D-7358, December 1973.

Experiment was done at Mach 6 on a lifting body configuration and compared with theoretical models. The horizontal wing-tip-type control surfaces were adjustable in 5° increments from $+15^\circ$ to -30° . HABP was used for theoretical predictions. The tangent-cone method gave the best agreement at control settings between $+5^\circ$ and -5° and at positive lift coefficients except for directional characteristics. None of the methods predicted characteristics well at negative lift coefficients and large control deflections.

9. Clark, L.E. and Richie, C.B., "Aerodynamic Characteristics at Mach 6 of a Hypersonic Research Airplane Concept Having a 70° Swept Delta Wing," NASA TM X-3475, May 1977.

The study was a configuration build up and includes effect of elevon deflection on trim characteristics. Elevon data are given for deflections of 10° to -20° in 5° increments for seven different configurations. Speed brake deflection data are also included.

10. Covell, P.F., Wood, R.M., Bauer, S.X., and Malker, I.J., "Configuration Trade and Code Validation Study on a Conical Hypersonic Vehicle," AIAA Paper 88-4505, September 1988.

Test Mach numbers were between 2.5 and 4.5. Effect of canard shape, vertical tail shape, wing location, and wing incidence on aerodynamic characteristics included. A comparison is also made between the experimental results and three theoretical analysis programs: HABP, LT (Linear Theory), and SIMP (Supersonic Implicit Marching).

11. Decker, J.P. and Spencer, B. Jr., "Low-Subsonic Aerodynamic Characteristics of a Model of a Fixed-Wing Space Shuttle Concept at Angles of Attack to 76° ," NASA TM X-1996, April 1970.

These tests were done on an early shuttle concept at a Mach number of 0.25. Longitudinal stability and control are provided by a horizontal tail with an elevator. Elevator deflections of 20° to -20° were effective at low angles of attack where flow separation is not a major problem.

12. Dillon, J.L. and Creel, T.R. Jr., "Aerodynamic Characteristics at Mach Number 0.2 of a Wing Body Concept for a Hypersonic Research Airplane," NASA TP 1189, 1978.

The experiment consisted of configuration buildup from the basic body by adding a wing, center vertical tail and scramjet engines. The test angle of attack range was approximately -5° to 30° at constant angles of sideslip of 0° and 4° . The elevons were deflected from 5° to -15° . Roll and yaw control were investigated. Also includes rudder deflection data.

13. Dillon, J.L. and Pittman, J.L., "Aerodynamic Characteristics at Mach Numbers from 0.33 to 1.20 of a Wing-Body Design Concept for a Hypersonic Research Airplane," NASA TP 1044, 1977.

The tests were done at seven different transonic Mach numbers. Control deflection data includes: symmetrical elevon deflections of 0° , -10° , and -20° ; differentially deflected elevons at $\pm 20^\circ$; and rudder deflections of 0° and 15.6° .

14. Dillon, J.L. and Pittman, J.L., "Aerodynamic Characteristics at Mach 6 of a Wing-Body Concept for a Hypersonic Research Airplane," NASA TP 1249, August 1978.

Similar configuration build-up of model in TP 1044 (item 13) and TP 1189 (item 12) at Mach 6. The elevons were deflected from 10° to -15° for pitch control and yaw and roll control were also investigated. HARP was used and gave good predictions for the longitudinal but not for the lateral-directional aerodynamic characteristics.

15. Ellison, J.C., "Investigation of the Aerodynamic Characteristics of a Hypersonic Transport Model at Mach Numbers to 6," NASA TN D-6191, April 1971.

Tests were done at Mach numbers from 0.36 to 6.0. Results for elevon deflections from 5° to -20° are included for all Mach numbers. The configuration also had strakes which helped provide positive C_M .

16. Fetterman, D.E. Jr., Penland, J.A., "Static Longitudinal, Directional, and Lateral Stability and Control Data from an Investigation at a Mach Number of 6.83 of Two Developmental X-15 Airplane Configurations," NASA TM X-209, March 1960.

Directional control data were obtained by testing vertical tail deflections of 0° and -5° , and lateral control data were obtained by testing differential horizontal tail deflections of 0° , -10° , and -20° . Results for speed brake deflections of 20° are also included.

17. Freeman, D.C. Jr., "Dynamic Stability Derivatives of Space Shuttle Orbiter Obtained from Wind-Tunnel and Approach and Landing Flight Tests," NASA TP 1634, April 1980.

Wind tunnel and flight test data were compared with ADDB values at subsonic Mach numbers for the parameters of pitch, yaw and roll damping, as well as the yawing moment due to rolling velocity and the rolling moment due to yawing velocity.

18. Freeman, D.C. and Boyden, R.P., "Supersonic Dynamic Stability Characteristics of a Space Shuttle Orbiter," NASA TN D-8043, January 1976.

Similar results to NASA TN D-8042 (item 5) except for different Mach numbers. Elevon data are also included.

19. Freeman, D.C. and Fournier, R.H., "Static Aerodynamic Characteristics of a Single-Stage-to-Orbit Vehicle With Low Planform Loading at Mach Numbers from 0.3 to 4.63," NASA TM 74056, November 1977.

Tests were run at eight different Mach numbers. At a Mach number of 0.9, elevon deflections of 10° became completely ineffective at angles of attack above 6° . The resulting nonlinearity in $C_{M\delta_e}$ was also seen in the Space Shuttle.

20. Freeman, D.C. and Fournier, R.H., "Static Aerodynamic Characteristics of a Winged Single-Stage-to-Orbit Vehicle at Mach Numbers from 0.3 to 4.63," NASA TP 1233, August 1978.

Tests were done to determine the static longitudinal stability and trim, the static lateral-directional stability, and the aileron control effectiveness. Elevons were deflected from 0° to -20° for all eight Mach numbers tested.

21. Freeman, D.C. and Jones, R.S., "Low-Speed Static Stability and Control Characteristics of Two Small-Scale, Hypersonic Cruise Configurations," NASA TM X-2021, June 1970.

The first model was a distinct wing-body with a conventional rudder for directional control and differential deflections of the all-movable horizontal tail for roll control. The second model was a blended wing-body with elevons for both pitch and roll control and a center vertical rudder for directional control.

22. Freeman, D.C. and Spencer, B. Jr., "Comparison of Space Shuttle Orbiter Low-Speed Static Stability and Control Derivatives Obtained from Wind-Tunnel and Approach and Landing Flight Tests," NASA TP 1779, December 1980.

The longitudinal stability, elevon effectiveness, lateral directional stability and aileron effectiveness derivatives were compared from wind tunnel tests, approach and landing flight tests and ADDB values. Body flap and speed brake deflections are included.

23. "Hypersonic Aerodynamic Characteristics of Two Delta-Wing X-15 Airplane Configurations," NASA TN D-5498, October 1969.

The effects of wing geometry and longitudinal position, wing fins, nose cant, strakes, and speed brakes were looked at for elevon deflections to -45° . The experimental aerodynamic characteristics were compared with the analytical results from HABP. At the time of the investigation, HABP was very new and the results were not very good.

24. Kelly, M.W., "Wind-Tunnel Investigation of the Low-Speed Aerodynamic Characteristics of a Hypersonic Glider Configuration," NACA RM A58F03, September 1958.

The tests were done to investigate the adequacy of the low speed stability and control characteristics for landing. Trailing-edge flaps at the wing tips supplied both yaw and roll control. The effect of wing tip droop on lateral and directional stability is also reported.

25. McCandless, R.S. and Cruz, C.I., "Hypersonic Characteristics of an Advanced Aerospace Plane," AIAA Paper 85-0346, January 1985.

Tests were run at Mach numbers of 6, 10, and 20. Results include elevator, elevon and rudder deflection data. The experimental data were then compared with APAS II predicted values.

26. McCandless, R.S., "Hypersonic Characteristics of an Advanced Aerospace Plane at Mach 20.3," NASA TM 86435.

Aerodynamic control effectiveness was determined by deflecting the elevators, the elevons, and the rudder. Tests were run at a Mach number of 20.3 at various Reynolds numbers.

27. McKinney, R.L. and Lancaster, J.A., "Investigation of the Aerodynamic Characteristics of a 0.02-Scale Model of the X-15 Airplane at Mach Numbers of 2.96, 3.96, and 4.65 at High Angles of Attack," NASA TM X-820, June 1963.

Supersonic tests on the final X-15 configuration. Results include deflections of the horizontal tail, asymmetric deflections of the upper and lower verticals, and deflections of upper and lower speed brakes.

28. Mellinger, G.R., "Design and Operation of the X-15," *Shell Aviation News*, April 1961, pp 14-21.

Includes a description of the X-15 design. The article discusses design decisions such the need for the wedge airfoil for the upper and lower vertical tails.

29. Moore, M.E. and Williams, J.E., "Aerodynamic Prediction Rationale for Analyses of Hypersonic Configurations," AIAA Paper 89-0525, January 1989.

A method selection rationale was developed for S/HABP. They suggest braking the configuration into three basic parts: nose, body, and aerodynamic surfaces. Analyses were done on the Space Shuttle, the FDL-7, and the X-24C-10D. No comparisons for control deflections.

30. Nelms, W.P. and Ames, J.A., "Longitudinal Aerodynamic Characteristics of Three Representative Hypersonic Cruise Configurations at Mach Numbers from 0.65 to 10.70," NASA TM X-2113, October 1970.

Two configurations were discrete wing-body concepts and the third was a blended wing-body design. Effects of varying angle of attack, Mach number, and configuration build-up were considered. There are no control deflection data in this report.

31. Nelms, W.P. and Thomas, C.L., "Aerodynamic Characteristics of an All-Body Hypersonic Aircraft Configuration at Mach Numbers from 0.65 to 10.6," NASA TN D-6577, November 1971.

The effectiveness of horizontal tail, vertical tail and canard stabilizing and control surfaces were investigated. The horizontal tail was deflected both symmetrically and differentially. The rudder was deflected asymmetrically and flared as a speed brake.

32. Osbourne, R.S., "Aerodynamic Characteristics of a 0.0667 Scale Model of the N.A. X-15 Research Airplane at Transonic Speeds," NASA TM X-24, 1959.

Tests were run at eight Mach numbers between 0.6 and 21.43. The tests were not run on the final X-15 configuration (does not include vertical wedge airfoil). Results are presented for symmetrical and differential deflections of the horizontal tail.

33. Penland, J.A., "Low-Speed Aerodynamic Characteristics for a Hypersonic Research Airplane Concept Having a 70° Swept Delta Wing," NASA TM X-71974, August 1974.

Tests were conducted at a Mach number of 0.06 on a model like that in NASA reports: TP 1252 (item 38), TP 1552 (item 39), TM X-3475 (item 9), and TN D-8065 (item 37). Eight model configurations were tested with various elevon and aileron deflections.

34. Penland, J.A. and Fetterman, D.E. Jr., "Static Longitudinal, Directional, and Lateral Stability and Control Data at a Mach Number of 6.83 of the Final Configuration of the X-15 Research Airplane," NASA TM X-236, April 1960.

Data are presented in comparison plots to show the effects of component breakdown and control deflection. Control surfaces include: vertical tail, horizontal tail (symmetrical and differential deflections), speed brakes. The configuration geometry is well documented in the report (0.02 scale model).

35. Penland, J.A. and Creel, T.R. Jr., "Low-Speed Aerodynamic Characteristics of a Lifting-Body Hypersonic Research Aircraft Configuration," NASA TN D-7851, February 1975.

Configuration is similar to that of NASA TN D-7358. The model was tested with two sets of horizontal and vertical tip controls, a center vertical tail, and two sets of canard controls.

36. Penland, J.A., Creel, T.R. Jr., and Howard, "Experimental Low-Speed and Calculated High-Speed Aerodynamic Characteristics of a Hypersonic Research Airplane Concept Having a 65° Swept Delta Wing," NASA TN D-7633, August 1974.

Experimental low speed tests were done to determine lift and stability during landing. Calculated results using HABP are presented for Mach numbers from 3 to 12. Results are given for elevon, aileron, and wing tip rudder deflections.

37. Penland, J.A., Fournier, R.H., and Marcum, D.C. Jr., "Aerodynamic Characteristics of a Hypersonic Research Airplane Concept Having a 70° Swept Double-Delta Wing at Mach Numbers from 1.50 to 2.86," NASA TN D-8065, December 1975.

A configuration build-up was done as well as the effect of elevon deflections. Data for elevon deflections of 0°, -10°, and -20° are presented at four supersonic Mach numbers. Aileron effectiveness data are also presented.

38. Penland, J.A., Creel, T.R. Jr., and Dillon, J.L., "Aerodynamic Characteristics of a Hypersonic Research Airplane Concept Having a 70° Swept Double-Delta Wing at Mach Number 0.2," NASA TP 1252, September 1978.

Tests were done at a Mach number of 0.2 for various Reynolds numbers. The elevons were deflected from 0° to -20° in 5° increments. Roll control was also investigated.

39. Penland, J.A., Hallissy, and Dillon, J.L., "Aerodynamic Characteristics of a Hypersonic Research Airplane Concept Having a 70° Swept Double-Delta Wing at Mach Numbers from 0.80 to 1.20, With Summary of Data from 0.20 to 6.0," NASA TP 1552, December 1979.

Wind tunnel data of static longitudinal, lateral, and directional stability characteristics of a hypersonic research airplane, for angles of attack from -4° to 23° , and at angles of sideslip of 0° and 5° . The configuration variables included wing planform, tip fins, and the center vertical tail. The second area is a summary of the variations of the more important aerodynamic parameters with $M = 0.2$ to 6.0. Elevon deflections are included.

40. Pittman, J.L and Riebe, G.D., "Experimental and Theoretical Aerodynamic Characteristics of Two Hypersonic Cruise Aircraft Concepts at Mach Numbers of 2.96, 3.96, and 4.63," NASA TP 1767, December 1980.

Comparison of wind tunnel tests with results from various theoretical methods including HABP. The control deflections studied were for horizontal and vertical tails.

41. Powell, R.W. and Freeman, D.C., Jr., "Application of a Tip-Fin Controller to the Shuttle Orbiter for Improved Yaw Control," *Journal of Guidance and Control*, AIAA Paper 81-0074R, 1982.

Looks at possibility of implementing tip-fins on the Shuttle Orbiter for improved yaw control. Results compared effectiveness of speed brakes on the two configurations.

42. Powell, R.W. and Freeman, D.C. Jr., "Aerodynamic Control of the Space Shuttle Orbiter with Tip-Fin Controllers," *Journal of Spacecraft*, AIAA Paper 84-0488, September-October 1985.

Results show that the orbiter with tip-fin controllers can successfully perform the required maneuvers during entry. They do however exhibit less control authority in some flight regimes than the current configuration.

43. Putman, L.E. and Trescot, C.D. Jr., "Hypersonic Aerodynamic Characteristics of Plain and Ported Elevon Controls on a 75° Swept Modified Delta-Wing Configuration," NASA TM X-987, July 1964.

The tests were run at a Mach number of 10.03 and at various Reynolds numbers. The relative effectiveness of plain and ported elevons and the effect of wing position on elevon effectiveness were reported. Newtonian impact theory was used to predict the control characteristics but was not adequate for this configuration.

44. Putnam, L.E. and Brooks, C.W. Jr., "Hypersonic Aerodynamic Characteristics of Wing-Body Configurations with Canard Controls," NASA TN D-3728, December 1966.

Similar to work in NASA TN D-3374 (item 6) but with different canards.

45. Rainey, R.W., Fetterman, D.E. Jr., and Smith, R., "Summary of the Static Stability and Control Results of a Hypersonic Glider Investigation," NASA TM X-277, May 1960.

Test Mach numbers of 6.7 to 18.4. Wing trailing edge flaps provided longitudinal and lateral control, and the wing-tip fins with rudders provided directinal stability and control. Other control surfaces tested include delta tripanel tip controls, pyramidal tip controls, and conical tip controls.

46. Romere, P.D. and Young, J.C., "Space Shuttle Entry Aerodynamic Comparisons of Flight 2 with Preflight Predictions," AIAA Paper 82-0565, March 1982.

Control deflection data given only for the speed brakes.

47. Ross, A.J. and Thomas, H.H.B.M., "A Survey of Experimental Data on the Aerodynamics of Controls, in the Light of Future Needs," *Aerodynamics of Controls - Paper 2*, AGARD CP 262.

This paper is a good overview of both conventional and unconventional motivators. A bibliography of control data for pitch, roll, yaw, and lift motivators is included. They are further broken down into different speed regimes.

48. Shuttle Performance: Lessons Learned, "Space Shuttle Entry Longitudinal Aerodynamic Comparisons of Flights 1-4 with Preflight Predictions," NASA CP 2283, March 8-10, 1983.

Analysis results of the STS 2 and 4 maneuvers during entry indicate that the hypersonic trim discrepancy is due to an error in the prediction of the basic vehicle pitching moment and not an error in prediction of the elevon and body flap effectiveness. Speed brake data are included.

49. Small W.J., Kirkham, F.S., and Fetterman, D.E., "Aerodynamic Characteristics of a Hypersonic Transport Configuration at Mach 6.86," NASA TN D-5885, June 1970.

Configuration was a low-wing, distinct wing-body with a vertical tail. Elevon deflection data are included. The analytical prediction methods used were found to be inadequate. At $\alpha = 6.85^\circ$ the vertical tail became ineffective due to interference and shielding effects.

50. Spearman, M.L. and Driver, C., "Longitudinal and Lateral Stability and Control Characteristics at a Mach Number of 2.01 of a 60° Delta-Wing Airplane Configuration Equipped with a Canard Control and with Wing Trailing-Edge Flap Controls," NACA RM L58A20, March 1958.

51. Spencer, B. Jr., "Effects of Stabilizer Configuration on Transonic Aerodynamic Characteristics of a Variable-Geometry High-Hypersonic-Performance Spacecraft," NASA TM X-1865, September 1969.

The configuration has an adjustable wing which is stowed at high speeds and is deployed at low speeds. Elevon controls were deflected 0° , -10° , and -20° for pitch control and differentially for roll control. The results are given for various horizontal stabilizer configurations.

52. Spencer, B. Jr., Henry, B.Z. Jr., and Putnam, L.E., "The Transonic Longitudinal and Lateral Aerodynamic Characteristics of a Low-Fineness-Ratio Elliptic Hypersonic Configuration Employing Variable-Sweep Wing Panels for Improving Subsonic Lift and Performance," NASA TM X-768, March 1963.

Results are given for body-base flap deflections at various transonic Mach numbers. The wing leading edge sweep angle was also varied with body flap deflections.

53. Suit, W.T. and Schiess, J.R., "Lateral and Longitudinal Stability and Control Parameters for the Space Shuttle *Discovery* as Determined from Flight test Data," NASA TM 100555, February 1988.

Comparison of flight test data with predictions. Results include: rolling and yawing moments due to aileron deflection; rolling and yawing moments due to rudder deflection; and pitching moment due to elevon deflection. These results are given versus Mach number from 25.0 to 0.

54. Syvertson, C.A., Gloria, H.R., and Sarabia, M.F., "Aerodynamic Performance and Static Stability and Control for Flat-Top Hypersonic Gliders at Mach Numbers from 0.6 to 18," NACA RM A58G17, September 1958.

The model was a 77.4° swept arrow wing with deflected wing tips, a retractable ventral fin, plain trailing edge flaps, a rudder on the ventral fin, and body flaps that could also be used for speed brakes. All of the test results are presented in tabular form.

55. Trescot, C.D. and Spencer, B. Jr., "Hypersonic Aerodynamic Characteristics of a Lifting Reentry Vehicle Model with Four Types of Longitudinal Control Surfaces," NASA TM X-1173, November 1965.

Tests were at a Mach number of 10.03. The baseline configuration is that of TM X-768 (item 52) with the wing in the 75° leading edge sweep position. The four types of controls tested were aft-mounted fins, a canard, a chin flap, and two body trailing edge flaps (one each on upper and lower surfaces).

56. Underwood, J.M. and Cooke, D.R., "A Preliminary Correlation of the Orbiter Stability and Control Aerodynamics from the First Two Space Shuttle Flights (STS 1 and 2) with Preflight Predictions," AIAA Paper 82-0564, March 1982.

Data from STS-1 and STS-2 are compared with Shuttle Data Book values. Results are presented for aileron and rudder effectiveness.

57. Walker, H.J. and Wolowicz, C.H., "Stability and Control Derivative Characteristics of the X-15 Airplane," NASA TM X-714, March 1962.

Results compare actual flight test data with wind tunnel test predictions. Control deflections include horizontal tail, upper vertical tail rudder, and speed brakes.

58. Yancy, R.B., Rediess, H.A., and Robinson, G.H., "Aerodynamic Derivative Characteristics of the X-15 Research Airplane as Determined from Flight Tests for Mach Numbers from 0.6 to 3.4," NASA TN D-1060, January 1962.

Flight test results are derived from pulse, pull-up and sideslip maneuvers and are compared to wind tunnel results for corresponding conditions. Results are given for aileron, vertical tail and horizontal stabilizer deflections.